

**DETECTING NONLINEARITY IN CONCRETE BEAMS
USING BI-COHERENCE OF VIBRATION DATA**

by

Fahim Ahmed

MASTER OF SCIENCE IN CIVIL ENGINEERING (STRUCTURAL)

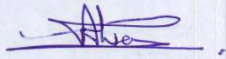


**DEPARTMENT OF CIVIL ENGINEERING
BANGLADESH UNIVERSITY OF ENGINEERING AND TECHNOLOGY**

June, 2016

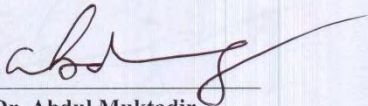
This thesis titled “**DETECTING NONLINEARITY IN CONCRETE BEAMS USING BI-COHERENCE OF VIBRATION DATA**”, submitted by Fahim Ahmed, Roll No. **0413042312F**, Session: April 2013, has been accepted as satisfactory in partial fulfillment of the requirement for the degree of **Master of Science in Civil Engineering (Structural)** on 4th June, 2016.

BOARD OF EXAMINERS



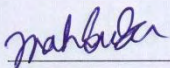
Dr. Raquib Ahsan
Professor
Department of Civil Engineering, BUET

Chairman
(Supervisor)



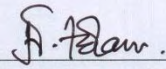
Dr. Abdul Muktadir
Professor and Head
Department of Civil Engineering, BUET

Member
(Ex-officio)



Dr. Mahbuba Begum
Professor
Department of Civil Engineering, BUET

Member



Dr. Mohammad Nazmul Islam
Professor
Department of Civil Engineering,
North South University

Member
(External)

DECLARATION

It is hereby declared that this project or any of it has not been submitted elsewhere for the award of any degree or diploma.

F. Ahmed
(Fahim Ahmed)

DEDICATION

This Thesis is Dedicated to My Parents and Teachers

ACKNOWLEDGEMENTS

First of all the author would like to give thanks to almighty Allah who is very kind to allow completing this thesis effectively.

The author expresses his profound gratitude and heartiest thanks to his thesis supervisor Professor Dr. Raquib Ahsan, Department of Civil Engineering, Bangladesh University of Engineering and Technology (BUET) for his constant guidance, supervision, keen interest as well as resource management in making this project success. His helpful guidance has benefited the author greatly.

The author is grateful to the members of thesis defence committee Prof. Dr. Abdul Muktadir, Prof. Dr. Mahbuba Begum and Prof. Dr. Mohammad Nazmul Islam for their advice and help in reviewing this thesis.

The author expresses his deep gratitude to Dr. Md. Ali Ahammad Shoukat Choudhury, professor and Head of the Department, Department of Chemical Engineering, BUET, for giving permission to use his book and program. Without these, it would have been impossible to complete the research work.

The author is very thankful to Md. Ashraf Kamal Himel and Md. Maruful Hasan for their cooperation and would like to express his thanks to all laboratory members for their advice and technical support throughout the experimental program.

The author is very grateful to his family members and friends for their unconditional love, encouragement, blessings and co-operation.

ABSTRACT

Vibration characteristics of structures have gained recent popularity in detecting damage of structures. Most of these works have been based on the assumption that the vibrating system behaves linearly. The aim of the present work is to explore possibility of identifying change in the nonlinear vibration characteristics to detect damage in RC beams.

To understand the nonlinearities in the vibration characteristics, a time series data based model is discussed which is based on the bicoherence of vibration data. The model is capable of identifying the extent of nonlinearity in any time series and it also proposes some indexes to measure the extent of nonlinearity in vibrating time series.

Static loads were applied to RC beams to induce damage and vibrating time series data at various damage levels were recorded. Time series data were recorded for four different vibrating conditions, ambient, one impact, interval impact and continuous impact excitations. These time series data were used to calculate the indexes proposed by the time series based model. These indexes were used to develop some relations with the increasing nonlinearity due to damage loading in RC beams. After that frequency domain data of time series were further studied to know the extent of cracks in RC beams due to the loading.

The beam tests demonstrated that there was a change in nonlinear vibration behavior with damage. The change in frequency domain data and corresponding area is more prominent for flexure control beams. In case of shear control beams we can identify the propagation of crack from the change of frequency domain data of time series.

TABLE OF CONTENTS

ACKNOWLEDGEMENTS.....	v
ABSTRACT.....	vi
TABLE OF CONTENTS.....	vii
LIST OF FIGURES	xi
LIST OF TABLES.....	xiv
CHAPTER ONE : INTRODUCTION.....	15
1.1 General.....	15
1.2 Background of the study	15
1.3 Objectives of the Research.....	16
1.4 Methodology	16
1.5 Scope of the Work.....	17
1.6 Organization of the Thesis	17
CHAPTER TWO : LITERATURE REVIEW.....	18
2.1 General.....	18
2.2 Linear Modal Method.....	18
2.2.1 Natural Frequency.....	18
2.2.2 Damping Ratios	19
2.2.3 Modal Shapes.....	19
2.2.4 Finite Element Models and Model Updating Methods.....	21
2.2.5 Problems to Overcome.....	22
2.3 Nonlinear Modal Methods	23
2.3.1 Modeling Cracked Beams.....	23
2.3.2 Nonlinear Vibration	24
2.4 Time Series Based Measures of Nonlinearity	25

2.4.1	Bispectrum and Bicoherence	25
2.4.2	Test of Gaussianity and Linearity of a Signal.....	26
2.5	Nonlinear Testing of Concrete Beams	29
2.6	Nonlinear Testing Methods of Concrete Beams	30
2.7	Conclusion Drawn from the Literature Review	31
CHAPTER THREE : TESTING of CONCRETE BEAMS		33
3.1	General	33
3.2	Model Preparation	33
3.2.1	Selection of Geometric Properties of Models	33
3.2.2	Test set-up, instrumentation and data acquisition.....	35
3.3	Testing of Concrete Beams	36
3.3.1	Applying Loads.....	36
3.3.2	Vibration Testing	37
3.4	Experimental Procedure	37
3.5	Summary	38
CHAPTER FOUR : ANALYSIS of BEAM TEST RESULTS		39
4.1	Generals.....	39
4.2	Damage Loading	39
4.3	Bispectrum and Bicoherence Based Measure of nonlinearity	39
4.3.1	Ambient Excitation	40
4.3.2	One Impact Excitation	42
4.3.3	Interval Impact Excitation.....	45
4.3.4	Continuous Impact Excitation.....	48
4.4	Outcome of Bispectrum and Bicoherence Based Measure of Nonlinearity.....	51
4.5	Normalized Fourier Spectrum of Time Series Data.....	52
4.6	Normalized FFT and Area under the Curve: Ambient Excitation	52
4.6.1	Flexure Control Beam.....	52

4.6.2	Shear Control Beam.....	57
4.7	Normalized FFT and Area under the Curve: One Impact Excitation	65
4.7.1	Flexure Control Beam.....	65
4.7.2	Shear Control Beam.....	69
4.8	Normalized FFT and Area under the Curve: Interval Impact Excitation.....	75
4.8.1	Flexure Control Beam.....	75
4.8.2	Shear Control beam.....	79
4.9	Normalized FFT and Area under the Curve: Continuous Impact Excitation.....	85
4.9.1	Flexure Control Beam.....	85
4.9.2	Shear Control Beam.....	90
CHAPTER FIVE : CONCLUSIONS		97
5.1	General	97
5.2	Conclusions	98
5.3	Recommendation for Future Studies	98
REFERENCES		99
APPENDIX-A.....		103
APPENDIX-B.....		123
APPENDIX- C.....		127

LIST OF FIGURES

Figure 3.1: Dimensions and Detailing of Shear Control Beam	34
Figure 3.2: Dimensions and Detailing of Flexure Control Beam	34
Figure 3.3: Experimental Setup of Testing Beam.....	35
Figure 3.4: Load Application Mechanism in RC Beam	36
Figure 3.5: sensor and Data Acquisition System of MT.....	37
Figure 4.6: Load Deflection Curve of Flexure and Shear Control Beams.....	39
Figure 4.7: Ambient Time History Recording for Flexure Control Beam-2.....	40
Figure 4.8: Non-Gaussianity Index (NGI) of Beam at Ambient Excitation	41
Figure 4.9: Non-Linearity Index (NLI) of Beam at Ambient Excitation.....	42
Figure 4.10: One Impact Time History Recording for Flexure Control Beam-2	43
Figure 4.11: Non-Gaussianity Index (NGI) of Beams at One Impact Excitation.....	44
Figure 4.12: Non-Linearity Index of Beam at One Impact Excitation	45
Figure 4.13: Interval Impact Time History Recording for Flexure Control Beam-2.....	46
Figure 4.14: Non-Gaussianity Index (NGI) of Beam at Interval Impact Excitation	47
Figure 4.15: Non-Linearity Index (NLI) of Beam at Interval Impact Excitation	48
Figure 4.16: Continuous Impact Time History Recording for Flexure Control Beam-2.....	49
Figure 4.17: Non-Gaussianity Index (NGI) of Beam at Continuous Impact Excitation	50
Figure 4.18: Non-Linearity Index (NLI) of Beam at Continuous Impact Excitation	51
Figure 4.19: Normalized FFT Curve of Flexure Control Beam-2 (FB-2).....	54
Figure 4.20: Normalized FFT Curve of Flexure Control Beam-3 (FB-3).....	57
Figure 4.21: Area under the FFT Curve of Flexure Control Beam at Ambient Excitation	57
Figure 4.22: Normalized FFT Curve of Shear Control Beam-1 (SB-1) at Ambient Excitation	60
Figure 4.23: Normalized FFT Curve of Shear Control Beam-2 (SB-2)	62
Figure 4.24: Normalized FFT Curve of Shear Control Beam-3 (SB-3)	64
Figure 4.25: Area under the FFT Curve of Shear Control Beam at Ambient Excitation	65
Figure 4.26: Normalized FFT Curve of Flexure Control Beam-2 (FB-2).....	67
Figure 4.27: Normalized FFT Curve of Flexure Control Beam-3 (FB-3).....	68
Figure 4.28: Area under the FFT Curve of Flexure Control Beam at One Impact Excitation	69
Figure 4.29: Normalized FFT Curve of Shear Control Beam-1 (SB-1) at One Impact Excitation	71

Figure 4.30: Normalized FFT Curve of Shear Control Beam-2 (SB-2) at One Impact Excitation	72
Figure 4.31: Normalized FFT Curve of Shear Control Beam-3 (SB-3) at One Impact Excitation	74
Figure 4.32: Area under the FFT Curve of Shear Control Beam at One Impact Excitation ...	75
Figure 4.33: Normalized FFT Curve of Flexure Control Beam-2 (FB-2)	77
Figure 4.34: Normalized FFT Curve of Flexure Control beam-3 (FB-3)	78
Figure 4.35: Area under the FFT Curve of Flexure Control Beam at One Impact Excitation	79
Figure 4.36: Normalized FFT Curve of Shear Control Beam-2 (SB-2)	80
Figure 4.37: Normalized FFT Curve of Shear Control Beam-2 (SB-2) for Interval Impact Excitation	82
Figure 4.38: Normalized FFT Curve of Shear Control Beam-3 (SB-3) for Interval Impact Excitation	84
Figure 4.39: Area under the FFT Curve of Shear Control Beam at Interval Impact Excitation	85
Figure 4.40: Normalized FFT curve of Flexure Control Beam-2 (FB-2) for Continuous Impact Excitation	87
Figure 4.41: Normalized FFT Curve of Flexure Control Beam-3 (FB-3) for Continuous Impact Excitation	89
Figure 4.42: Area under the FFT Curve of Flexure Control Beam at Continuous Impact Excitation	89
Figure 4.43: Normalized FFT Curve of Shear Control Beam-1 (SB-1) for Continuous Impact Excitation	91
Figure 4.44: Normalized FFT Curve of Shear Control Beam-2 (SB-2) for Continuous Impact Excitation	93
Figure 4.45: Normalized FFT Curve of Shear Control Beam-3 (SB-3) for Continuous Impact Excitation	95
Figure 4.46: Area under the FFT Curve of Shear Control Beam at Continuous Impact Excitation	96
Figure A1: Ambient Time History Recording for Flexure Control Beam-2	103
Figure A2: One Impact Time History Recording for Flexure Control Beam-2	104
Figure A3: Interval Impact Time History Recording for Flexure Control Beam-2	105
Figure A4: Continuous Impact Time History Recording for Flexure Control Beam-2	106
Figure A5: Ambient Time History Recording for Flexure Control Beam-3	107

Figure A6: One Impact Time History Recording for Flexure Control Beam-3	108
Figure A7: Interval Impact Time History Recording for Flexure Control Beam-3.....	109
Figure A8: Continuous Impact Time History Recording for Flexure Control Beam-3.....	110
Figure A9: Ambient Time History Recording for Shear Control Beam-1	111
Figure A10: One Impact Time History Recording for Shear Control Beam-1.....	112
Figure A11: Interval Impact Time History Recording for Shear Control Beam-1	113
Figure A12: Continuous Impact Time History Recording for Shear Control Beam-1	114
Figure A13: Ambient Time History Recording for Shear Control Beam-2	115
Figure A14: One Impact Time History Recording for Shear Control Beam-2.....	116
Figure A15: Interval Impact Time History Recording for Shear Control Beam-2.....	117
Figure A16: Continuous Impact Time History Recording for Shear Control Beam-2.....	118
Figure A17: Ambient Time History Recording for Shear Control Beam-3	119
Figure A18: One Impact Time History Recording for Shear Control Beam-3.....	120
Figure A19: Interval Impact Time History Recording for Shear Control Beam-3.....	121
Figure A20: Continuous Impact Time History Recording for Shear Control Beam-3.....	122
Figure B1: Grain Size Distribution of Fine Aggregate	123
Figure B2: Grain Size Distribution of Fine Aggregate	125

LIST OF TABLES

Table 4.1: Various Damage Levels of FB-2	52
Table 4.2: Various Damage Levels of FB-3	55
Table 4.3: Various Damage Levels of SB-1	58
Table 4.4: Various Damage Levels of SB-2	60
Table 4.5: Various Damage Levels of SB-3	62
Table B1: Sieve Analysis of Fine Aggregate.....	123
Table B2: Specific Gravity and Absorption Capacity of Sand	124
Table B3: Unit Wt of Fine Aggregate.....	124
Table B4: Grain Size Analysis of Coarse Aggregate.....	125
Table B5: Specific Gravity and Absorption Capacity of Coarse Aggregate	126
Table B6: Unit Wt of Coarse Aggregate.....	126
Table B7: Mix Design for Beam Casting	126

CHAPTER ONE

INTRODUCTION

1.1 General

Detecting damage within structure at an early stage of its development recently has gained attentions from researchers. Current detection methods are either visualized or localized experimental methods (ultrasonic or acoustic methods). These methods require that the damage location is known and accessible. The need for a more global damage detection method has lead to the development of methods that investigate changes in the vibration properties of the structures.

1.2 Background of the study

The basic idea of vibration-based damage diagnosis is that changes in geometry and physical properties of structures cause changes in structural dynamic behavior. Typically, damage is characterized by changes in the modal parameters, namely natural frequencies, modal damping ratios and mode shapes. Damage may also be detected on the basis of other damage-sensitive effects without the need of identifying modal parameters. Damage causes changes in structural parameters, namely the matrices of mass, damping, stiffness and flexibility of structures.

In contrast to the large amount of work on developing methods of detecting damage assuming linear vibration, there has been very little research on the feasibility of using the vibration nonlinearities to assess the condition of structures. Most of the non-linear vibration damage detection work has centered on fatigue cracks in metals. Significant progress has been made in detecting damage in, for example, aero plane wings (Tsyfansky and Beresnevich 2000). On the whole, one of two possible ways of detecting nonlinearities in the vibration characteristics is employed; either using forced vibration tests at a natural frequency and inspecting how the response deviates from a pure sine wave at the forcing frequency, or using impact excitation and inspecting the change in natural frequencies as the vibration decays. Very little work,

however, has been conducted on the non-linear testing and analysis of damaged concrete beams.

1.3 Objectives of the Research

The main objective of the work presented here is to assess the feasibility of using nonlinearities, in the vibration characteristics of damaged concrete beams to detect the damage. The terminal objectives are:

- Identification of Nonlinearity in RC beams, induced by structural distress, for flexure control beam.
- Identification of Nonlinearity in RC beams, induced by structural distress, for shear control beam.

1.4 Methodology

To detect the nonlinearity in concrete beams due to crack two types of failure conditions will be considered. One is Flexural failure and the other is Shear failure. To observe these failure conditions two different types of simple supported RC beams will be made. All the sample beams will be 125 x 125 x 1500 mm. Gradual incremental load will be applied to the beams to induce cracks. A micro-tremor with five sensors will be used to measure the vibration of the beams. This measurement will be used to compute the bi-coherence for the system in two operating conditions: when the beam is linear or crack free and when the beam is non-linear or cracked. When cracks are formed then the cracks origin and extent were observed. When the beam is non-linear or cracked the change of bi-coherence value from the linear or un-cracked beam will be used as a condition monitoring tool.

A total of 6 RC beam samples will be prepared for the above study:

- Three flexure control beams will be constructed using two 10 mm diameter bottom bar and stirrup with 8 mm diameter at 4 inch spacing.
- Three shear control beams will be constructed using two 10 mm and one 8mm diameter bottom bar and provide 3-8mm diameter stirrup. One stirrup at the middle of the beams and other two are at the end of the beams.

Finally, some indicators will be proposed by using the change of bi-coherence values or other parameters from vibration time series for convenient detection of nonlinearity and its extent in RC beams.

1.5 Scope of the Work

It is expected that the research work will unveil the suitability of using bi-coherence as a crack detection tool for RC beams. Since failure of RC structure often occurs due to structural cracks. The research will facilitate us to develop a Nondestructive Test to determine the crack and to measure the extent of non-linearity due to the crack in RC beams.

1.6 Organization of the Thesis

The thesis paper is organized into total six chapters. Apart from chapter one, the following chapters are organized as follows:

Chapter Two: A literature review is presented, the main conclusion of which was to conduct vibration excitation tests on concrete beams at various levels of over-load damage to assess the effect of damage on the non-linear vibration characteristics of a beam.

Chapter Three: This chapter presents the experimental program of research consisting of sample preparation of half scale concrete beams. The model preparation, test setup procedures were discussed in this chapter.

Chapter Four: Experimental results and analysis are presented in Chapter Four. Change of frequency domain data of time series vibration data, at various damage levels of RC beams were discussed in this chapter.

Chapter Five: This chapter summarizes the research and lists out the conclusions based on the outcome of the experimental study and recommend scopes for future studies.

CHAPTER TWO

LITERATURE REVIEW

2.1 General

A summary of the literature pertaining to the various methods for damage identification and health monitoring of structures based on changes in their measured dynamic properties is presented in this section. The vibration testing literature may be divided into two sections: those papers that assume that the vibration is linear and those that are concerned with the nonlinearities in the vibration response. Firstly, the linear and then the non-linear methods will be explored in this section of thesis.

2.2 Linear Modal Method

The idea of using vibration measurements to detect damage was proposed by Cawley and Adams (1979). It is based on the fact that damage will reduce the local stiffness of the structure, which in turn reduces the natural frequencies of the whole structure. Most studies into using vibration measurements to detect damage examine changes in modal properties and assume that these properties are linear. The types of indicators can be split into several main groups, each of which is briefly described below with some examples of their application.

2.2.1 Natural Frequency

The amount of literature related to damage detection using shifts in natural frequencies is quite large. The observation that changes in structural properties cause changes in vibration frequencies was the main assumption for using modal methods for damage identification.

Maguire and Severn (1987) conducted tests on four simply-supported pre-cast post tensioned concrete bridge beams with a span of 27.6 m. They reported a drop in frequency when the cover concrete was removed exposing the pre-stressing tendons. However, the changes were very small (in the order of 2%) and comparable to their frequency resolution.

Salawu (1997) conducted tests on a concrete bridge before and after the support bearings had been replaced and reported an average change in frequency of only 1.7% for the first six modes of vibration.

There have also been a large number of laboratory tests reported. For example, Eccles et al. (1997) found that for concrete beams that were damaged by four-point loading, the fundamental frequency dropped initially by around 12% but for greater damage (between 20% and 80% of the final load) the additional change in frequency was only 2.5%.

It is clear from above literatures that frequency shifts have significant practical limitations for applications to the type of structures considered in this review, although ongoing and future work may help resolve these difficulties. The somewhat low sensitivity of frequency shifts to damage requires either very precise measurements or large levels of damage. In addition there is an effect of temperature on natural frequency which was further discussed by Wahab and De Roeck (1997) and Roberts (1995).

2.2.2 Damping Ratios

There have been some attempts to use damping ratios as a measure of damage but they have proven to be unsuccessful. Salane and Baldwin Jr (1990) tested a steel girder bridge with concrete decking and concluded that, although damping ratios were affected by deterioration, they were unsuitable indicators as they initially increased and then fell with increasing damage. This finding is supported by Farrar and Jauregui (1998), who also found that damping of a steel plate girder bridge did not consistently increase or decrease with increasing damage. Casas and Aparicio (1994) conducted tests on small concrete beams and reported no clear relationship between damage and changes in damping.

2.2.3 Modal Shapes

Detecting damage using modal shapes have been generally far more positive than for damping ratios and natural frequencies. A large number of methods of interpreting the mode shape data have been suggested.

MAC and COMAC Numbers

Most of the work on mode shapes has concentrated on looking at the Modal Assurance Criterion (MAC). This compares the damaged mode shape for mode j against the undamaged reference mode shape for mode k , for all the modes J and k measured, and produces a correlation value between each damaged mode shape and each reference mode shape. For an undamaged structure it would be expected that for all $J = k$ the MAC is 1 and for all $J \neq k$ it is 0. The Co-Ordinate Modal Assurance Criterion (COMAC) is also commonly used. This is an extension to the MAC, intended to identify the location where two sets of mode shape data disagree and hence to find the location of the damage.

Alampalli et al. (1997) found that for a steel bridge no clear trend was detectable for increasing damage states when looking at the modal properties averaged over several tests for each of the first 12 modes. However, when statistical methods were applied to the results some success was reported although only at high damage levels. Salawu and Williams (1995) also reported some success when using mode shape data taken before and after repairs to a reinforced concrete bridge. They reported that although nothing could be concluded from inspection of the mode shapes directly, the MAC values did indicate some damage and the COMAC indicated four locations for damage, of which two were correct and two incorrect once a suitable threshold value for damage had been selected. A third actual damage site was not detected.

In contrast, Das et al. (1997) conducted tests on reinforced concrete beams damaged by static four-point loading and found that for lower modes the change in MAC number was extremely small, the greatest difference being when the damage was very localized, i.e. at first cracking and at the point where the steel first yielded. They also found that when the damage became more uniform the mode shape returned to a similar one to its undamaged state.

Curvature

If a crack is introduced there is a reduction in stiffness EI and this should cause a local increase in curvature, which is equal to bending moment divided by stiffness. Pandey et al. (1991) used a finite element model of a simply-supported beam with a reduction in E of 50% at the one-third span point over a region of 0.05 of the total span. They found that modal curvature was a far more sensitive damage indicator than the MAC or COMAC methods. The

changes in MAC and COMAC numbers were less than 0.5%, but using curvature a fairly clear damage region could be seen. This method was tested on a bridge and a finite element model of a bridge by Farrar and Jauregui (1998). They found that damage could be detected and that the location could be narrowed down to two or three sites. However, they noted that their damage sites were extremely localized and that the method was unlikely to be as successful in locating a larger damaged region. Also, to calculate curvature accurately, a large number of measurement points were needed. This method of damage detection was further extended by Ratcliffe (1997).

Flexibility

Maeck et al. (1999) extended the use of curvature to detect damage by using it to calculate the local beam stiffness. A smoothed version of the curvature was calculated from the mode shape data then the stiffness was calculated using the curvature and the moment distribution along the beam (which may be derived using the mode shapes). Maeck et al. (2000) looked at using this method along with changes in natural frequency firstly to establish the state of a concrete beam and then to locate any damage that was present. The method is reasonably successful for a distributed damage region. It does, however, require a dense measurement grid and an accurate undamaged stiffness profile.

Pandey and Biswas (1994) presented a damage-detection and location method based on changes in the measured flexibility of the structure. This method is applied to several numerical examples and to an actual spliced beam where the damage is linear in nature. Results of the numerical and experimental examples showed that estimates of the damage condition and the location of the damage could be obtained from just the first two measured modes of the structure.

2.2.4 Finite Element Models and Model Updating Methods

There has been a large quantity of work investigating the use of a numerical model of a structure in conjunction with test data to detect damage, a few examples of which are outlined below.

The method of combining frequency information with a numerical model has largely been extended from a method proposed by Cawley and Adams (1979), who looked at the change in the stiffness matrices necessary for two natural frequencies to match the corresponding natural frequencies in the damaged specimen. They then used this change in the stiffness matrix to find a locus of possible damage sites. By looking at several pairs of frequencies, several sets of loci of damage sites were calculated and a damage probability map could be generated. The tests they conducted were quite successful, although they were examining a sheet of aluminium with a saw cut representing the damage, which is relatively easy to model in comparison to a bridge, modeled by Thyagarajan et al. (1998)

Several authors have reported methods which use the natural frequencies of a structure in conjunction with a theoretical model to find damage location and severity. For example, Rizos et al. (1990) reported a method of measuring the amplitude of a steel beam at two points during forced vibration at a natural frequency, then using a model of the beam to predict the crack length and position by fitting the amplitudes to the equations of motion at the natural frequency. Morassi (2001) used the equations of motion of a simple beam to calculate the position and the size of a crack using the frequencies of the m^{th} and $2m^{\text{th}}$ modes. Armon et al. (1994) used a system of rank ordering the change in natural frequencies of a structure and then related this to the damage using a finite element model. A further problem with these methods is that an accurate model of the undamaged structure is required before using the model to assess the damaged structure.

Owen and Choo (1998) stated that the problem with the application of this type of method to a civil engineering structure is that the model will not predict the behavior of the structure as accurately as for a mechanical engineering application. Salawu (1997) held the same view and stated that methods that rely only on measured data would be more appropriate to large civil engineering structures.

2.2.5 Problems to Overcome

The review of previous work employing linear methods indicates that some substantial progress has been made in detecting damage using vibration techniques. There are however some major problems to overcome.

The relationship between the modal properties and environmental conditions needs further investigation. The effect of temperature on natural frequencies has already been mentioned and is believed to be the most influential factor but other factors such as humidity and rainfall must also be investigated. More detailed work on the environmental effects is being conducted. For example, C. Kramer et al. (1999) reported testing a bridge for a nine-month period, recording the environmental conditions and frequency response.

Since reinforced concrete structures are non-linear in behavior, important information is lost when the linear assumption is made. If non-linear behavior, i.e. the effects of amplitude of oscillation on the frequencies, can be used to detect damage it might be possible to test the structure just once and from examining the nonlinearities assess whether the structure is damaged so eliminating the need for a baseline measurement.

2.3 Nonlinear Modal Methods

In contrast to the vast quantity of work reported on linear damage detection techniques, little has been done to investigate non-linear time-dependent vibrational properties of civil engineering structures.

2.3.1 Modeling Cracked Beams

There has been interest for many years in the vibrational behavior of cracked beams in the condition-monitoring field. Numerous models of beams with cracks have been developed. These generally include either a crack that is permanently open or a “breathing” crack which opens and closes during vibration.

Many models represent the cracked beam as a series of undamaged beam finite elements, with the crack represented as either a reduced stiffness in one element or a mass less rotational spring at the joint between two of the beam elements. Rizos et al. (1990) modeled a beam with an open crack as two undamaged beams connected by a spring. They used the general form of the modal shapes of the two undamaged beams, along with the boundary conditions at the crack location, to develop equations for the displacements either side of the crack. The spring compliance was found using the strain energy function of the crack. A

similar approach was used by Narkis (1994) to relate the natural frequency of a beam with a double-edged crack to the crack position and depth. The method was extended to a beam with a series of cracks by Shifrin and Ruotolo (1999) and to a crack in a beam with variable cross-section by Nandwana and Maiti (1997).

An alternative method was proposed by Mahmoud et al. (1999). They divided the beam along its length into many elements and, after lumping the mass of each element at its center, derived a matrix equation relating the forces and displacements of one end of an element to the other. The open crack was included as a reduced stiffness of one of the elements. A root searching technique was then used to find the natural frequencies using the matrix equations and boundary conditions. For most applications, applying a simple stiffness reduction is unrealistic, since most cracks open and close during oscillations unless a static load is also applied.

Kisa and Brandon (2000) developed a finite element model of a steel beam with a fatigue crack with varying degrees of closure. They then used modal superposition to model the transition region and calculate the natural frequency of the cracked beam. These models include crack nonlinearities to enable a better prediction of the natural frequency of a cracked beam but do not investigate any changes in frequency due to a change in amplitude of oscillation. Instead, the vibration was assumed to be linear with amplitude.

2.3.2 Nonlinear Vibration

Sundermeyer and Weaver (1995) demonstrated the potential use of the non-linear behavior of a breathing crack in detecting the existence of the crack. They used a model with a bilinear spring representing the crack to show that, in theory, for a beam that is excited at two frequencies simultaneously the steady state signal consists not only of the two driving frequencies, as expected, but also of a component at a frequency equal to the difference between the two driving frequencies. This was thought to be due to the bilinear stiffness properties of the spring. They concluded that this additional frequency component could be a useful indicator of bilinear behavior that resulted from damage.

Rivola and White (1998) investigated the possibility of using the auto-bispectrum to detect nonlinearities in a bilinear system using a simple model. The auto-bispectrum detects

coherence between the phases of the signal at different resonant frequencies. If a non-linearity is present there will be some relationship between the phases causing a peak in the auto-bispectrum. They concluded that the auto-bispectrum was more sensitive to changes in behavior than the power spectral density, but it was far more difficult to interpret. Worden and Tomlinson (2001) also used the auto-bispectrum to analyze a non-linear three degree of freedom model.

2.4 Time Series Based Measures of Nonlinearity

Time series approach requires only the output time series to assess nonlinearity. Classical signal processing tools utilizes only the first and second-order moments, i.e. the mean, variance, covariance and correlation. Such tools are mainly useful for analyzing signals from linear processes. The distribution of signals from nonlinear processes is often skewed and non-Gaussian. This necessitates the use of higher order statistical tools. The third and fourth order moments and their frequency domain counterparts (bispectrum and trispectrum) are found to be useful in communication signals and machine condition monitoring (Collis et al. 1998; Nikiyas and Petropulu 1993). These higher order statistical techniques have also been used to detect and diagnose nonlinearities in control valves used in process industries.

2.4.1 Bispectrum and Bicoherence

The bispectrum is the simplest of the various frequency domain higher order statistics (HOS) measures. It is the frequency domain counter part of the third-order moment and is defined as

$$B(f_1, f_2) \triangleq E[X(f_1)X(f_2)X^*(f_1 + f_2)] \dots\dots\dots(2.1)$$

Where $X(f)$ is the Fourier transform of the time series $x(t)$. Equation 2.1 shows that it is a complex quantity having both magnitude and phase. It can be plotted against two independent frequency variables f_1 and f_2 , in the three dimensional plot. Each point in the plot represents the bispectral energy content of the signal at the bifrequency, (f_1, f_2) . In fact, the bispectrum, $B(f_1, f_2)$, at point (f_1, f_2) measures the nonlinear interaction between frequencies f_1 and f_2 . This interaction between frequencies can be related to the nonlinearity present in the signal

generating system and therein lies its usefulness in the detection and diagnosis of nonlinearity (Choudhury et al. 2006).

The bispectrum is normalized in the following way to give a measure called bicoherence whose magnitude is bounded between 0 and 1:

$$bic^2(f_1, f_2) \triangleq \frac{|E[B(f_1, f_2)]|^2}{E[|X(f_1)X(f_2)|^2]E[|X(f_1+f_2)|^2]} \dots\dots\dots(2.2)$$

Where „bic“ is the bicoherence function. Equation (2.2) can be rewritten as

$$bic^2(f_1, f_2) \triangleq \frac{|E[X(f_1)X(f_2)X^*(f_1+f_2)]|^2}{E[|X(f_1)X(f_2)|^2]E[|X(f_1+f_2)|^2]} \dots\dots\dots(2.3)$$

2.4.2 Test of Gaussianity and Linearity of a Signal

Collis et al. (1998) used the bicoherence function whose magnitude is bound between 0 and 1 to check the linearity of a signal or time series. However they did not construct any statistical test. Choudhury et al. (2006a) used bicoherence to construct a chi-square test for examining the nonlinearity of a time series or signal and proposed two new indices the Non-Gaussianity Index (NGI) and Nonlinearity Index (NLI). The magnitude of these two indices always bounded between -1 and 1 because magnitude of bicoherence is always bound between 0 and 1. The indices allow users to apply them for comparing multiple time series. A short form of the derivation is described here the detail derivation and development of these indices can be found in Choudhury et al. (2006).

A discrete stationary time series, $X(K)$, is called linear if it can be represented by

$$X(K) = \sum_{n=0}^{M-1} h(n)e(k - n) \dots\dots\dots(2.4)$$

Where $e(K)$ is a sequence of independent distributed random variables with $E[e(K)]$, $\sigma_e^2 = E[e^2(K)]$ and $\mu_3 = E[e^3(K)]$. For this case, the following frequency domain relationship can be obtained.

$$\text{The power spectrum: } P(f) = \sigma_e^2 |H(f)|^2 \equiv |X(f)X^*(f)| \dots\dots\dots(2.5)$$

$$\text{And the bispectrum: } B(f_1, f_2) = \mu_3 H(f_1)H(f_2)H^*(f_1 + f_2) \dots\dots\dots(2.6)$$

Where $H(f) = \sum_{n=0}^{M-1} h(n)\exp(-2\pi ifn)$. Equation (6.2) can be rewritten as

$$\begin{aligned} bic^2(f_1, f_2) &\triangleq \frac{|B(f_1, f_2)|^2}{E[|X(f_1)X^*(f_1)|] E[|X(f_1)X^*(f_2)|] E[|X(f_1+f_2)X^*(f_1+f_2)|]} \\ &\equiv \frac{|B(f_1, f_2)|^2}{E[|P(f_1)|] E[|P(f_2)|] E[|P(f_1+f_2)|]} \dots\dots\dots(2.7) \end{aligned}$$

For the linear time series substituting expression from Eq (2.5) and (2.6) it can be shown that

$$bic^2(f_1, f_2) = \frac{\mu_3^2}{\sigma_e^6} \dots\dots\dots(2.8)$$

Equation (2.8) shows that for any linear signal, x , the squared bicoherence will be independent of bifrequencies (f_1, f_2) . If the squared bicoherence is zero the signal x is non-skewed or Gaussian because skewness or μ_3 is also zero. In most of the HOS literature non-skewed or Gaussian have been used interchangeably. To check whether is constant, two tests are required. One is to determine whether the squared bicoherence is zero, which would show that the signal is Gaussian and thereby the signal generating process is linear. The other is to test for a non-zero constant squared bicoherence, which would show that the signal is non-Gaussian but the signal generating process is linear (Choudhury et al. 2006).

The following statistical test is suggested to check for the significance of bicoherence magnitude at each individual bifrequencies:

$$P \{ 2K bic^2(f_1, f_2) > C_\alpha^{\chi^2} \} = \alpha$$

or

$$P \left\{ bic^2(f_1, f_2) > \frac{C_\alpha^{\chi^2}}{2k} \right\} = \alpha \dots\dots\dots(2.9)$$

Where K is the number of data segment used in bicoherence estimation and $C_\alpha^{\chi^2}$ the critical value calculated from the central χ^2 distrebution table for a significance level of α with two degrees of freedom. For example, for $\alpha = 0.05$ the value of $C_{0.05}^{\chi^2}$ is 5.99.

Often the principal domain of the bicoherence plot contains more than a hundred bifrequencies. The hupothesis test results for this large number of bifrequencies can be conveniently summarized into the following Non-Gaussianity Index (NGI):

$$NGI \triangleq \frac{\Sigma bic_{significant}^2}{L} - \frac{C_\alpha^{\chi^2}}{2k} \dots\dots\dots(2.10)$$

Where $bic_{significant}^2$ are those bicoherence values which satisfy equation (2.9) and L is the number of $bic_{significant}^2$. Therefore following rule-based decision is suggested by:

- if $NGI \leq 0$, the signal is Gaussian
- if $NGI > 0$, the signal is Non-Gaussian

Thus a signal is non-skewed or Gaussian at a confidence level of α if the NGI is ≤ 0 . Thus NGI facilitate the automation of this statistical hypothesis test.

Rao and Gabr (1980) showed that if a signal is found to be Gaussian, the signal generating process is linear. In the case of a non-Gaussian or skewed signal the signal generating process should be tested for its linearity. As shown in Eq (2.8), if the signal is non-Gaussian or skewed and linear, the magnitude of the squared bicoherence should be a non-zero constant in such a case (Choudhury et al. 2006).

Choudhury et al. (2006) proposed a simple way to confirm the constancy of squared bicoherence is to examine the three dimensional squared bicoherence plot and observe the flatness of the plot. This method can be cumbersome when it is applied to a large number of

time series. To check the flatness of the plot or the constancy of the squared bicoherence, a nonlinearity index has been reported in Choudhury et al. (2004b) in which the maximum squared bicoherence is compared with the average squared bicoherence plus two times the standard deviation of the estimated squared bicoherence. The disadvantage of using this index is that the presence of a few large peaks significantly bias the standard deviation and mean of the estimated bicoherence, which leads to some false negatives. In order to avoid these limitations, the nonlinearity index defined in Choudhury et al. (2004b) was modified in Choudhury et al. (2006a).

$$NLI \triangleq \sum bic_{max}^2 - \left(\overline{bic_{max}^2} + 2 \sigma_{bic^2, robust} \right) \dots \dots \dots (2.11)$$

Where $\overline{bic_{max}^2}$ and $\sigma_{bic^2, robust}$ are respectively the robust mean and the robust standard deviation of the estimated squared bicoherence.

Therefore it can be concluded that:

- if $NLI \leq 0$, the signal generating process is LINEAR
- if $NLI > 0$, the signal generating process is NONLINEAR

Since the squared bicoherence is bound between 0 and 1, the Nonlinearity Index (NLI) is also bound between -1 and 1.

2.5 Nonlinear Testing of Concrete Beams

There is very little published work which examines the non-linear amplitude-dependent modal properties of concrete beams. Eccles et al. (1997) conducted impact excitation tests on several beams. They showed that, initially, when the amplitude of oscillation is largest the frequency is lower than that when the amplitude of oscillation is small. The frequency increases approximately linearly with time until the amplitude of oscillation is small, at which point the frequency stabilizes and no further amplitude dependence can be detected. The gradient at which the frequency increases with time is larger for higher levels of damage. However the beams tested had a fundamental frequency far higher than would be expected for a bridge and the excitation decayed away extremely quickly.

These findings have been backed up by small scale beam tests conducted by Goldsmith (1999) who found that, although there was some amplitude dependence when the beam was undamaged, this increased when the beam was damaged up to the point where the reinforcing bars started to yield. After steel yield, the strength of the amplitude dependence stopped increasing and only a drop in the overall frequency was noted.

Forced vibration tests were conducted by Van Den Abeele and De Visscher (2000). They used continuous wave excitation at various amplitudes to build up a picture of the natural frequencies at different amplitudes of oscillation. The tests demonstrated that although the beam did not behave linearly when undamaged, once the beam was damaged using four-point loading the nonlinearities became far more pronounced. This approach was also explored by Owen (2001); Van Den Abeele and De Visscher (2000) also demonstrated similar trends using time domain tests. However, there is the disadvantage that the tests required shaker equipment, which adds to the complexity, especially if the method were to be employed on a large structure.

2.6 Nonlinear Testing Methods of Concrete Beams

Test methods may be split into three main categories;

- Ambient excitation
- Impact excitation
- Forced vibration

There has been much work published on the advantages and disadvantages of the three types of tests including sizeable reviews conducted by Prakash Rao et al. (1983); Salawu and Williams (1995). These tests are mainly performed for bridge health monitoring.

Ambient excitation tests are the easiest and cheapest to perform, relying simply on traffic or other environmental excitation. There is no need for expensive excitation equipment or to disrupt traffic flow and it would be possible to record the bridge vibration remotely using permanently installed accelerometers and data acquisition equipment (C. Kramer et al. 1999). However, it is the most difficult excitation method to interpret. There is a continuously

changing mass distribution on the bridge and vibration due to interaction with the vehicle suspensions (Humar and Kashif 1993). The input excitation is unknown and must be assumed to be white noise Farrar and James III (1997); Felber and Ventura (1996).

Tests on a bridge using impact excitation have been conducted by Raghavendrachar and Aktan (1992), who constructed a bump on the road surface and drove a truck over it. Although, as with forced vibration tests, the bridge must be closed for the duration of the test, it is reported that the disruption to traffic is less as each test is quicker and traffic can be allowed over the bridge between tests. A problem with this type of excitation is that the truck movement over the bridge results in a change of mass distribution. Another test method was employed by C. Kr̄amer et al. (1999), that of dropping a weight onto the bridge. Although this is more complex than truck excitation and may prevent reopening of the bridge between tests, it is easier to measure the input force.

Forced vibration tests consist of exciting the bridge using a shaker over either a broad band of frequencies, at one frequency or at a gradually changing frequency. The main benefit of forced vibration tests is that the amplitude of the bridge vibration may be held at a certain level giving a cleaner shape of the response. Other advantages of forced vibration tests are that the input excitation is known and that the frequency range may be controlled. A disadvantage is that for a bridge to be excited at reasonable amplitude a large shaker is required, which increases the cost of the tests. Also the bridge must be closed so that vehicle excitation does not affect the tests. Tests on bridges using forced excitation tests include Salawu and Williams (1995) and C. Kr̄amer et al. (1999), who reported the need for two shakers at different locations on the bridge to minimize the effect of traffic vibration from the road beneath the bridge.

2.7 Conclusion Drawn from the Literature Review

From an examination of the literature, it is clear that, although some promising work has been reported on damage detection in concrete structures using linear methods, there are still major problems to overcome, particularly those of sensitivity and the effect of environmental conditions. Nonlinear methods that detect any amplitude dependence of the natural frequencies should therefore be further investigated. Another important thing is that none of

the proposed methods has quantified the extent of nonlinearity. Time series based measure of nonlinearity proposed by Choudhury et al. (2006) provides a good starting point in quantifying the nonlinearity.

It requires only the output time series from a system. As a starting approach this method of detecting nonlinearity is used to measure extent of nonlinearity in simple supported concrete beams. To be coherent with the previous test methods the output time series of the beam is taken from three test condition ambient excitation, impact excitation and forced excitation.

CHAPTER THREE

TESTING OF CONCRETE BEAMS

3.1 General

This chapter presents the experimental program of research consisting of sample preparation of half scale concrete beams. To study the change of NGI and NLI index with the increase of nonlinearity in concrete beams, two different types of beams were made in laboratory. Material properties, sample preparation, test setup and testing of beam are described in this chapter.

3.2 Model Preparation

3.2.1 Selection of Geometric Properties of Models

To detect the nonlinearity in concrete beams due to crack two types of failure conditions are considered. One is Flexural failure and the other is Shear failure. To observe these failure conditions two different types of simple supported RC beams were made. All the sample beams were half scale model of actual beams.

The shear control beam had cross sectional area of 125 x 125 mm and a longitudinal length of 1500 mm. it had 2- ϕ 10 mm top bar with 2- ϕ 10 mm and 1- ϕ 8 mm bottom bar. To control the shear crack only three shear reinforcement of ϕ 8 mm are provided, one in the middle and other two in two end support point. All the shear reinforcement had 135 degree hook. Three shear control beams were prepared in the laboratory. Fig.3.1 shows dimension sand detailing of shear control beams. The Flexural moment capacity of the beam was 209 N-m and shear capacity of the beam was 15kN. The following Fig. 3.1 shows the detailing of flexure control beam.

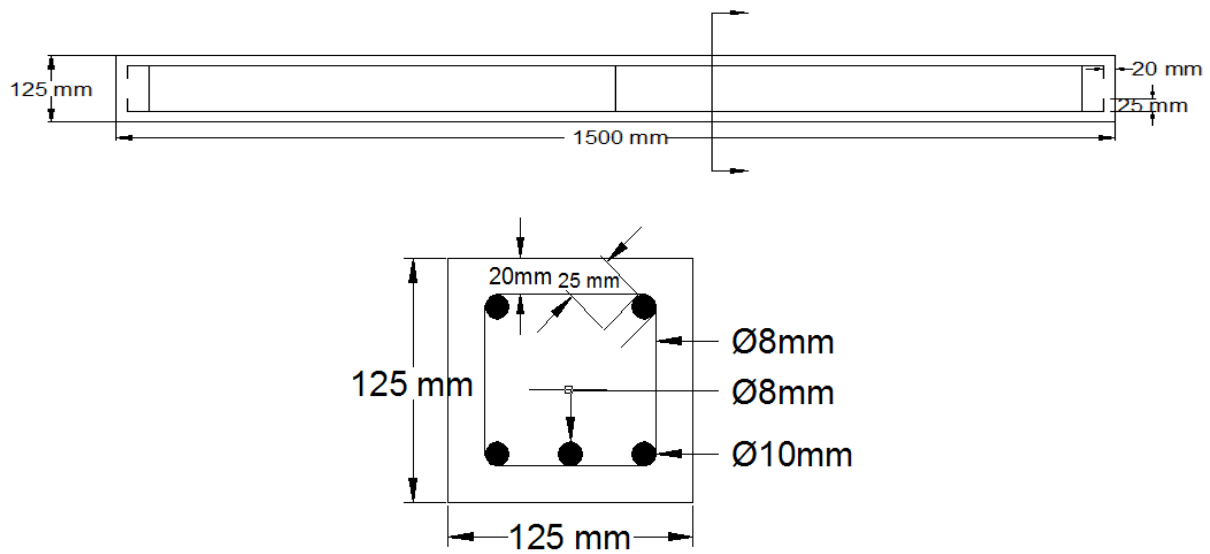


Figure 3.1: Dimensions and Detailing of Shear Control Beam

The flexure control beam had cross sectional area of 125 x 125 mm and a longitudinal length of 1500 mm. it had 2-φ 10 mm top and bottom bar. To control the flexure crack shear reinforcement of φ 8 mm are provided @ 100mm spacing with 135 degree hook. Three flexure control beams were prepared in the laboratory. It was estimated that the moment capacity of flexure control beam was 140 N-m, corresponding to a single point loading of 13.24 kN at mid span of the beam. Fig 3.2 shows the reinforcement detailing of the flexure control beam.

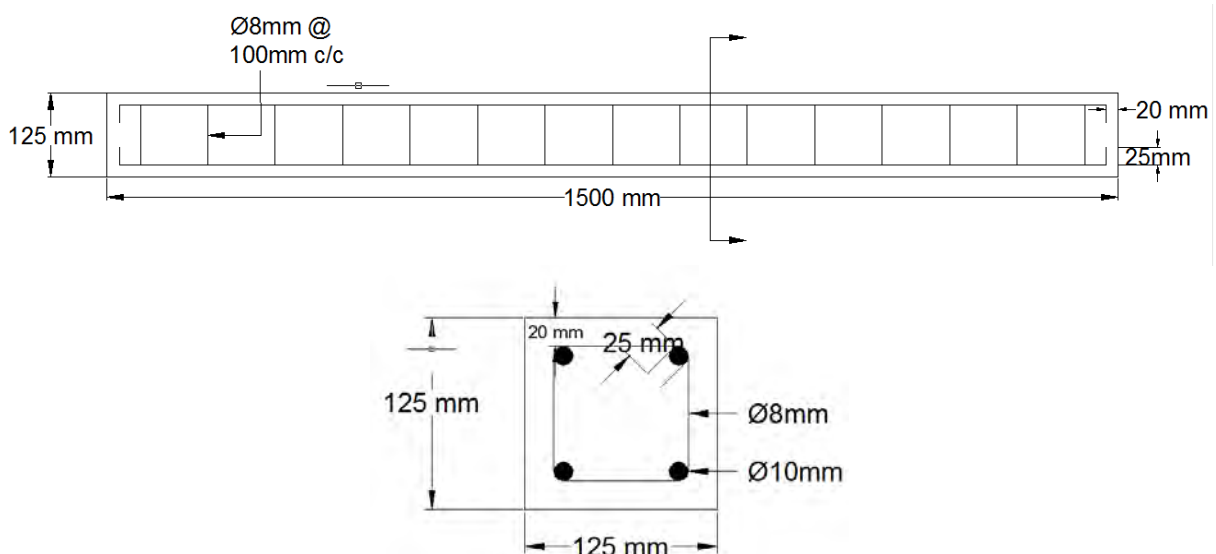


Figure 3.2: Dimensions and Detailing of Flexure Control Beam

A concrete mix giving 28 days design cylinder strength of 29.6 MPa was used. Due to the duration of the tests (each load level requiring a day of testing), the beams were cured for 28 days before testing to minimize any change in the concrete properties over the test period

3.2.2 Test set-up, instrumentation and data acquisition

Beam Set-up

Beams were tested under one point loading at mid span. They are supported by roller bearing action which represents the simple support condition. Specimens were placed over the two steel rollers bearing leaving 75mm from ends of beam.

Instrumentation

After installing the beam in proper position, the sensors of Microtremor (MT) were placed at the top of the beam. It has five sensors and each sensor has three channels representing X, Y, Z. Sensors were placed at every $\frac{L}{4}$ distance of the beam that is 375 mm. every sensor has X, Y, Z orientation marked in their body and beam were marked accordingly, which is shown in the following Fig. 3.3. A dial gauge was placed at the mid span of the beam to measure the deflection.

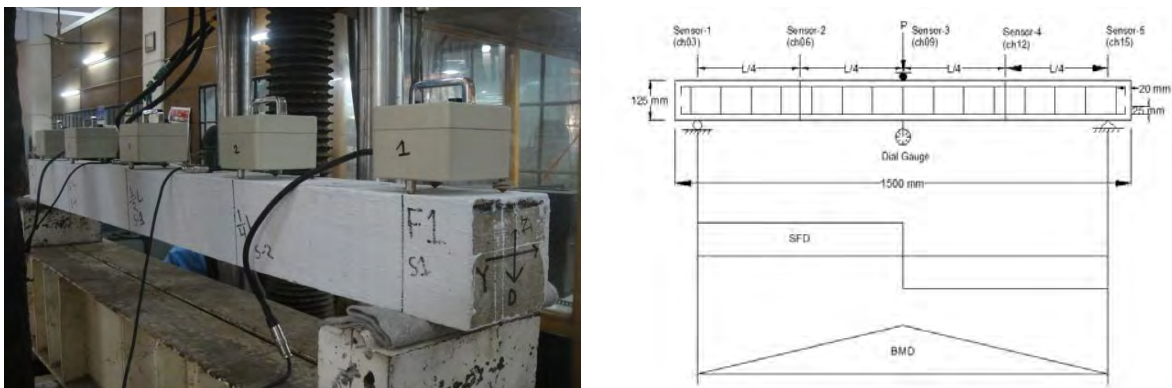


Figure 3.3: Experimental Setup of Testing Beam

Data Acquisition

The specimen beams were tested for gradual incremental vertical load, with an increment of 5 kN. After each increment of load mid span deflection and vibration of the beam were measured. Vibration data was recorded with a sampling frequency of 200 HZ. Four different

vibrating conditions were used; **Ambient Vibration**: only the ambient vibration of the beam was recorded, **One Impact Excitation**: in this case an impact load was given by hammering in a point of beam in the data recording time, **Interval Impact Excitation**: in this case an impact load was given by hammering at a point of beam with certain time interval in the vibration data recording time, **Continuous Impact Excitation**: continuous impact load was given by hammering in the whole duration of data recording. After each increment of load these cycle was repeated up to complete failure of the beam.

3.3 Testing of Concrete Beams

3.3.1 Applying Loads

The beam was damaged using single point loading at mid span of the beam. The damage levels were in steps of 5 kN. Failure was defined as the point where the beam could sustain no further increase in load. The load was applied using a Universal Testing Machine. To measure the deflection at mid span of the beam a dial gauge was used. This data is used to develop load deflection curve of the beam. The following Fig. 3.4 shows the load applying mechanism.



Figure 3.4: Load Application Mechanism in RC Beam

3.3.2 Vibration Testing

Once the beam was unloaded, the vibration of the beam was recorded for four different conditions: Ambient Vibration, Vibration after one impact, Vibration at certain interval impact and vibration at continuous impact. The vibration was recorded using a Microtremor (MT) with 5 sensors in it. Each sensor had three channels for measuring vibration in three direction (x,y and z). Sampling frequency of the MT was 200 Hz and total data recording time was 42 sec. the velocity data was recorded in micro meter/s and time was in second. The following Fig. 3.5 shows the MT sensor arrangement and data logger.



Figure 3.5: sensor and Data Acquisition System of MT

3.4 Experimental Procedure

Initially tests were conducted to assess the support conditions. Once they were confirmed as being satisfactory, the undamaged (UD) tests were performed and then the subsequent damage levels (D1 to D5). Failure (D5) was defined as the point where the beam was no longer capable of sustaining higher loading. For each damage level the vibration tests were carried out immediately after damage loading.

After each loading is removed vibration of the beam was tested for four conditions mentioned earlier. First for ambient vibration condition the natural or ambient vibration of the bema was recorded. No external excitation was provided to the beam and all other external noise coming from the laboratory machine was reduced by stopping them. For one impact excitation test the beam was excited manually by hammering once in the surface of the beam

during the data recording time. There appeared a clear pick in the data stream monitor in the MT screen. For interval impact test impact was given by hammering after certain time interval in the data recording period. Uniform interval in the impact was not possible due to manual application of hammering. In case of continuous interval continuous hammering was done during the whole data recording time of MT.

Time history data is not suitable to estimate the dynamic properties. So, transformation of time domain data to frequency domain data is required with Fourier Transformation. Therefore First Fourier Transformation (FFT) was used to transfer time domain data to frequency domain data.

3.5 Summary

To summarize, experiments were performed on concrete beams to assess the change in non-linear behavior with increasing damage. The experiments were performed at increasing levels of over-load damage. After each of these damage levels vibration responses to various excitations were measured. Deflection at mid span of the beam was also measured using dial gauge to find the load deflection relation. These will aid understanding of vibration pattern with increasing nonlinear of concrete beams due to damage loading.

CHAPTER FOUR

ANALYSIS OF BEAM TEST RESULTS

4.1 Generals

The analysis of beam test results can be divided into four different vibrating conditions as stated earlier.

- Ambient Excitation
- One impact Excitation
- Interval Impact Excitation
- Continuous Impact Excitation

4.2 Damage Loading

Damage levels are in steps of 5 kN ranging from UD (undamaged, no load case) to D5 the final damage level at failure. Flexure beams failed at 22.7 and 23.65 kN load respectively. Shear control beams failed at 22, 19.5 and 24.2 kN load respectively.

Fig. 4.6 shows deflection at mid span of beam where maximum load was applied. Deflection was measured using a dial gauge. Deflection at each damage level was with respect to the initial undamaged condition. In addition to deflection crack locations were also identified cracks were located almost exclusively between sensor -2 and 4 (ch06 and ch12).

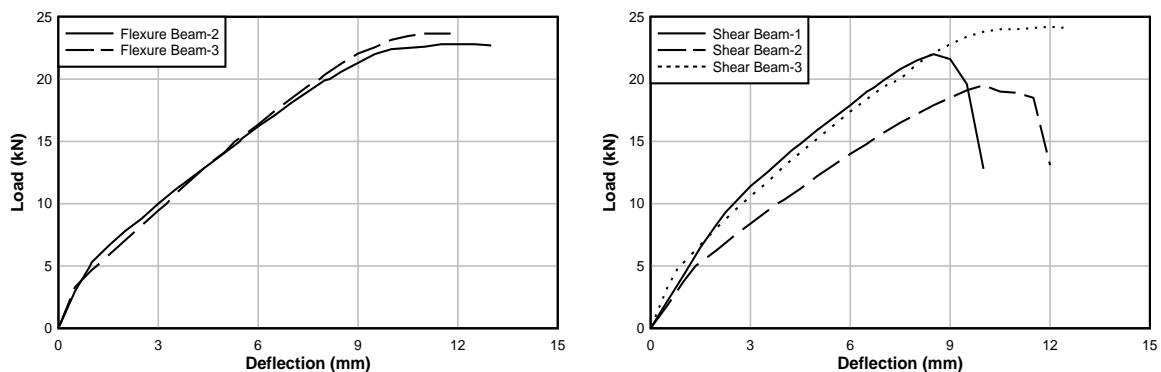


Figure 4.6: Load Deflection Curve of Flexure and Shear Control Beams

4.3 Bispectrum and Bicoherence Based Measure of nonlinearity

4.3.1 Ambient Excitation

For ambient excitation data vibration of each beam was recorded at undamaged condition as well as after removing the damaged load. To remove noise at recording time all running machine in the lab were stopped. The following Fig. 4.7 shows the recorded of ambient time history data of flexure control beam at various damage level. Other records can be found in appendix.

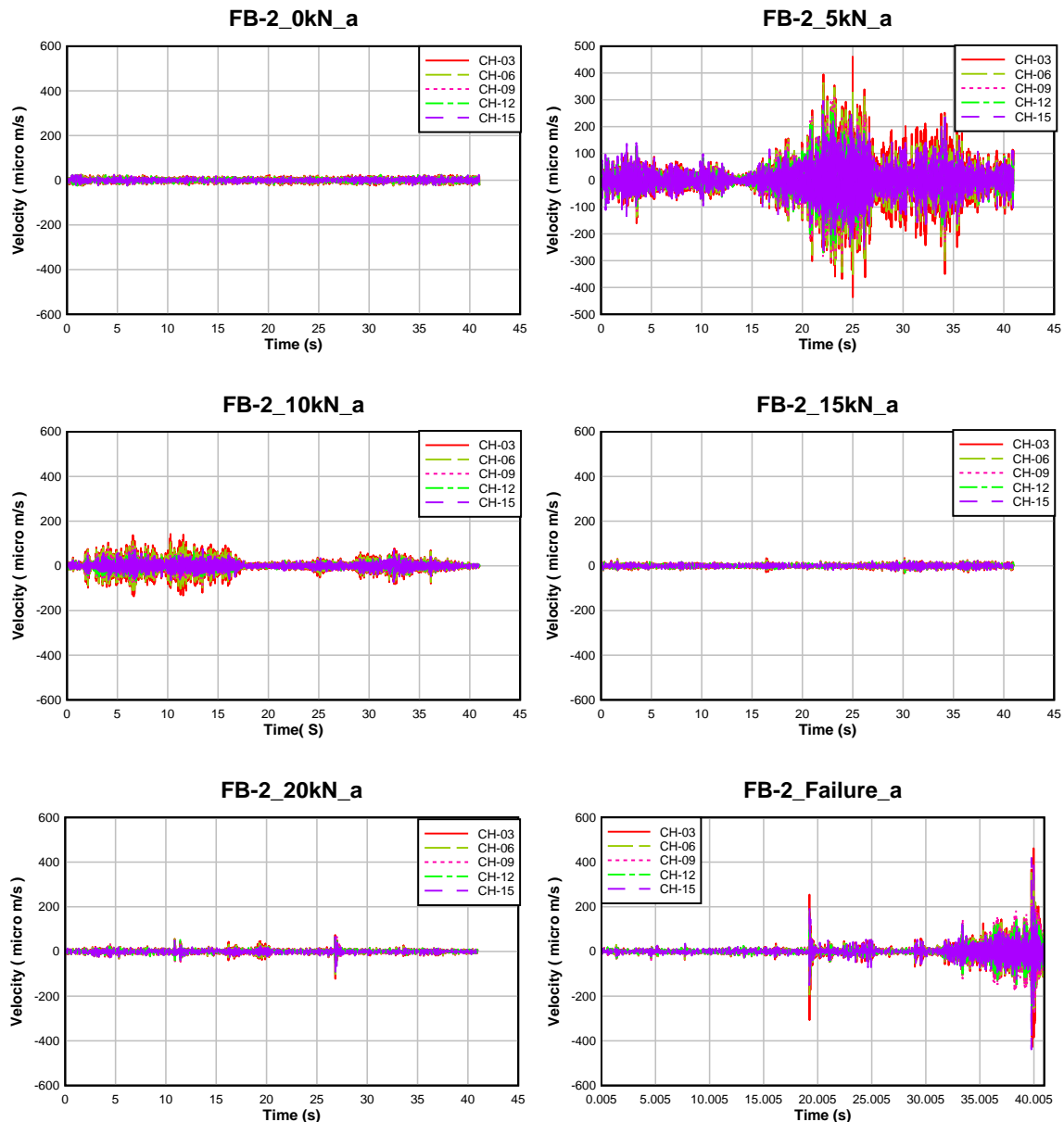


Figure 4.7: Ambient Time History Recording for Flexure Control Beam-2

This time series data was used to determine the distribution of the signal. According to Choudhury et al. (2006) if $NGI \leq 0$, the signal is GAUSSIAN and if $NGI \geq 0$, the signal is NON GAUSSIAN. Fig. 4.8 shows the Gaussianity test of the signals.

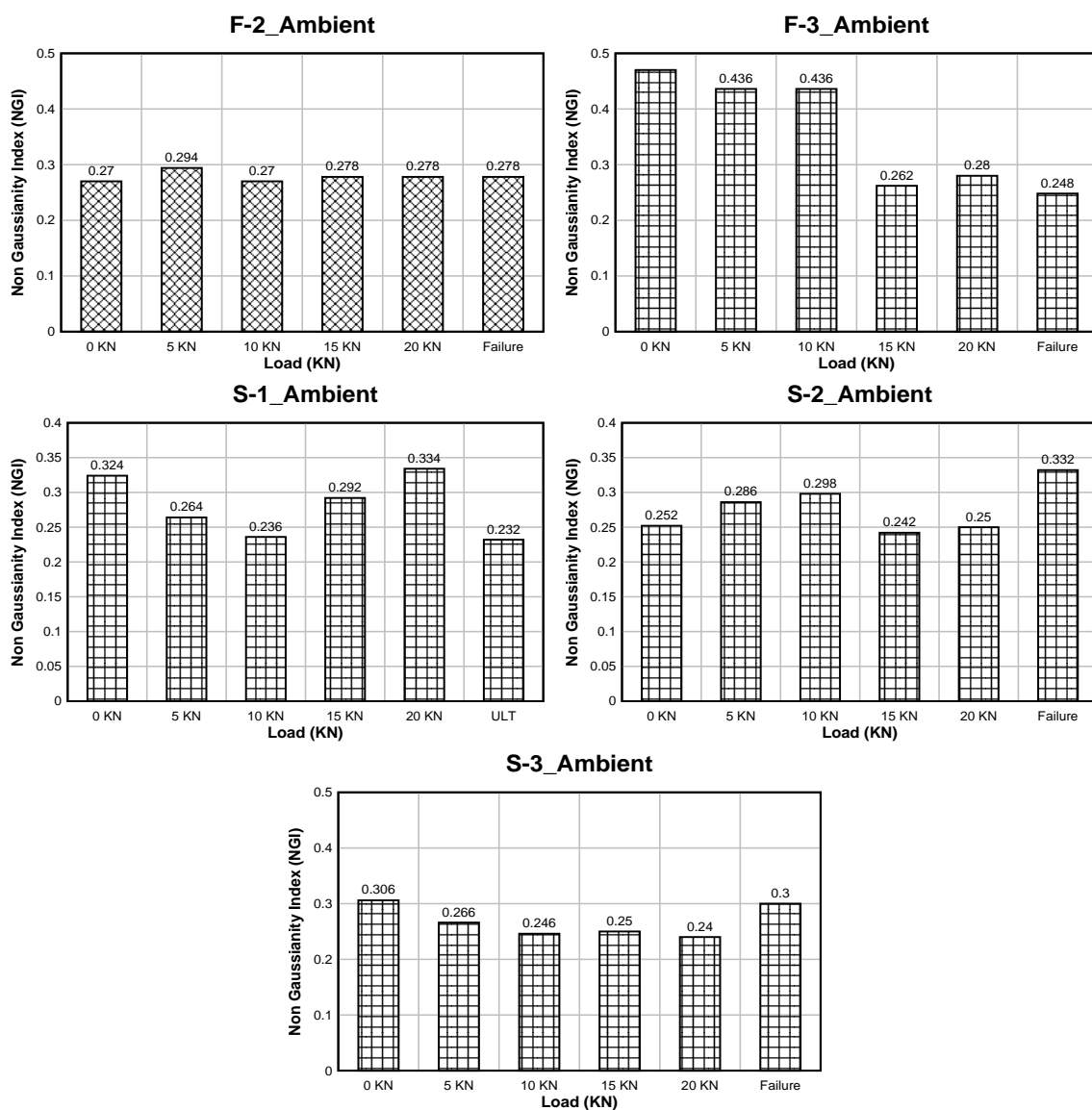


Figure 4.8: Non-Gaussianity Index (NGI) of Beam at Ambient Excitation

According to Choudhury et al. (2006) in the case of a non-Gaussian signal, signal generating process should be tested for its linearity and he defined the range of index as: if $NLI \leq 0$, the signal generating process is Linear; and if $NLI > 0$, the signal generating process is nonlinear. It is clear from the above Fig.4.8 that all the signals recorded from the beams had nongaussian distribution, so the nonlinearity of the signal is tested and the results are shown in flowing Fig. 4.9, which clearly indicates that the signal generating processes (tested beams) are nonlinear.

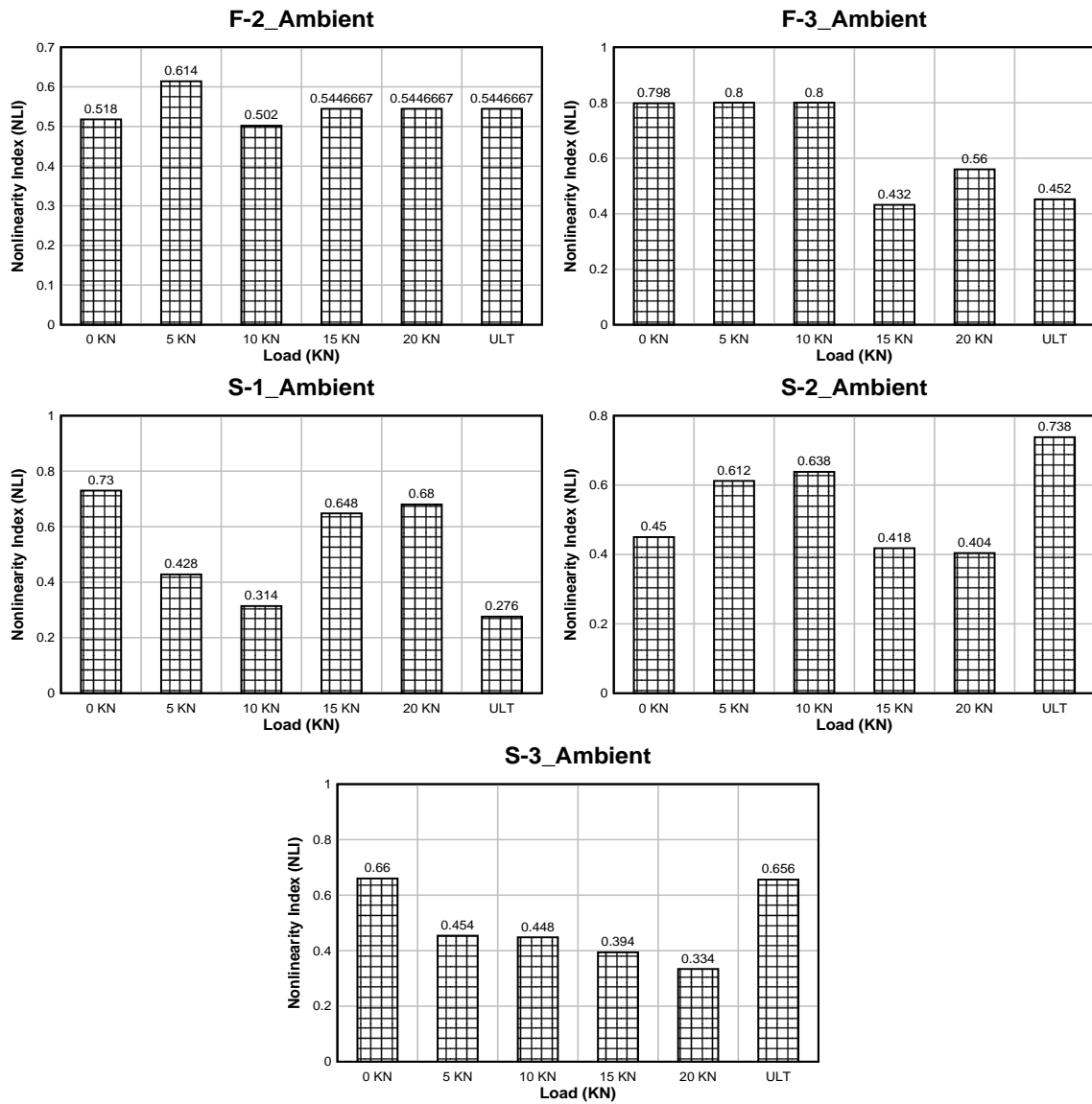


Figure 4.9: Non-Linearity Index (NLI) of Beam at Ambient Excitation

4.3.2 One Impact Excitation

For one impact excitation, vibration of each beam was recorded at undamaged condition as well as after removing the damaged load. During data recording time one single impact was provided in the beam by hammer. The following Fig. 4.10 shows the recording of one impact excitation of the flexure control beam. For other beams time series data is provided in Appendix-A.

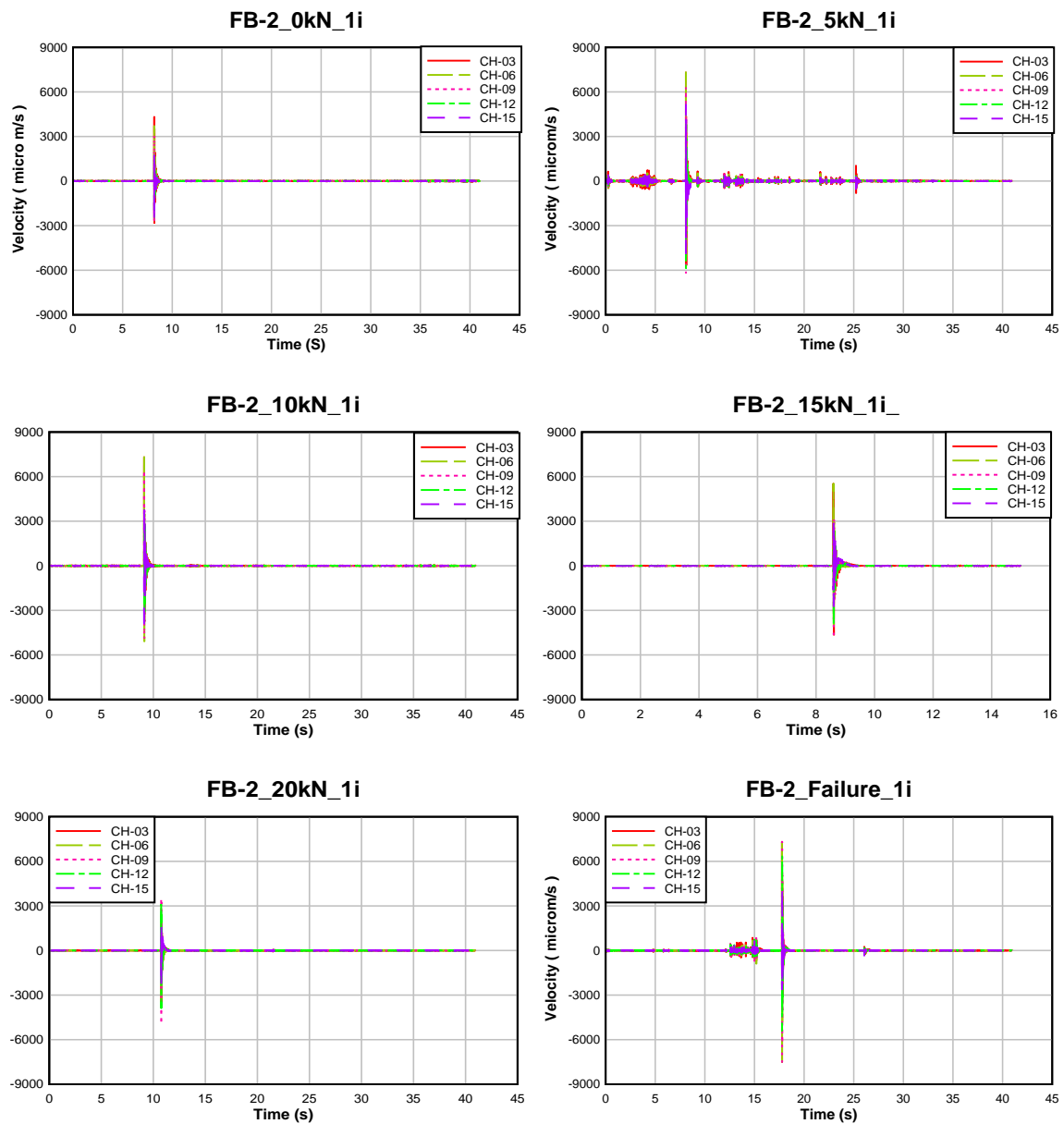


Figure 4.10: One Impact Time History Recording for Flexure Control Beam-2

This time series data was used to determine the distribution of the signal. According to Choudhury et al. (2006) if $NGI \leq 0$, the signal is GAUSSIAN and if $NGI \geq 0$, the signal was NON GAUSSIAN. Fig. 4.11 shows the Gaussianity test of the signals.

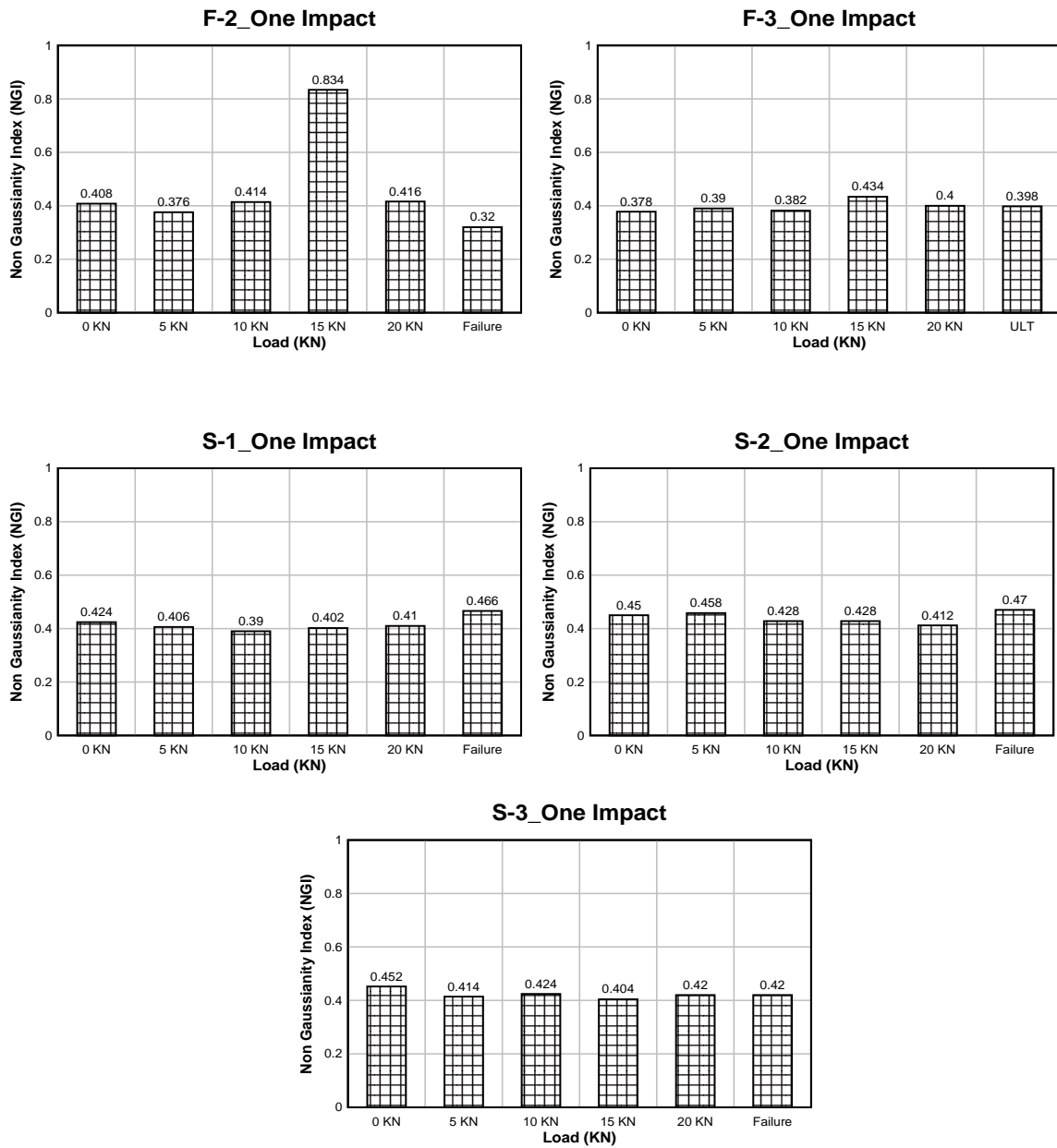


Figure 4.11: Non-Gaussianity Index (NGI) of Beams at One Impact Excitation

According to Choudhury et al. (2006) in the case of a non-Gaussian signal, signal generating process should be tested for its linearity and he defined the range of index as: if $NLI \leq 0$, the signal generating process is Linear; and if $NLI > 0$, the signal generating process is nonlinear. It is clear from the above Fig. 4.11 that all the signals recorded from the beams had nongaussian distribution, so the nonlinearity of the signal is tested and the results are shown in flowing Fig. 4.12, which clearly indicates that the signal generating processes (tested beams) were nonlinear.

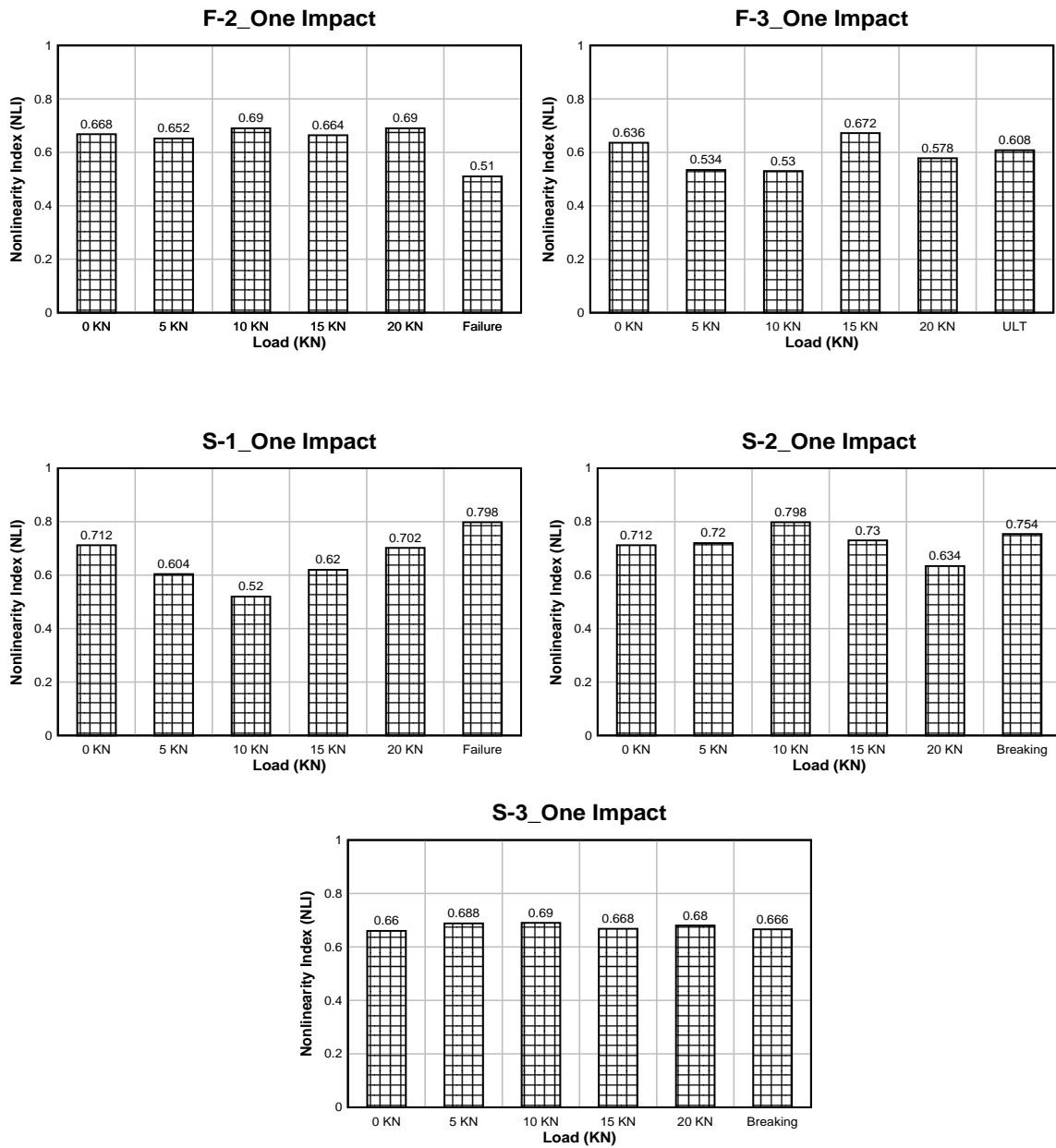


Figure 4.12: Non-Linearity Index of Beam at One Impact Excitation

4.3.3 Interval Impact Excitation

For interval impact excitation vibration of each beam was recorded at undamaged condition as well as after removing the damaged load. During data recording time impact excitations were provided in the beam by hammer at an interval. The interval time could not be maintained uniform because it was manual controlled. The following Fig. 4.13 shows the

recording of interval impact excitation of the flexure beam. For other beams time series data is provided in Appendix-A.

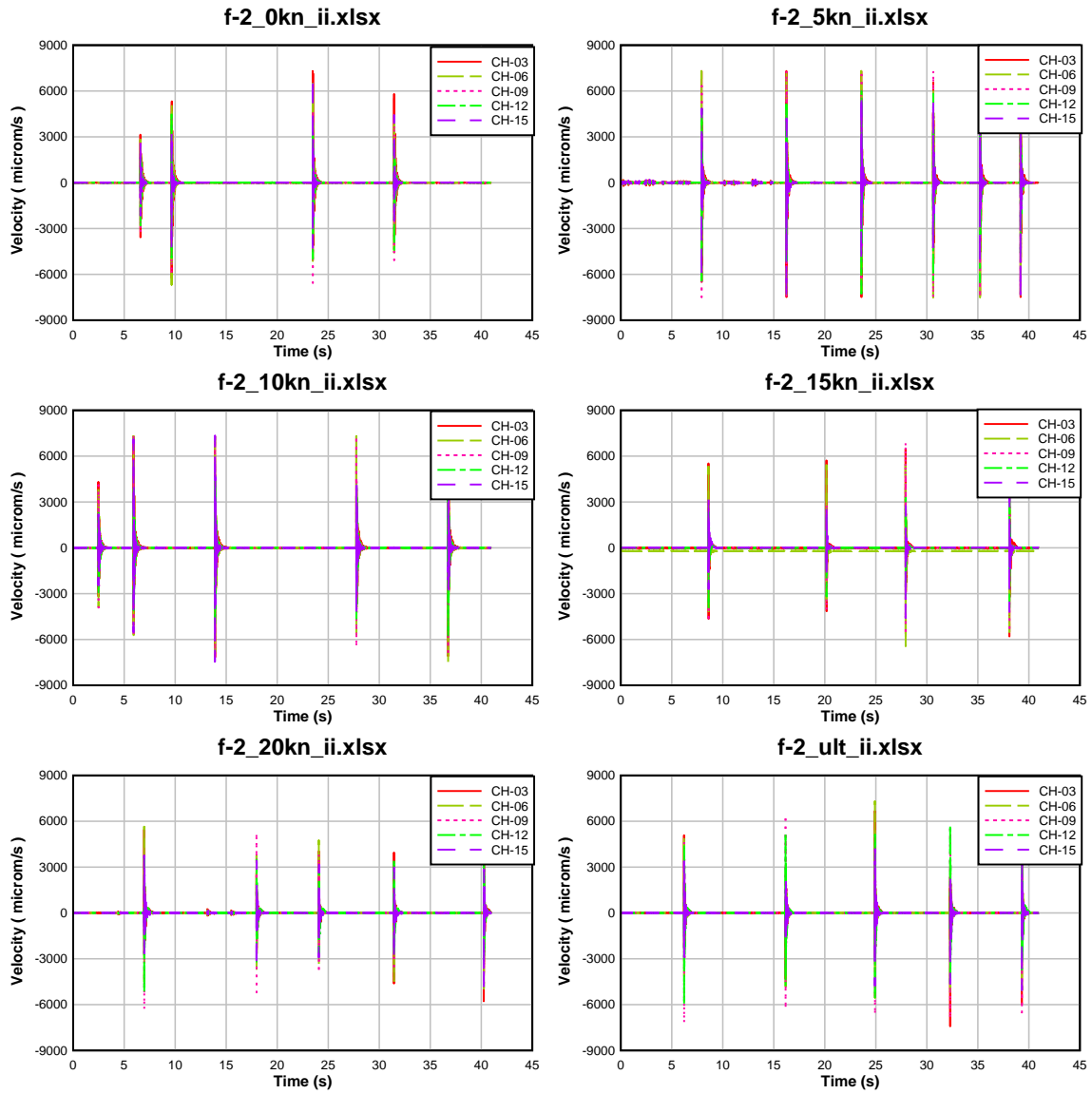


Figure 4.13: Interval Impact Time History Recording for Flexure Control Beam-2

This time series data was used to determine the distribution of the signal. According to Choudhury et al. (2006) if $NGI \leq 0$, the signal is GAUSSIAN and if $NGI \geq 0$, the signal was NON GAUSSIAN. Fig. 4.14 shows the Gaussianity test of the signals.

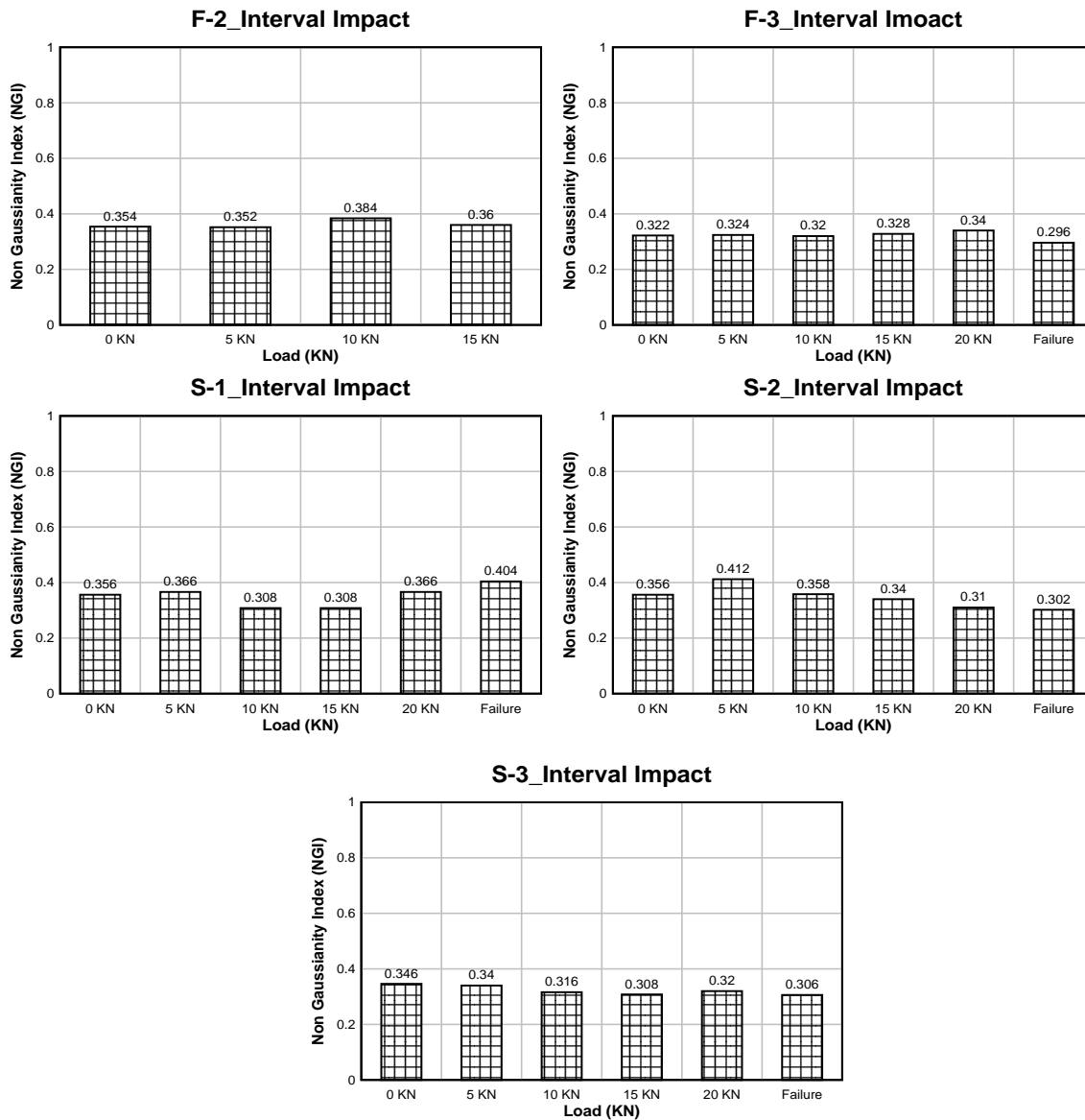


Figure 4.14: Non-Gaussianity Index (NGI) of Beam at Interval Impact Excitation

According to Choudhury et al. (2006) in the case of a non-Gaussian signal, signal generating process should be tested for its linearity and he defined the range of index as: if $NLI \leq 0$, the signal generating process is Linear; and if $NLI > 0$, the signal generating process is nonlinear. It is clear from the above Fig. 4.14 that all the signals recorded from the beams had nongaussian distribution, so the nonlinearity of the signal is tested and the results are shown in flowing Fig. 4.15, which clearly indicates that the signal generating processes (tested beams) were nonlinear.

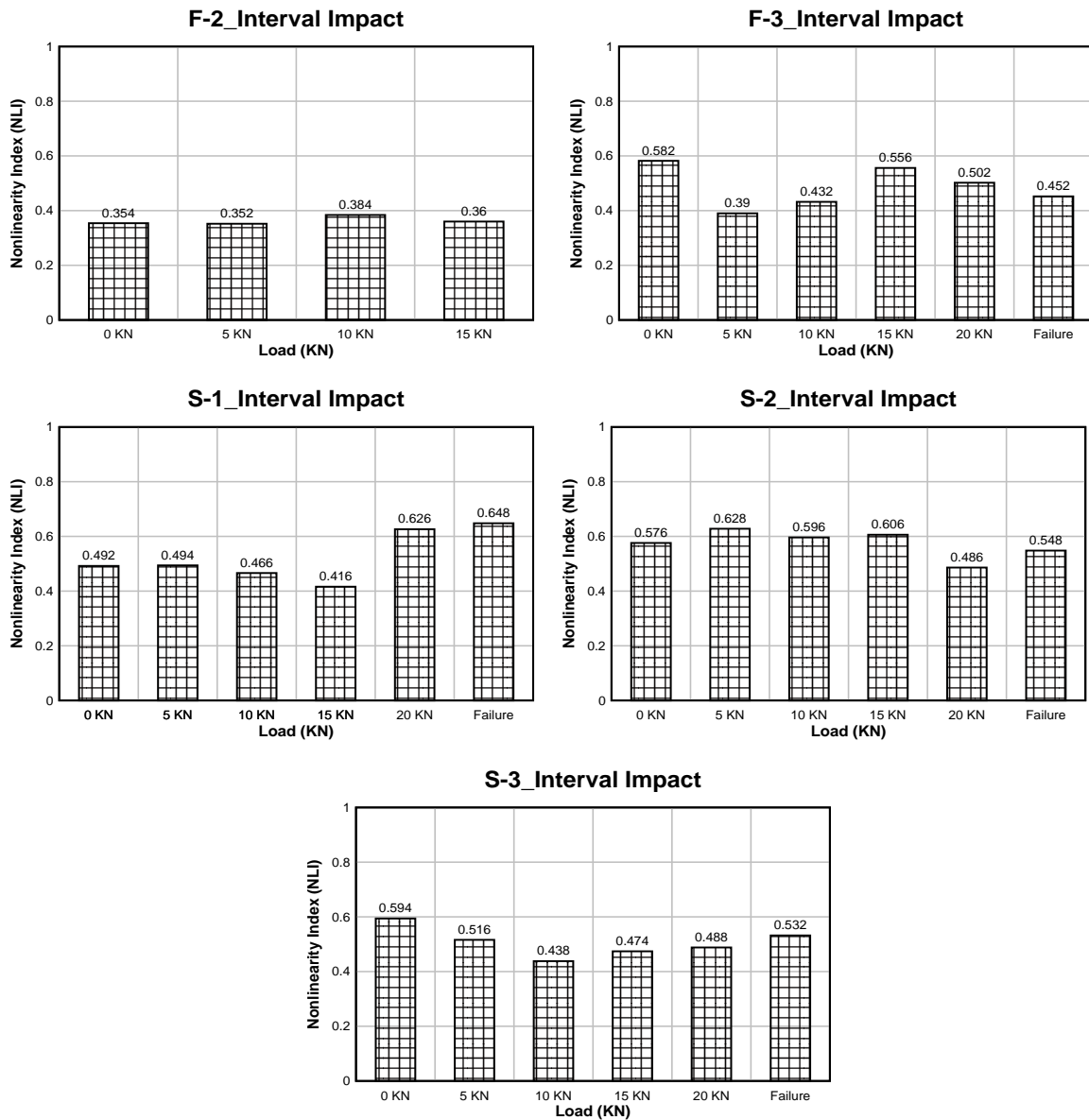


Figure 4.15: Non-Linearity Index (NLI) of Beam at Interval Impact Excitation

4.3.4 Continuous Impact Excitation

For continuous impact excitation vibration of each beam was recorded at undamaged condition as well as after removing the damaged load. During data recording time continuous impact excitations were provided in the beam by hammer throughout the data recording time. The following Fig. 4.16 shows the recording of continuous impact excitation of the flexure control beam. For other beams time series data is provided in Appendix-A.

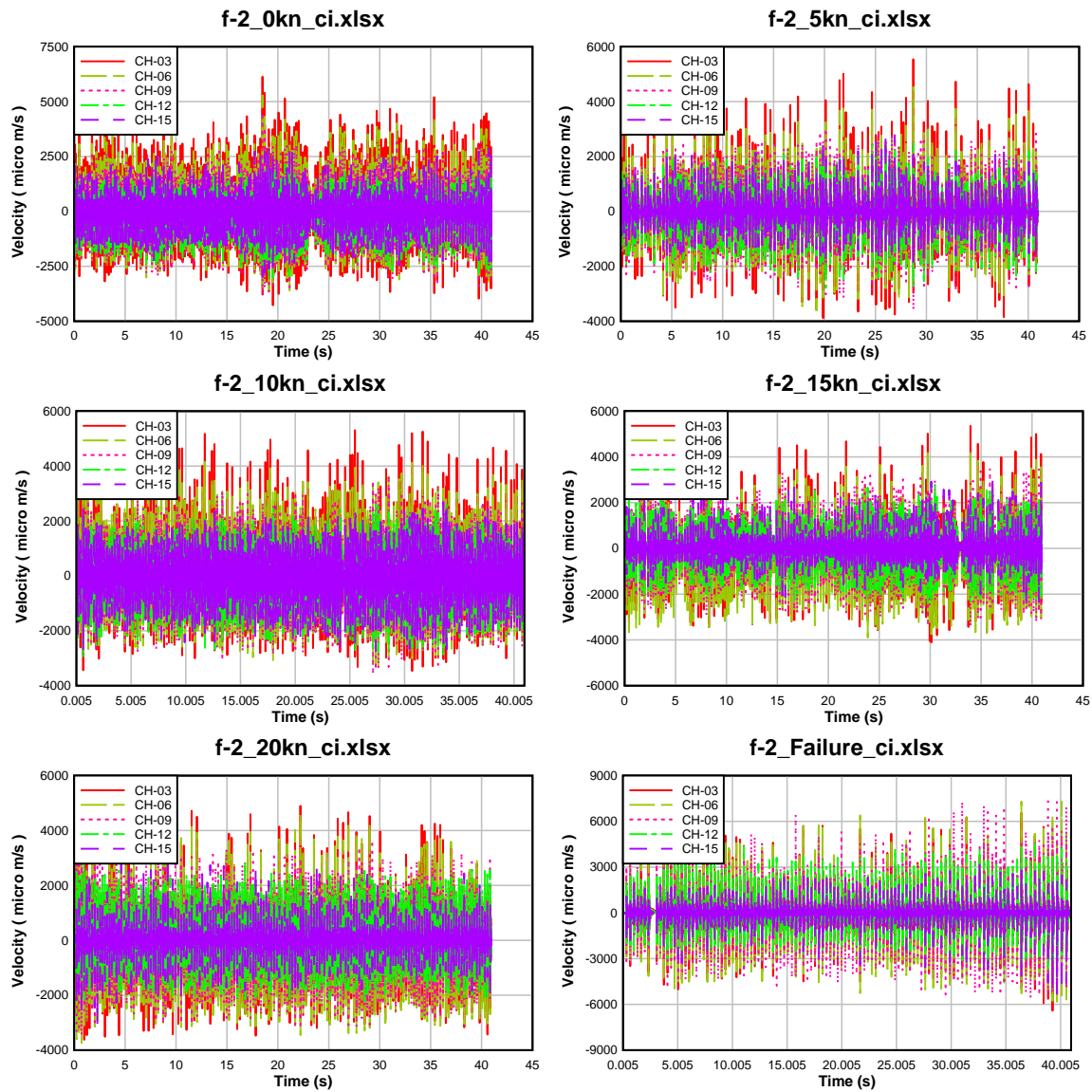


Figure 4.16: Continuous Impact Time History Recording for Flexure Control Beam-2

This time series data was used to determine the distribution of the signal. According to Choudhury et al. (2006) if $NGI \leq 0$, the signal is GAUSSIAN and if $NGI \geq 0$, the signal was NON GAUSSIAN. Fig. 4.17 shows the Gaussianity test of the signals.

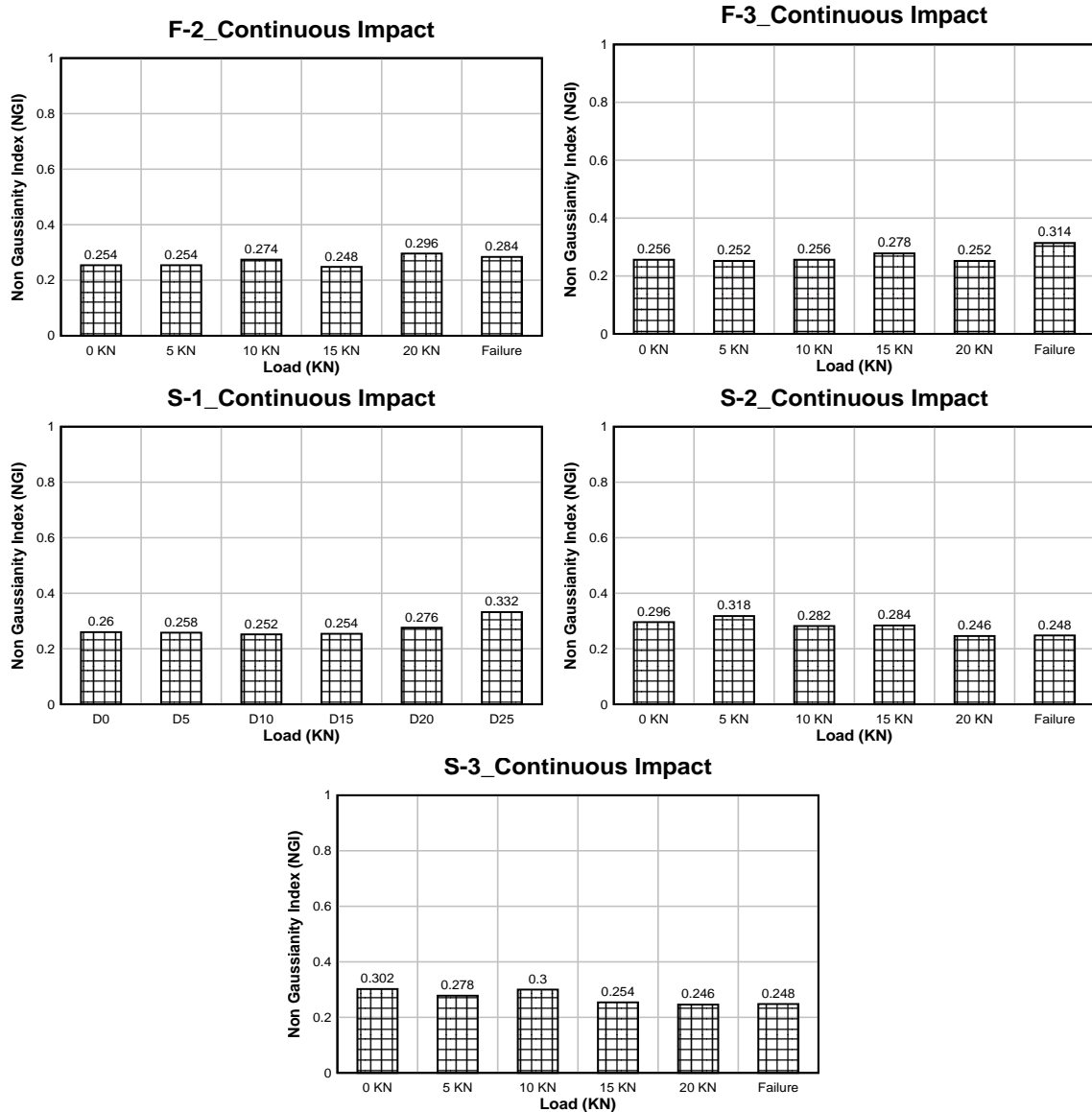


Figure 4.17: Non-Gaussianity Index (NGI) of Beam at Continuous Impact Excitation

According to Choudhury et al. (2006) in the case of a non-Gaussian signal, signal generating process should be tested for its linearity and he defined the range of index as: if $NLI \leq 0$, the signal generating process is Linear; and if $NLI > 0$, the signal generating process is nonlinear. It is clear from the above Fig. 4.17 that all the signals recorded from the beams had nongaussian distribution, so the nonlinearity of the signal is tested and the results are shown in flowing Fig. 4.18, which clearly indicates that the signal generating processes (tested beams) were nonlinear.

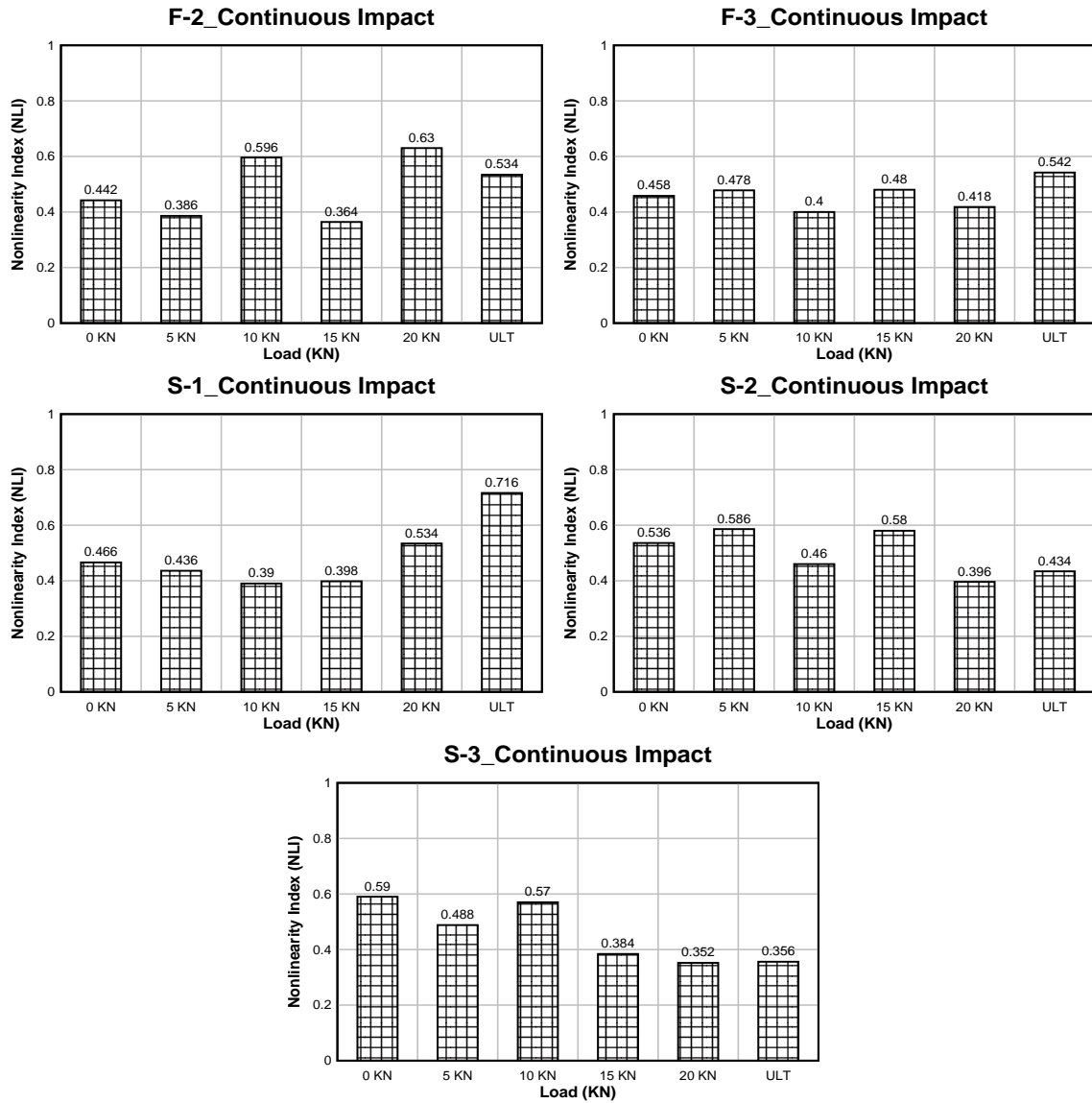


Figure 4.18: Non-Linearity Index (NLI) of Beam at Continuous Impact Excitation

4.4 Outcome of Bispectrum and Bicoherence Based Measure of Nonlinearity

From the above analysis it is clear that, though NGI indicates the non-Gaussian distribution of signals recorded from damaged and undamaged beam and following NLI also indicated the presence of nonlinearity in the concrete beams. But NLI index fails to perform as a clear and consistent indication of nonlinearity. To find a clear indication of increasing of nonlinearity with damage loading some other approach is needed.

4.5 Normalized Fourier Spectrum of Time Series Data

Time history data is not suitable to estimate the dynamic properties such as frequencies and amplitude. So, transformation of time domain data to frequency domain data is required with Fourier Transformation. Therefore, Fast Fourier transformation (FFT) has been used to transfer time domain data to frequency domain data

4.6 Normalized FFT and Area under the Curve: Ambient Excitation

First time series data of undamaged beam as well as damaged beams were converted to frequency domain data and plotted against frequency. Only ch03, 06,09,12,15 were used for analysis. As these channel data represents the vertical vibration. Then predominant frequency of each beam was determined. The damaged beam FFT plot was normalized with respect to predominant frequency of undamaged beam. The following Fig. 4.19 to 4.25 shows the normalized FFT plot of flexure and shear beam.

4.6.1 Flexure Control Beam

The following Table 4.1 shows various damage levels at various applied load for Flexure Beam-2 (FB-2).

Table 4.1: Various Damage Levels of FB-2

Beam Designation	Damage Level	Max Load (kN)	Max Deflection (mm)	Observed Damage
FB-2	UD	0	0	No Visible Crack
	D1	5	.95	Three small cracks appeared. One in between sensor- 2 and 3 (ch06 and ch09) . Other two is between sensor-3 and 4(ch09 and ch12)
	D2	10	3	Three new cracks appeared in between sensor - 2 and 3 (ch06 and ch09) . All other cracks propagated in length and width.

	D3	15	5.45	Several Cracks between Sensor- 2 & 3 (ch06 and ch09) . All other cracks propagated in length and width. Cracks prevailed all through the beam.
	D4	20	8.15	Two new cracks appeared at mid span of beam below sensor- 3 (ch 09) . All other cracks propagated in length and width.
	D5 / Failure	22.8	12	No new cracks were appeared only previous cracks were propagated. beam was not taking any further load as deflection was increasing without increasing load reading therefore in Failure condition

The following Fig. 4.19 shows the normalized FFT of flexure control beam-2 (FB-2) at ambient excitation at various damage levels. At UD (0kN) level there was no visible damage in the beam. The predominant frequency of undamaged beam was found to be 27.07 Hz. All the frequencies of damage level D1 to D5 were normalized with respect to this predominant frequency level.

At damage level D1 there were two small cracks between sensor-2&3 (ch06 and ch09) another two were between sensor-3 & 4 (ch09 and ch12). From the normalized FFT plot it is clear that there is a jump in ch6, 9, and 12.

At damage level D2 (10kN) some new cracks appeared between sensor-2 and 3 (ch06 and ch09) and there were jump in FFT plot of ch06 and ch09. Both of their increases were overwhelmed by ch12. As there were two previous crack in between sensor-3&4 (ch09 and ch12) and both of them propagated towards sensor-4 (ch12).

At damage level D3 (15kN) several cracks appeared between sensor- 2&3 (ch06 and ch09) there were no definite pattern in the normalized FFT plot. There was a sudden jump in sensor- 1 (ch03). Maximum damage occurred in this level as theoretical capacity of the beam was 140 N-m at single point loading of 13.24 kN.

At damage level D4 two new cracks appeared below sensor-3 (ch09) and from FFT plot it was clear that there is a jump in the ch09 plot. It was also observed that all other channels also showed jump in FFT plot. It was mainly because there were cracks prevailed all through the beam.

At damage level D5 (Failure) no new cracks appeared only previous cracks propagated in length and width. And FFT plot shows jump in all channels as cracks were increasing with

applied load. The beam was not taking any load which was clear from load-displacement curve in the Universal Testing machine (UTM) as displacement of the load cell was increasing without increasing load reading and thus indicated the failure stage of the beam. It is also clear from load-deflection curve of the beam that FB-2 was not taking any load after 22.8 kN.

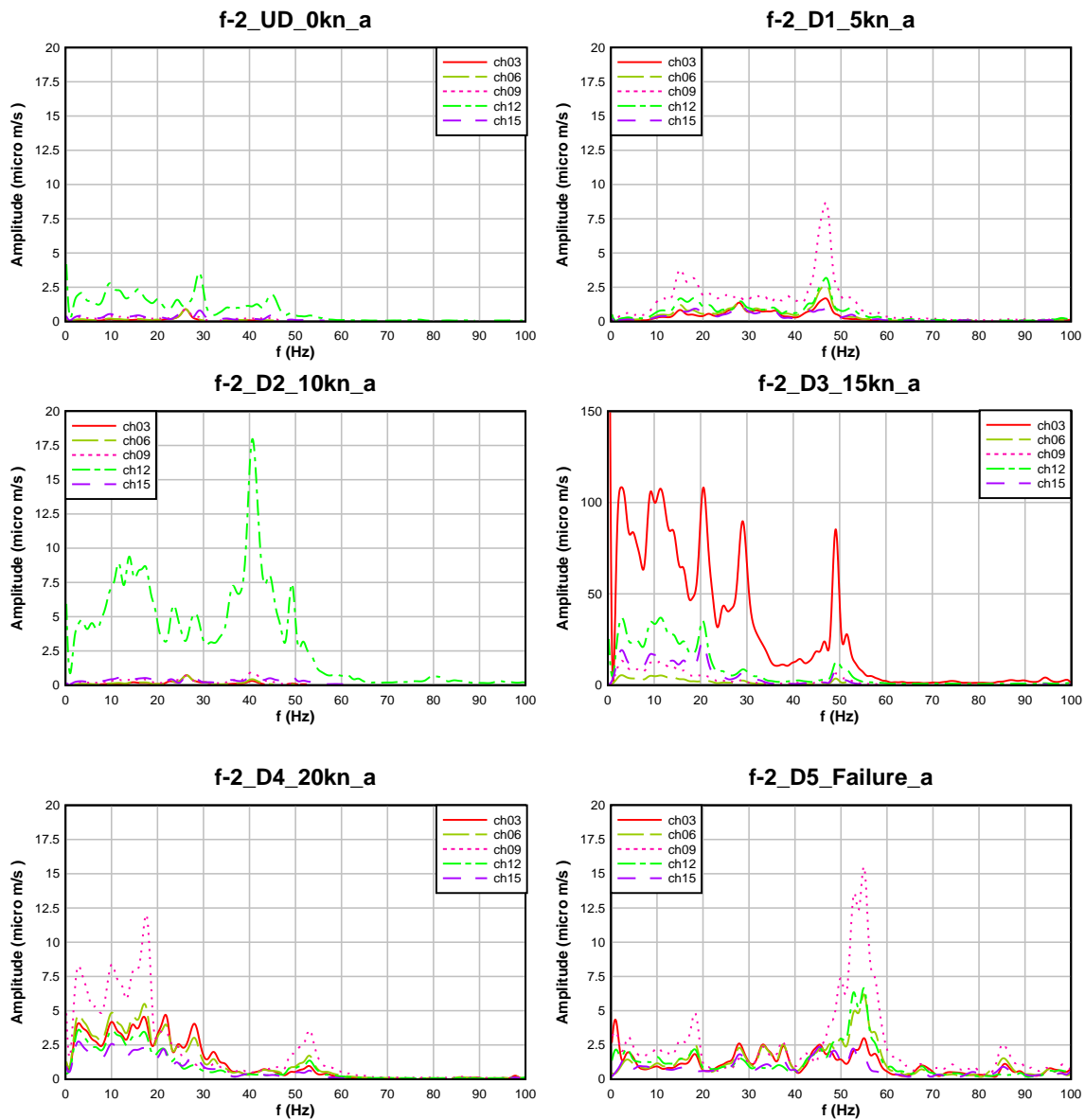


Figure 4.19: Normalized FFT Curve of Flexure Control Beam-2 (FB-2)

The following Table 4.2 shows various damage levels at various applied load for Flexure Beam-3 (FB-3).

Table 4.2: Various Damage Levels of FB-3

Beam Designation	Damage Level	Max Load (kN)	Max Deflection (mm)	Observed Damage
FB-3	UD	0	0	No Visible Crack
	D1	5	1.15	Three small cracks. One below sensor - 3 (ch 09) and two others between sensor 3 and 4 (ch09 and ch12) near to sensor-4 (ch12)
	D2	10	3.25	Four new cracks appeared. Two between sensor 2 and 3 (ch06 and ch09) and two between sensor 4 and 5 (ch12 and ch15) . All previous cracks propagated.
	D3	15	5.3	One new cracks appeared below sensor-2 (ch06) . Two previous cracks from D2 prevailed in sensor 4 and 5 (ch12 and ch15) were propagated more than the new one.
	D4	20	7.85	Three new cracks appeared between sensor- 2 and 3 (ch 03 and ch06) . All other crack increased in length and width than the newly appeared cracks.
	D5 / Failure	23.65	11	No new cracks were appeared only previous cracks were propagated. beam was not taking any further load as deflection was increasing without increasing load reading therefore in Failure condition

The following Fig. 4.20 shows the normalized FFT of flexure control beam-3 (FB-3) at ambient excitation at various damage levels. At UD (0kN) level there was no visible damage in the beam. The predominant frequency of undamaged beam was found to be 25.31 Hz. All the frequencies of damage level D1 to D5 were normalized with respect to this predominant frequency level.

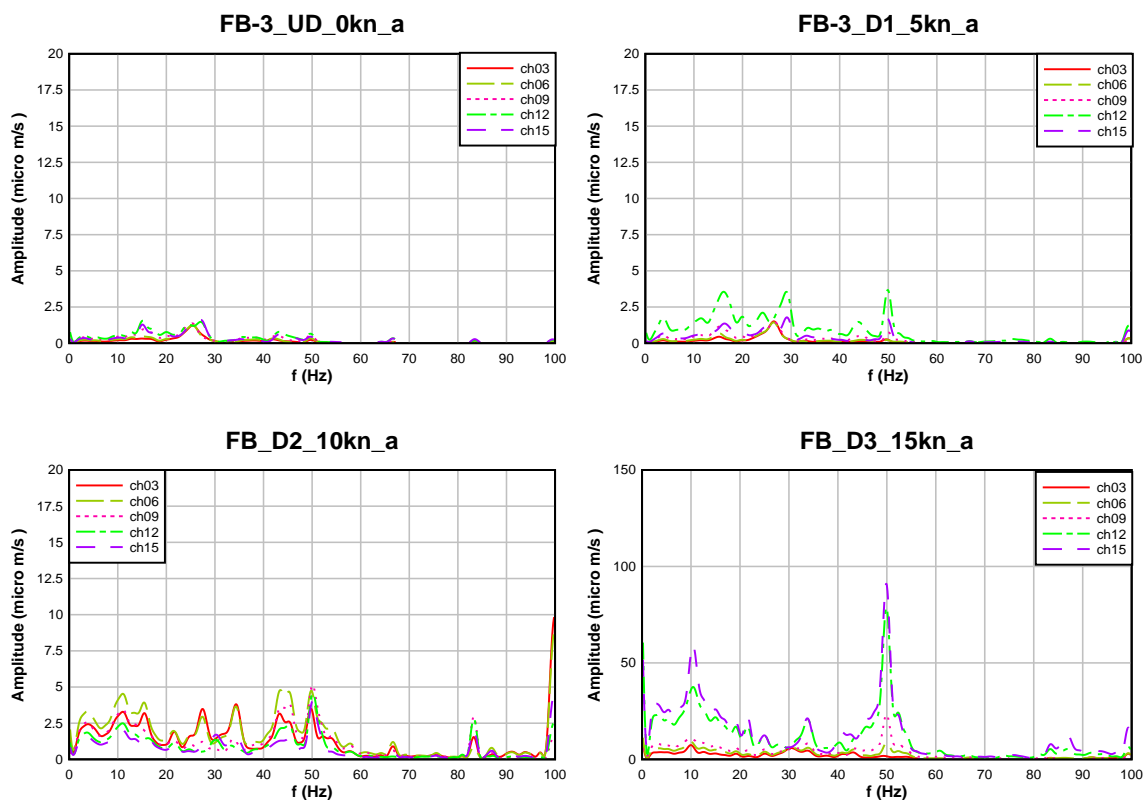
At damage level D1 there were three cracks one below sensor-3 (ch09) and two others between sensor- 3 and 4 (ch09 and ch12) near to sensor-4 (ch12). In FFT curve there was a jump in sensor-4 (ch12).

At damage level D2 (10kN) four new cracks appeared two between sensor-2 and 3 (ch06 and ch09) and two between sensor-4 and 5 (ch12 and ch15). In FFT curve there was a jump in ch03 and ch09. Most of the cracks were near sensor-3 and sensor-4 (ch09 and ch12).

At damage level D3 (15kN) one new crack appeared below sensor-2 (ch06). Two of the previous cracks from damage level D2, between sensor-4 and 5 (ch12 and ch15) were more propagated than the new crack. There was a slight jump in sensor-2 (ch06) of FFT plot but it was overwhelmed by the jump of ch12 and ch15. Maximum damage occurred in this level as theoretical moment capacity of the beam was 140 N-m at single point loading of 13.24 kN.

At damage level D4 (20kN) three new cracks appeared between sensor-2 and 3 (ch06 and ch09) all previous cracks increased in length and width than the newly appeared cracks and in FFT plot we observe a jump in sensor- 3, 4, 5 (ch09, 12, 15) more than the other channels.

At damage level D5 (Failure) no new cracks appeared only previous cracks propagated in length and width. And FFT plot shows jump in all channels as cracks were increasing with applied load but the jump is lower than the previous damage level. The beam was not taking any load which was clear from load-displacement curve in the Universal Testing machine (UTM) as displacement of the load cell was increasing without increasing load reading and thus indicated the failure stage of the beam. It is also clear from load-deflection curve of the beam that FB-3 was not taking any load after 23.65 kN.



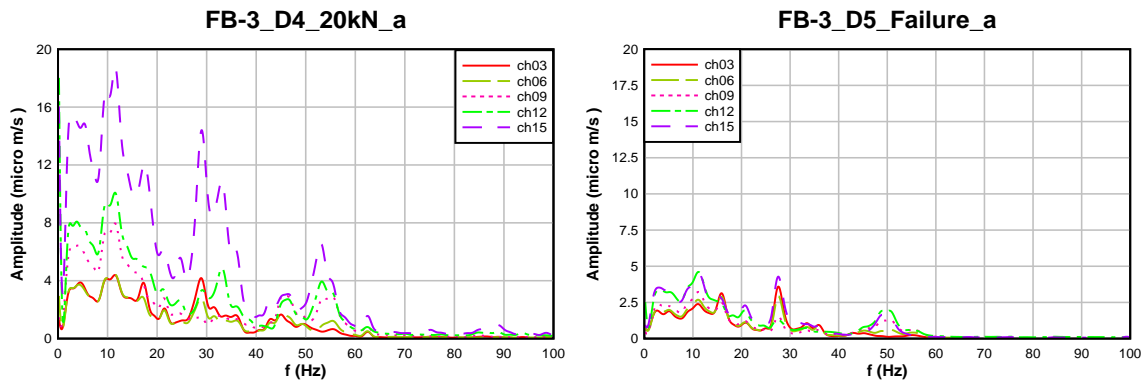


Figure 4.20: Normalized FFT Curve of Flexure Control Beam-3 (FB-3)

The following Fig. 4.21 shows the average area under the FFT curve, normalized with respect to undamaged state UD (0kN). For both of the flexure beams it is clear that there is a gradual increase in FFT area up to theoretical load capacity of the beam. And there is a gradual decrease in FFT area after the maximum theoretical load capacity. It is also clear from the Fig. 4.21 that FFT area is maximum when the beam works at its maximum capacity level and at failure stage RC flexure control beams does not disintegrate suddenly.

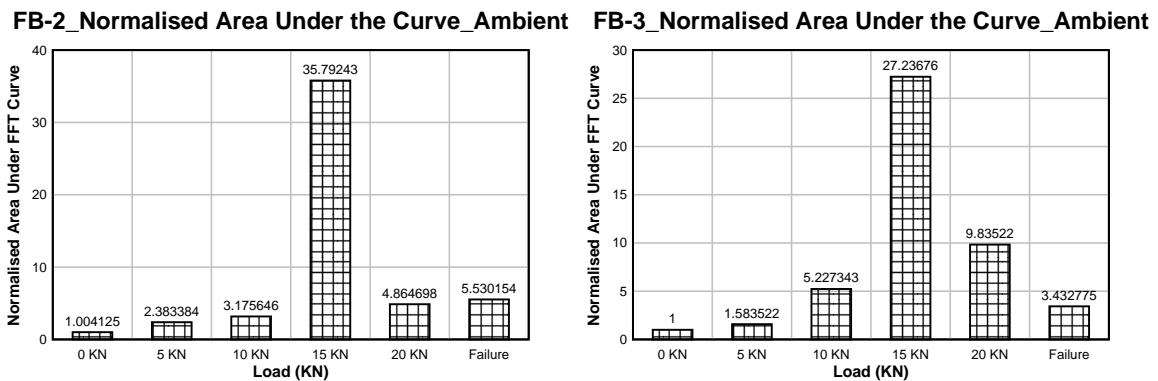


Figure 4.21: Area under the FFT Curve of Flexure Control Beam at Ambient Excitation

4.6.2 Shear Control Beam

The following Table 4.3 shows various damage levels at various applied load for Shear Control Beam-1 (SB-1).

Table 4.3: Various Damage Levels of SB-1

Beam Designation	Damage Level	Max Load (kN)	Max Deflection (mm)	Observed Damage
SB-1	UD	0	0	No Visible Crack
	D1	5	1	No Visible Crack
	D2	10	2.25	Multiple small crack at mid span. Below Sensor-3 (ch09) .
	D3	15	4.25	Multiple cracks appeared at mid span of the beam. Previous cracks were more propagated and increased in width. All the cracks were below sensor 2,3,4 . No crack below sensor 1
	D4	20	6.7	Previous all cracks propagated specially from damage level D3 . Two new cracks appeared. One was between sensor 1 & 2 and another one was between sensor 4 & 5
	D5 / Failure	22	8.5	Two new cracks appeared below sensor 2 . beam was not taking any further load as deflection was increasing without increasing load reading therefore in Failure condition

The following Fig. 4.22 shows the normalized FFT of Shear control beam-1 (SB-1) at ambient excitation at various damage levels.

At UD (0kN) level there was no visible damage in the beam. The predominant frequency of undamaged beam was found to be 47.31 Hz. All the frequencies of damage level D1 to D5 were normalized with respect to this predominant frequency level.

At damage level D1 (0kN) there were no visible crack in the beam and we could not find any significant jump in FFT plot of the channels.

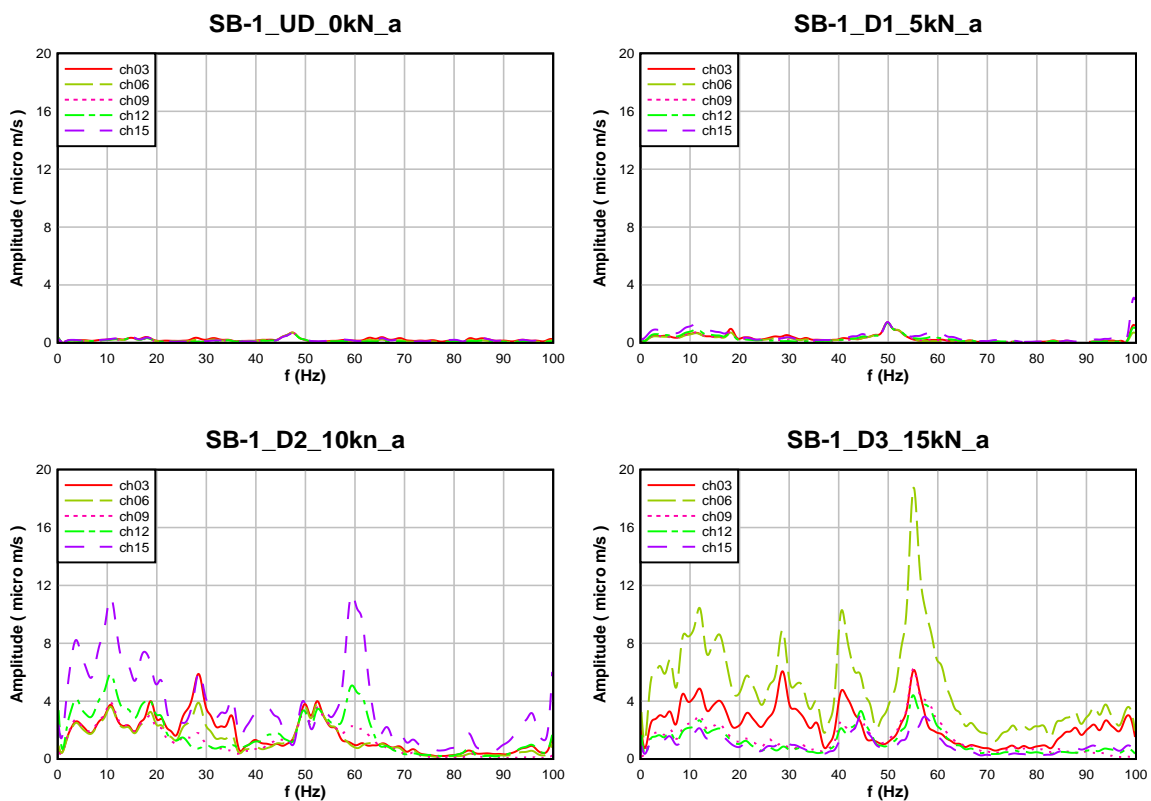
At damage level D2 (10kN) multiple small cracks appeared below Sensor-3 (ch09) at mid span of the beam. In FFT plot we found that there was highest level of jump in sensor -5 (ch15) followed by sensor- 4 and 3 (channel 12 and 09).

At damage level D3 (15kN) multiple cracks appeared at mid span of beam below sensor- 2, 3, 4 (ch06, 09, 12). From FFT plot it is clear that sensor-2 (ch06) showed highest level of peak

followed by sensor-3 (ch09) and sensor-4(ch12). Maximum damage occurred in this level as theoretical capacity of the beam was 209 N-m at single point loading and shear capacity of the beam was 15kN.

At damage level D4 (20kN) all cracks from previous damage level propagated in length and width and two new cracks appeared. One below sensor 1&2 (ch03 and ch06) and another one below sensor 4&5 (ch12 and ch15). From FFT plot we found that highest level of jump was in sensor-5 (ch12) followed by senso-3 (ch09). Both of them had peak lower than the previous damage level.

At damage level D5 (Failure) two new cracks appeared below sensor-2 (ch06). In FFT plot all the channels showed same level of jump there was no distinguished difference between them. In this stage the beam was not taking any load which was clear from load-displacement curve in the Universal Testing machine (UTM) as displacement of the load cell was increasing without increasing load reading and thus indicated the failure stage of the beam. It is also clear from load-deflection curve of the beam that SB-2 was not taking any load after 22 kN.



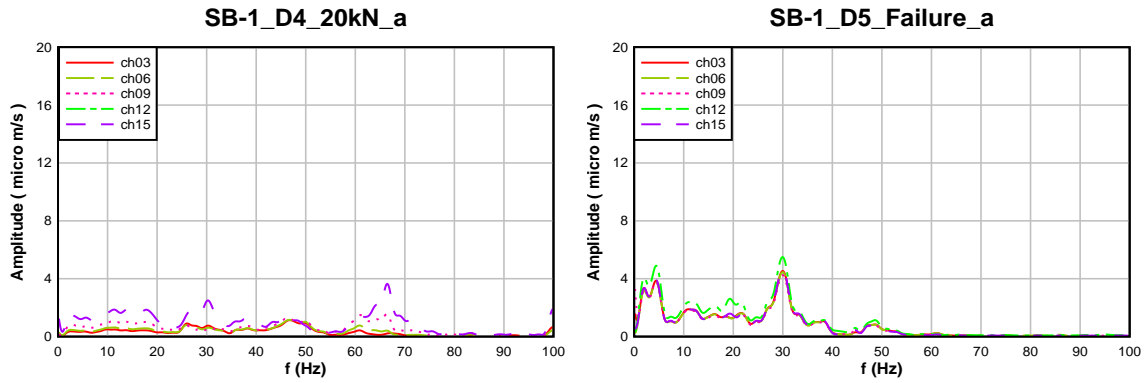


Figure 4.22: Normalized FFT Curve of Shear Control Beam-1 (SB-1) at Ambient Excitation

The following Table 4.4 shows various damage levels at various applied load for Shear Beam-2 (SB-2).

Table 4.4: Various Damage Levels of SB-2

Beam Designation	Damage Level	Max Load (kN)	Max Deflection (mm)	Observed Damage
SB-2	UD	0	0	No Visible Crack
	D1	5	1.35	No Visible Crack
	D2	10	3.8	Multiple small cracks appeared at various locations of beam. Below Sensor- 2 (ch06) & 3 (ch09)
	D3	15	6.6	All previous cracks were propagated. Two new cracks appeared below sensor- 3 (ch09)
	D4	20	10.5	All previous cracks were propagated. Two new cracks were identified directly below sensor -2 & 4 (ch06 and ch12). some more cracks were between sensor 2, 3,4 (ch06, ch09, ch12)
	D5 / Failure	21.5	11.5	No new cracks were appeared only previous cracks were propagated. beam was not taking any further load as deflection was increasing without increasing load reading therefore in Failure condition

The following Fig. 4.23 shows the normalized FFT of Shear Control Beam-2 (SB-2) at ambient excitation at various damage levels.

At UD (0kN) level there was no visible damage in the beam. The predominant frequency of undamaged beam was found to be 25.12 Hz. All the frequencies of damage level D1 to D5 were normalized with respect to this predominant frequency level.

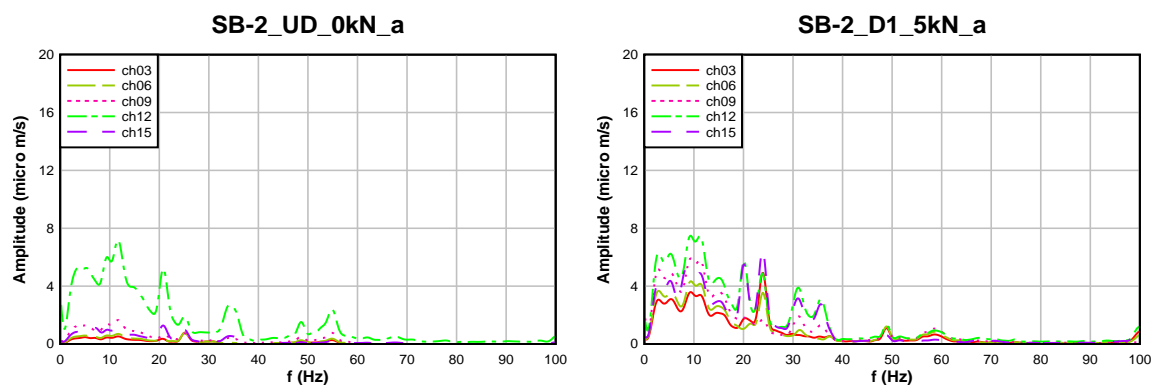
At damage level D1 (5kN) there were no visible crack in the beam and there were jump in all of the channels in FFT plot.

At damage level D2 (10kN) multiple small cracks appeared below Sensor-2 & 3(ch06 & 09) at mid span of the beam. In FFT plot we found that there was highest level of jump in sensor-3 (ch09) followed by sensor-2 (ch06).

At damage level D3 (15kN) two new cracks appeared below sensor-3 (ch09) at mid span of the beam. All previous cracks were propagated in length and width. From FFT plot it is clear that sensor -2 & 3 (ch06 & ch09) had the highest level of jump followed by sensor-1 (ch03). Maximum damage occurred in this level as theoretical capacity of the beam was 209 N-m at single point loading and shear capacity of the beam was 15kN.

At damage level D4 (20kN) two new cracks were identified below sensor-2&4 (ch06 & ch12). There were more cracks between sensor-2, 3, and 4(ch06, 09, 12). From FFT plot we found that highest jump was given by sensor-2, 3 (ch06, 09).

At damage level D5 (Failure) no new cracks appeared only previous cracks were propagated. In FFT plot all the channels showed same level of jump, no distinguished peak was observed. In this stage the beam was not taking any load which was clear from load-displacement curve in the Universal Testing machine (UTM) as displacement of the load cell was increasing without increasing load reading and thus indicated the failure stage of the beam. It is also clear from load-deflection curve of the beam that SB-2 was not taking any load after 21.5kN.



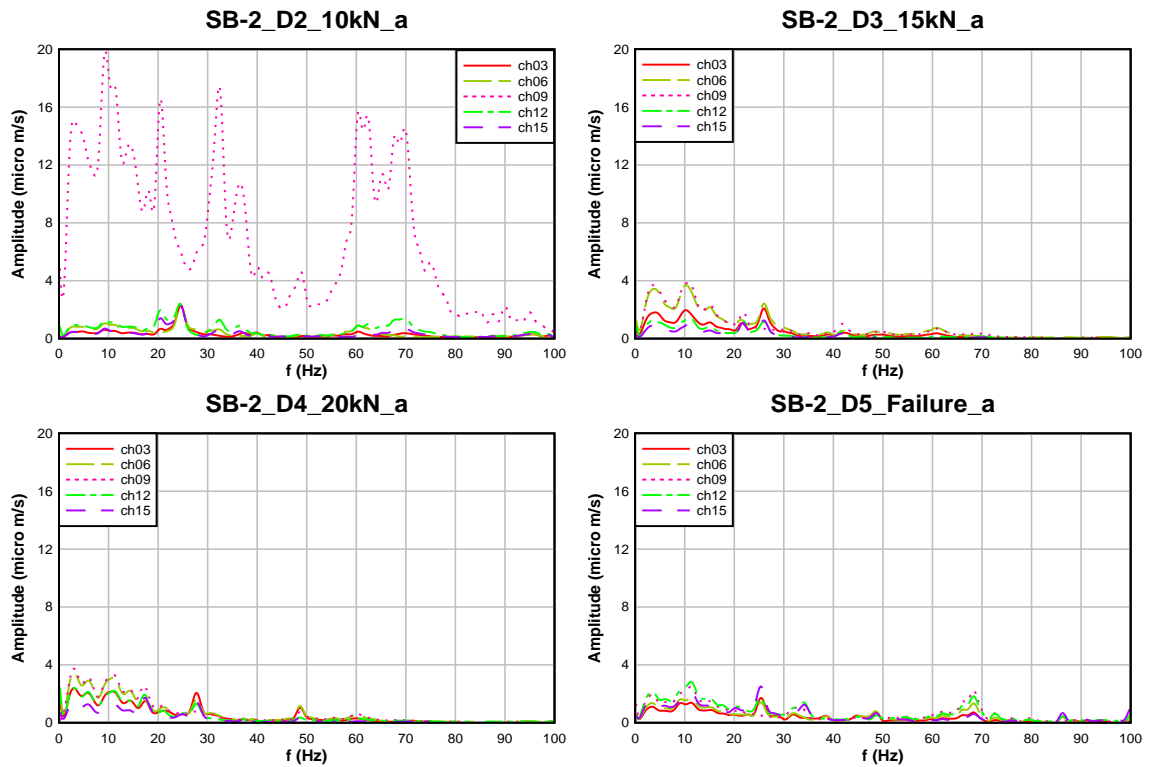


Figure 4.23: Normalized FFT Curve of Shear Control Beam-2 (SB-2)

The following Table 4.5 shows various damage levels at various applied load for Shear Beam-3 (SB-3).

Table 4.5: Various Damage Levels of SB-3

Beam Designation	Damage Level	Max Load (kN)	Max Deflection (mm)	Observed Damage
SB-3	UD	0	0	No Visible Crack
	D1	5	.85	One crack appeared below sensor-3 (ch09)
	D2	10	2.75	Multiple cracks appeared between the mid span of the beam. All of the cracks were between sensor-2, 3 & 4 (ch06, 09, 12) .

	D3	15	5	Only one new crack appeared below sensor-2 (ch06) . All the previous cracks were propagated.
	D4	20	7.5	Three new cracks appeared besides near sensor-3 (ch09) . All other cracks were propagated
	D5 / Failure	24.2	12	No new cracks were appeared only previous cracks were propagated. beam was not taking any further load as deflection was increasing without increasing load reading therefore in Failure condition

The following Fig. 4.24 shows the normalized FFT of Shear Control Beam-3 (SB-3) at ambient excitation at various damage levels.

At UD (0kN) level there was no visible damage in the beam. The predominant frequency of undamaged beam was found to be 29.27 Hz. All the frequencies of damage level D1 to D5 were normalized with respect to this predominant frequency level.

At damage level D1 (5kN) there was only one crack appeared below sensor-3 (ch09). In FFT plot we found that highest level of jump was found for Sensor-3(ch09).

At damage level D2 (10kN) multiple cracks appeared between the mid span of the beam. All of the cracks were between sensor-2, 3 &4 (ch06, 09, 12). In FFT plot highest level of jump was shown by sensor-3(ch09) followed by sensor-2, 4(ch06 & ch12).

At damage level D3 (15kN) only one new crack appeared below sensor-2 (ch06), all other cracks from previous damage level were propagated. From FFT plot we found that sensor-2 (ch06) showed the highest level of jump followed by ch09 & 03. Maximum damage occurred in this level as theoretical capacity of the beam was 209 N-m at single point loading and shear capacity of the beam was 15kN.

At damage level D4 (20kN) three new cracks appeared besides sensor-2 (ch06). In FFT plot we found that highest peak was achieved by sensor-3 & 4 (ch09, 12).

At damage level D5 (Failure) no new cracks appeared only previous cracks were propagated. In FFT plot sensor-4(ch12) showed highest level of jump, but peak was lower than previous damage level. All other channels showed same level of jump without any distinguished peak value. In this stage the beam was not taking any load which was clear from load-displacement curve in the Universal Testing machine (UTM) as displacement of the load cell was increasing without increasing load reading and thus indicated the failure stage of the beam. It

is also clear from load-deflection curve of the beam that SB-3 was not taking any load after 24.2 kN.

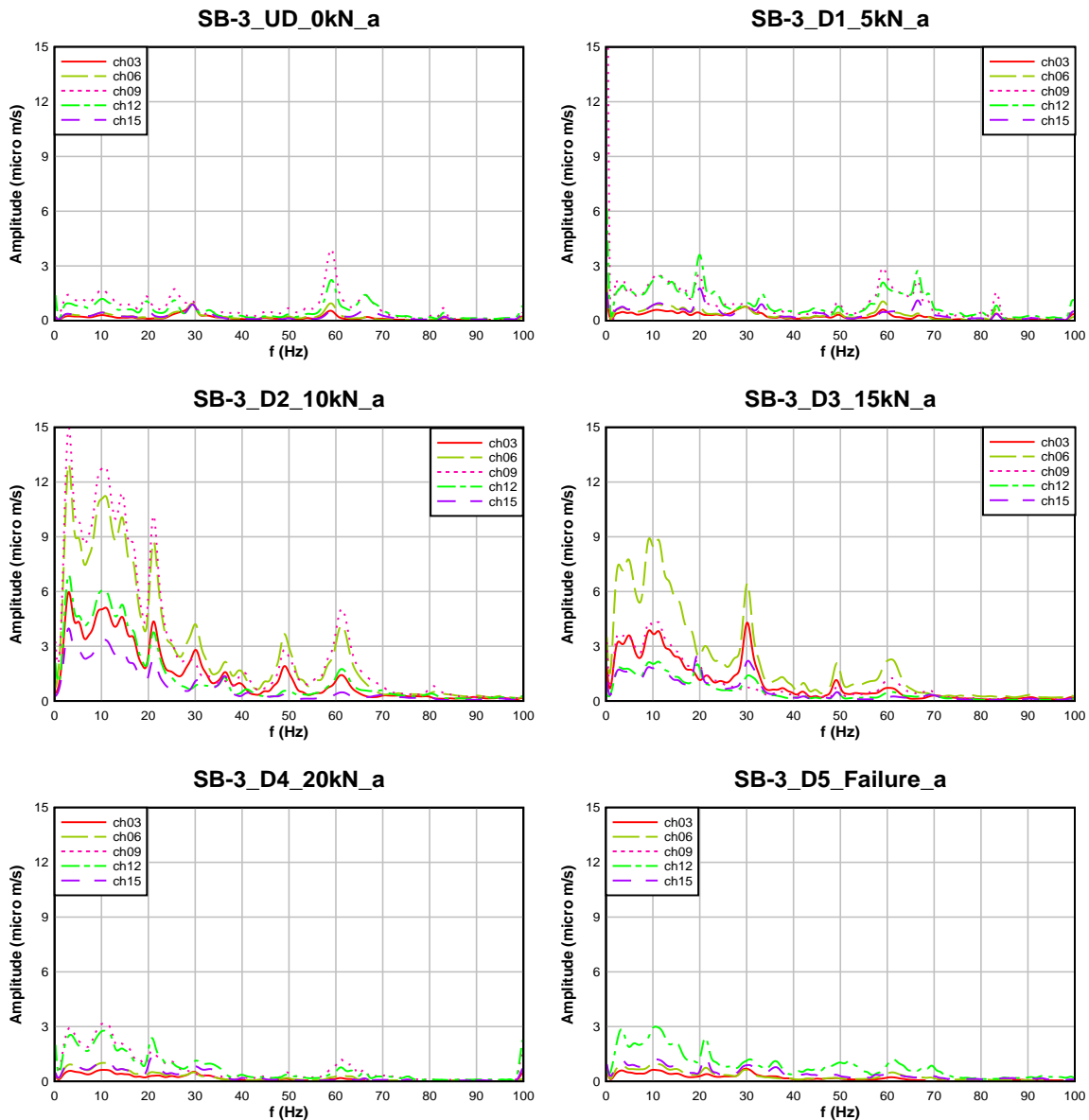


Figure 4.24: Normalized FFT Curve of Shear Control Beam-3 (SB-3)

The following Fig. 4.25 shows the average area under the FFT curve, and they were normalized with respect to undamaged state UD (0kN) state. From the figure it is clear that there is a no definite pattern in increasing the area under FFT curve. For SB-1 highest area was achieved at damage level D3 (15kN) but for SB-2 & 3 showed highest area for damage level D2 (10kN). For higher damage level SB-1&2 showed no definite pattern in decreasing areas. Only SB-3 showed a definite pattern in decreasing areas. It is also clear that a for shear control beams failure occurred in a random way after achieving the maximum load.

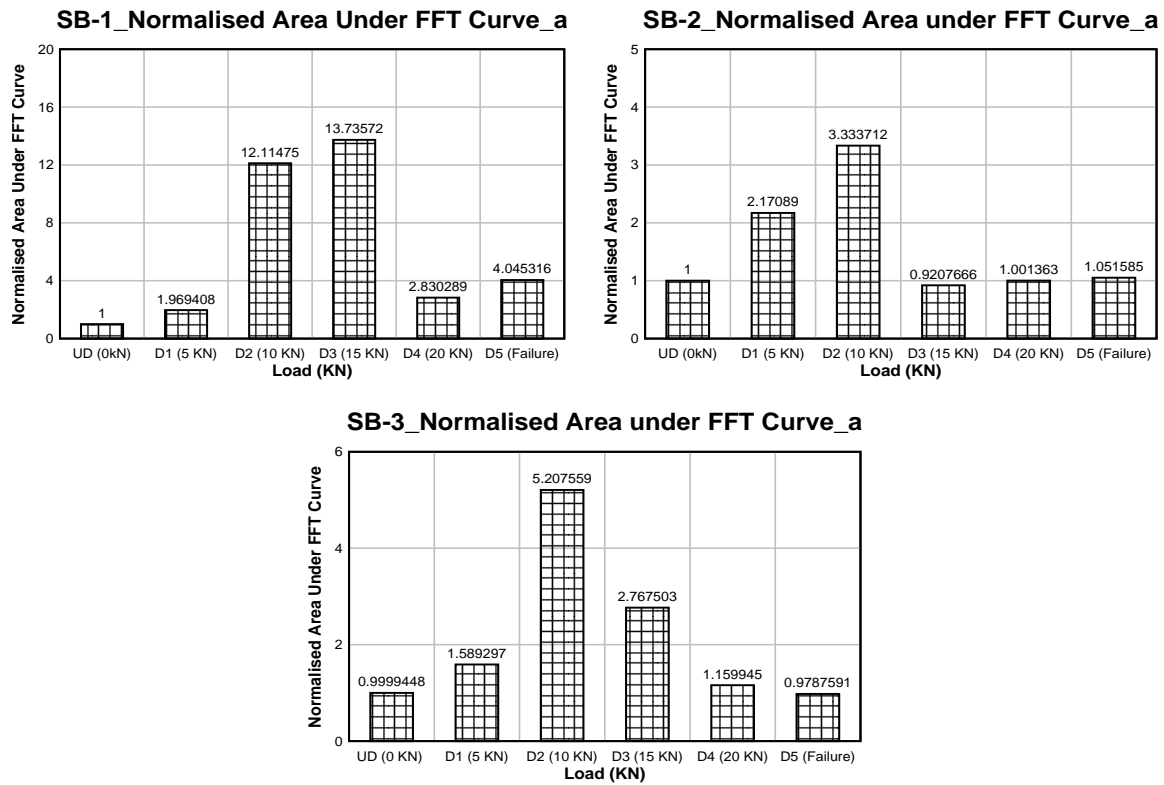


Figure 4.25: Area under the FFT Curve of Shear Control Beam at Ambient Excitation

4.7 Normalized FFT and Area under the Curve: One Impact Excitation

First time series data of undamaged beam as well as damaged beams were converted to frequency domain data and plotted against frequency. Only ch03, 06, 09, 12, 15 were used for analysis. As these channel data represents the vertical vibration. Then predominant frequency of each beam was determined. The damaged beam FFT plot was normalized with respect to predominant frequency of undamaged beam. The following Fig. 4.26 to 4.32 shows the normalized FFT plot of flexure and shear beam.

4.7.1 Flexure Control Beam

The following Fig. 4.25 shows the normalized FFT of flexure control beam-2 (FB-2) at one impact excitation at various damage levels, described previously in Table 4.1. At UD (0kN) level there was no visible damage in the beam. The predominant frequency of undamaged beam was found to be 40.84 Hz. All the frequencies of damage level D1 to D5 were normalized with respect to this predominant frequency level.

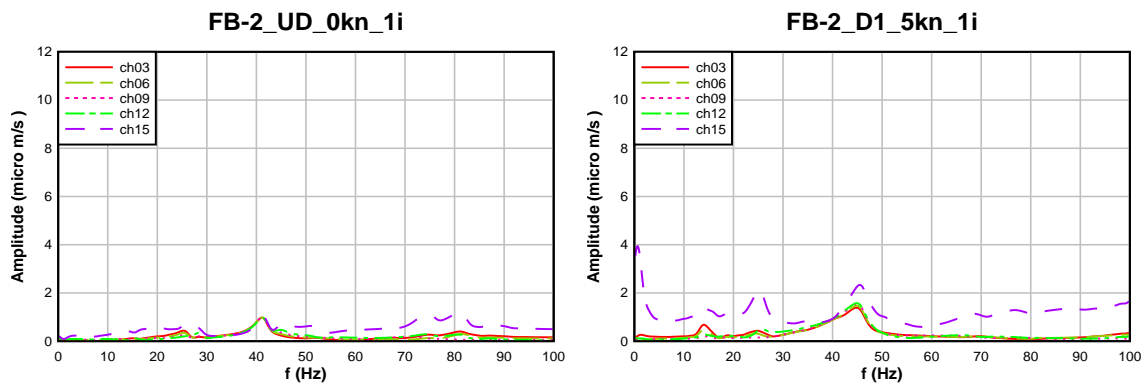
At damage level D1 there were two small cracks between sensor-2&3 (ch06 and ch09) another two were between sensor-3 & 4 (ch09 and ch12). From the normalized FFT plot it is clear that there were jump in all of the channels of FFT plot.

At damage level D2 (10kN) some new cracks appeared between sensor-2 and 3 (ch06 and ch09) and there were jump in FFT plot of all the channels. Ch03 has the highest jump.

At damage level D3 (15kN) several cracks appeared between sensor- 2&3 (ch06 and ch09) there were no definite pattern in the normalized FFT plot. Highest jump was occurred in Sensor-5 (ch15) and no definite pattern was observed in other channel plot. Maximum damage occurred in this level as theoretical capacity of the beam was 140 N-m at single point loading of 13.24 kN.

At damage level D4 two new cracks appeared below sensor-3 (ch09) and from FFT plot it was clear that there was no distinguished jump in channel plots rather all the channels showed a jump in a single point.

At damage level D5 (Failure) no new cracks appeared only previous cracks propagated in length and width. And FFT plot shows jump in all channels as cracks were increasing with applied load. The beam was not taking any load which was clear from load-displacement curve in the Universal Testing machine (UTM) as displacement of the load cell was increasing without increasing load reading and thus indicated the failure stage of the beam. It is also clear from load-deflection curve of the beam that FB-2 was not taking any load after 22.8 kN.



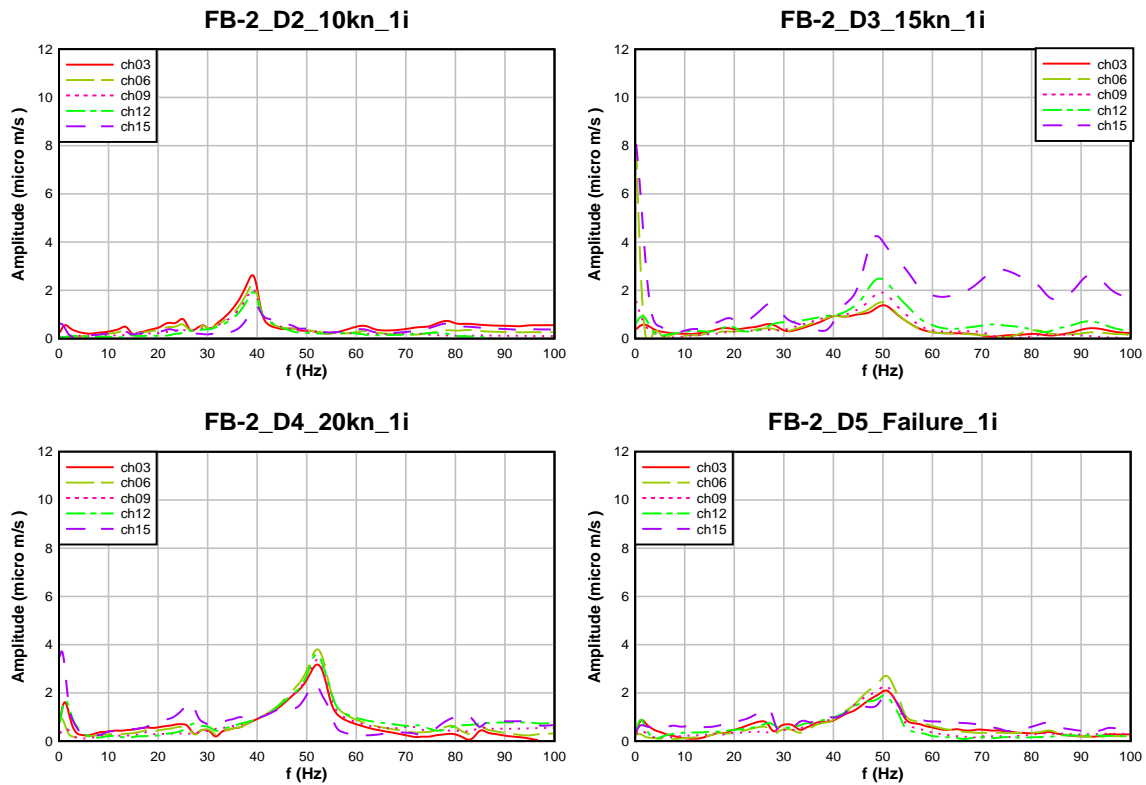


Figure 4.26: Normalized FFT Curve of Flexure Control Beam-2 (FB-2)

The following Fig. 4.27 shows the normalized FFT of flexure control beam-3 (FB-3) at one impact excitation at various damage levels. At UD (0kN) level there was no visible damage in the beam. The predominant frequency of undamaged beam was found to be 40.01 Hz. All the frequencies of damage level D1 to D5 were normalized with respect to this predominant frequency level.

At damage level D1 there were two small cracks between sensor-2&3 (ch06 and ch09) another two were between sensor-3 & 4 (ch09 and ch12). From the normalized FFT plot it is clear that there were jump in channels 6, 9, 12 of the FFT plot.

At damage level D2 (10kN) some new cracks appeared between sensor-2 and 3 (ch06 and ch09) and there were jump in FFT plot of channels ch06 and ch09.

At damage level D3 (15kN) several cracks appeared between sensor- 2&3 (ch06 and ch09). Highest jump was occurred in Sensor-2 (ch06) followed by sensor-3 (ch09). Other channels also showed some peaks. Maximum damage occurred in this level as theoretical capacity of the beam was 140 N-m at single point loading of 13.24 kN.

At damage level D4 two new cracks appeared below sensor-3 (ch09) and from FFT plot we found that sensor-3 and 4 (ch09 and ch12) showed a clear pick.

At damage level D5 (Failure) no new cracks appeared only previous cracks propagated in length and width. And FFT plot shows jump in all channels as cracks were increasing with applied load. The beam was not taking any load which was clear from load-displacement curve in the Universal Testing machine (UTM) as displacement of the load cell was increasing without increasing load reading and thus indicated the failure stage of the beam. It is also clear from load-deflection curve of the beam that FB-2 was not taking any load after 23.65 kN.

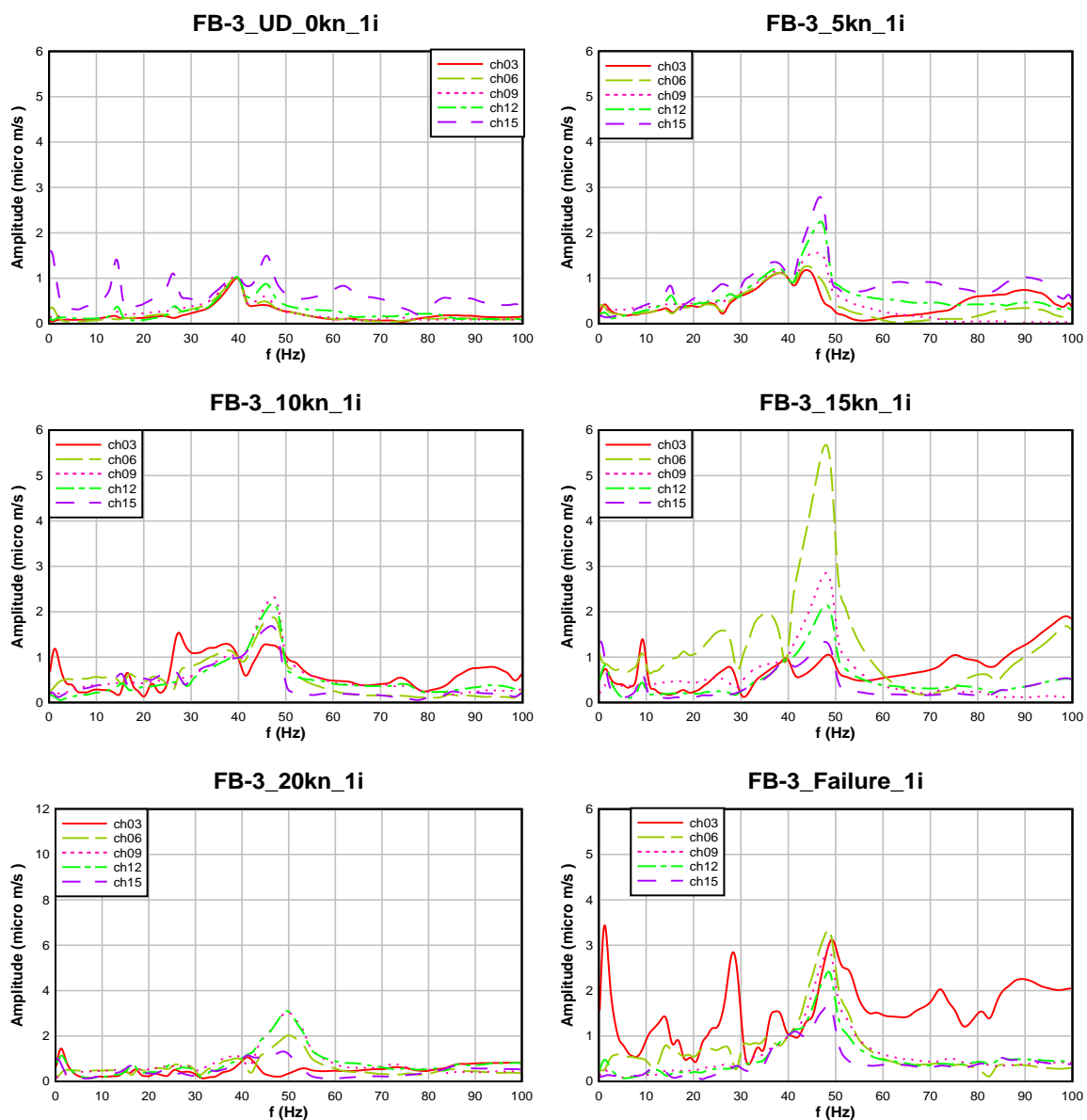


Figure 4.27: Normalized FFT Curve of Flexure Control Beam-3 (FB-3)

The following Fig. 4.28 shows the average area under the FFT curve normalized with respect to undamaged state UD (0kN). For both of the beams it is clear that there is no definite pattern in changing of FFT area. For FB-2 we found that at maximum damage level (D3) the area was three times of the Undamaged (UD) stage and for FB-3 it was 2.25 times. After that the area remained same for FB-2 and then decreases in damage level D5. For FB-3 it slightly decreased at damage level D4 but again it increased in damage level D5. It was clear from the Fig. 4.28 that at one impact excitation flexure control beams did not show any definite pattern in changing area of FFT curve.

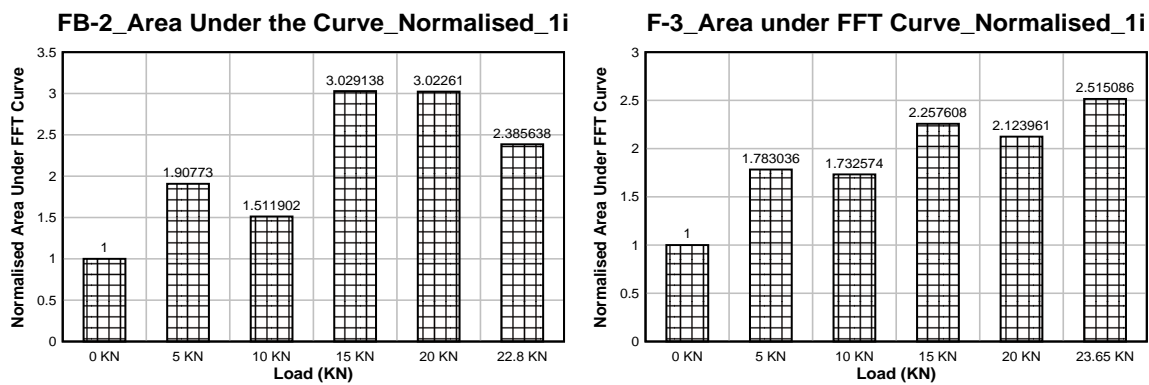


Figure 4.28: Area under the FFT Curve of Flexure Control Beam at One Impact Excitation

4.7.2 Shear Control Beam

The following Fig. 4.29 shows the normalized FFT of Shear Control Beam-1 (SB-1) at One Impact Excitation at various damage levels. At UD (0kN) level there was no visible damage in the beam. The predominant frequency of undamaged beam was found to be 45.67 Hz. All the frequencies of damage level D1 to D5 were normalized with respect to this predominant frequency level.

At damage level D1 (5kN) there were no visible crack in the beam and there was a pick in FFT plot of all the channels in a single point and the peak was slightly higher than the previous UD level. Highest peak was shown by sensor-1 (ch03) followed by sensor-2 and3 (ch06 & ch09).

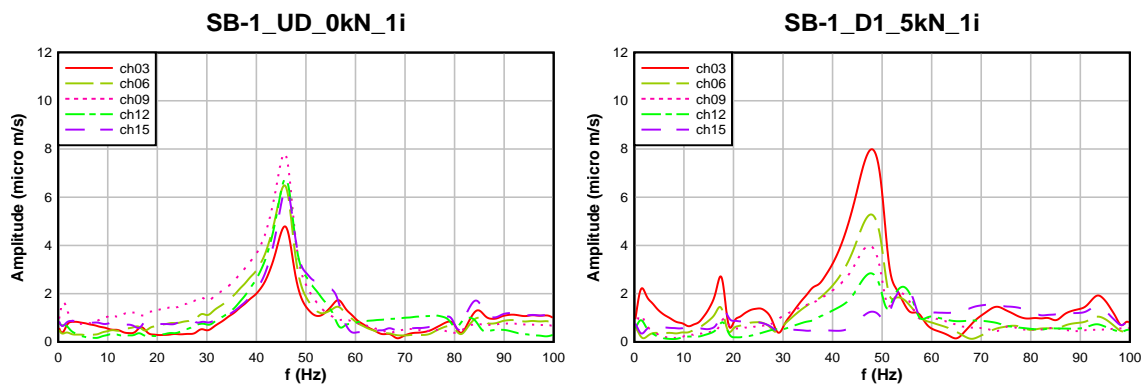
At damage level D2 (10kN) multiple small cracks appeared below Sensor-3 (ch09) at mid span of the beam. In FFT plot we observed that there were two consecutive peaks. Highest

peak was achieved by sensor-1, 2 and 3 (ch03, ch06& ch09). All peak values were less than the previous damage level.

At damage level D3 (15kN) multiple cracks appeared at mid span of beam below sensor- 2, 3, 4 (ch06, 09, 12). From FFT plot it is clear that sensor-1, 3, 4 (ch03, 09, 12) showed peaks, among them sensor-3 (ch09) showed highest level of peak. Maximum damage occurred in this level as theoretical capacity of the beam was 209 N-m at single point loading and shear capacity of the beam was 15 kN.

At damage level D4 (20kN) all cracks from previous damage level propagated in length and width and two new cracks appeared. One below sensor 1&2 (ch03 and ch06) and another one below sensor 4&5 (ch12 and ch15). From the FFT plot it is clear that all the channels showed a single pick as cracks were propagated all through the beam and peak values were lower than the previous damage level D3.

At damage level D5 (Failure) two new cracks appeared below sensor-2 (ch06). In FFT plot we found that all the channels showed abrupt and scattered peaks without any pattern. Here highest peak was shown by sensor-4 (ch-12).In this stage the beam was not taking any load which was clear from load-displacement curve in the Universal Testing machine (UTM) as displacement of the load cell was increasing without increasing load reading and thus indicated the failure stage of the beam. It is also clear from load-deflection curve of the beam that SB-1 was not taking any load after 22 kN.



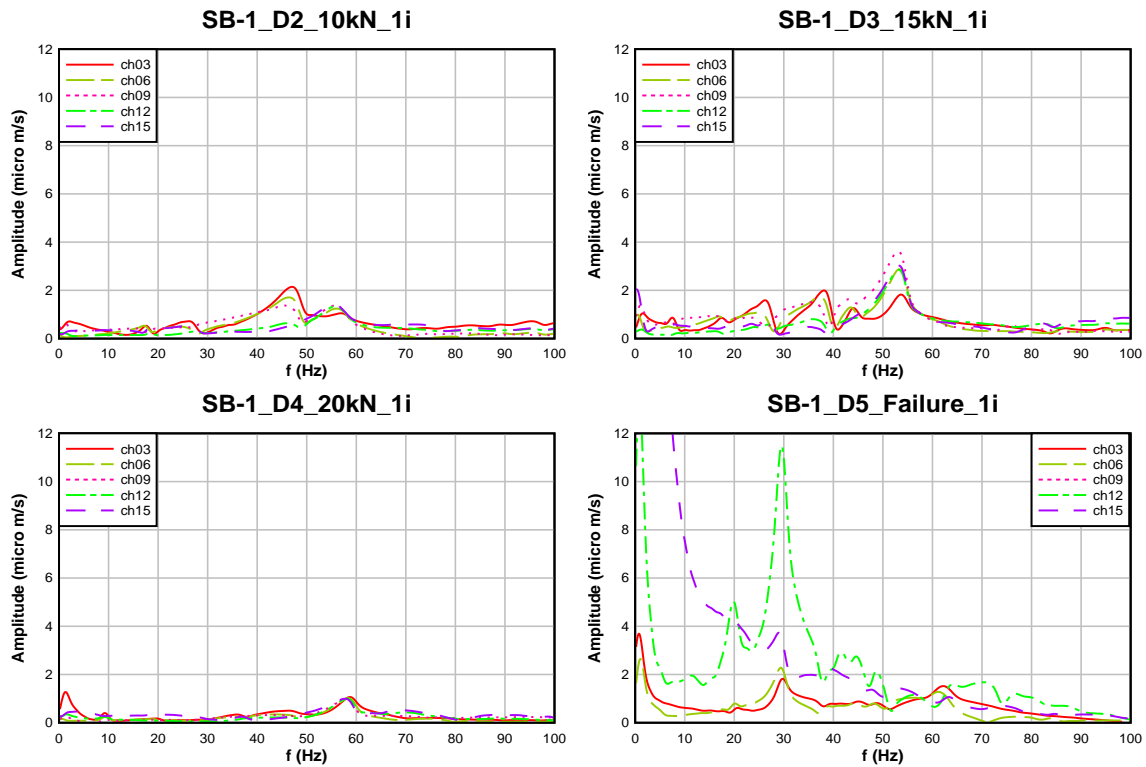


Figure 4.29: Normalized FFT Curve of Shear Control Beam-1 (SB-1) at One Impact Excitation

The following Fig. 4.30 shows the normalized FFT of Shear Control Beam-2 (SB-2) at ambient excitation at various damage levels.

At UD (0kN) level there was no visible damage in the beam. The predominant frequency of undamaged beam was found to be 53.46 Hz. All the frequencies of damage level D1 to D5 were normalized with respect to this predominant frequency level.

At damage level D1 (5kN) there were no visible crack in the beam and there were jump in all of the channels in FFT plot. Peak was slightly larger than the previous undamaged level.

At damage level D2 (10kN) multiple small cracks appeared below Sensor-2 & 3(ch06 & 09) at mid span of the beam. In FFT plot we found that there was no significant change in FFT plot from previous damage level D1.

At damage level D3 (15kN) two new cracks appeared below sensor-3 (ch09) at mid span of the beam. All previous cracks were propagated in length and width. in FFT plot sensor-5 (ch15) showed the highest level of jump. All other channels remained unchanged. Maximum damage occurred in this level as theoretical capacity of the beam was 209 N-m at single point loading and shear capacity of the beam was 15kN.

At damage level D4 (20kN) two new cracks were identified below sensor-2&4 (ch06 & ch12). There were more cracks between sensor-2, 3, and 4 (ch06, 09, 12). From FFT plot we found that there was no significant change in peak of FFT plot.

At damage level D5 (Failure) no new cracks appeared only previous cracks were propagated. In FFT plot all the channels showed same level of jump except sensor-5 (ch15). No distinguished peak was observed. In this stage the beam was not taking any load which was clear from load-displacement curve in the Universal Testing machine (UTM) as displacement of the load cell was increasing without increasing load reading and thus indicated the failure stage of the beam. It is also clear from load-deflection curve of the beam that SB-2 was not taking any load after 21.5 kN.

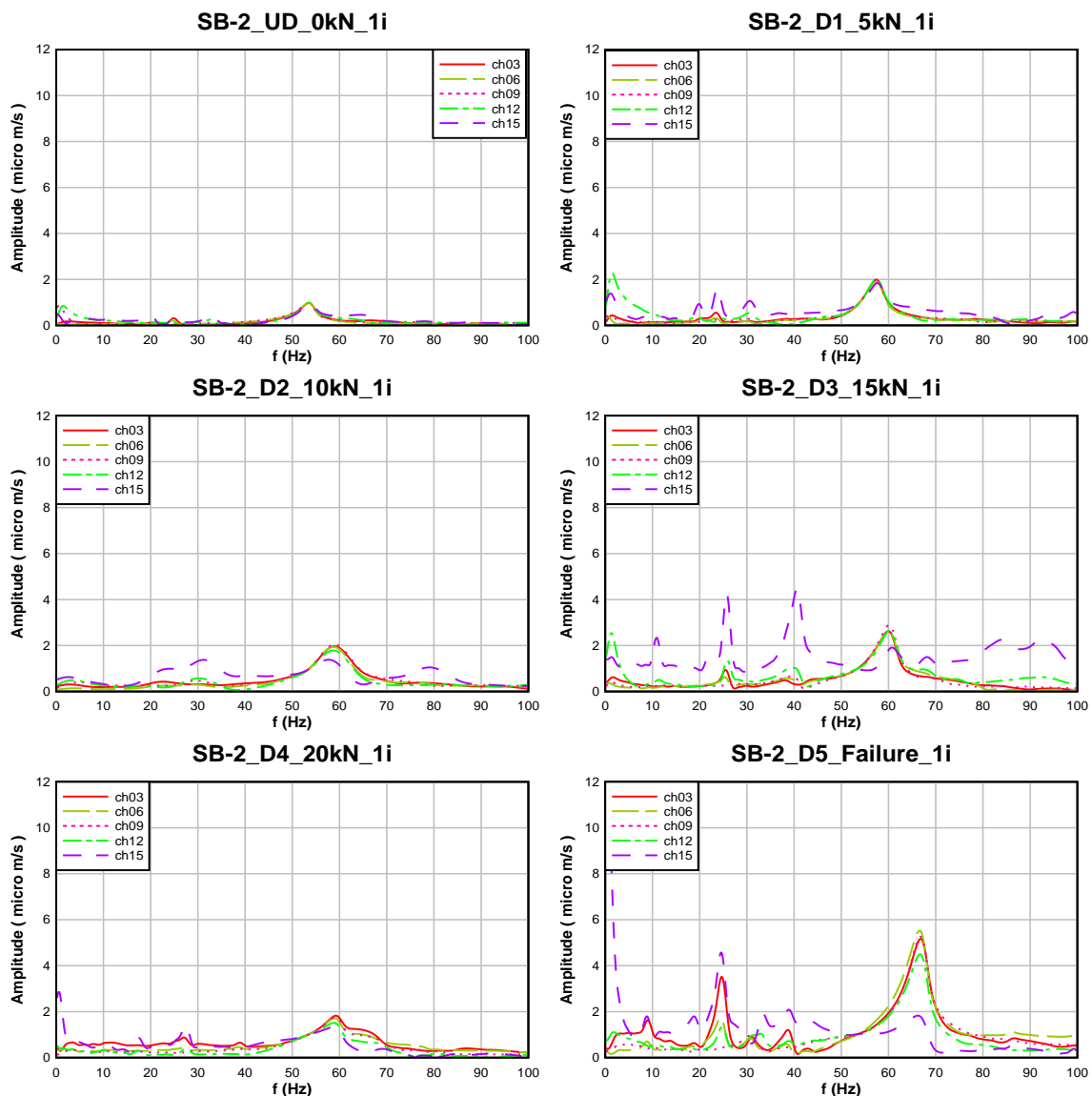


Figure 4.30: Normalized FFT Curve of Shear Control Beam-2 (SB-2) at One Impact Excitation

The following Fig. 4.31 shows the normalized FFT of Shear Control Beam-3 (SB-3) at One Impact Excitation at various damage levels. At UD (0kN) level there was no visible damage in the beam. The predominant frequency of undamaged beam was found to be 56.32 Hz. All the frequencies of damage level D1 to D5 were normalized with respect to this predominant frequency level.

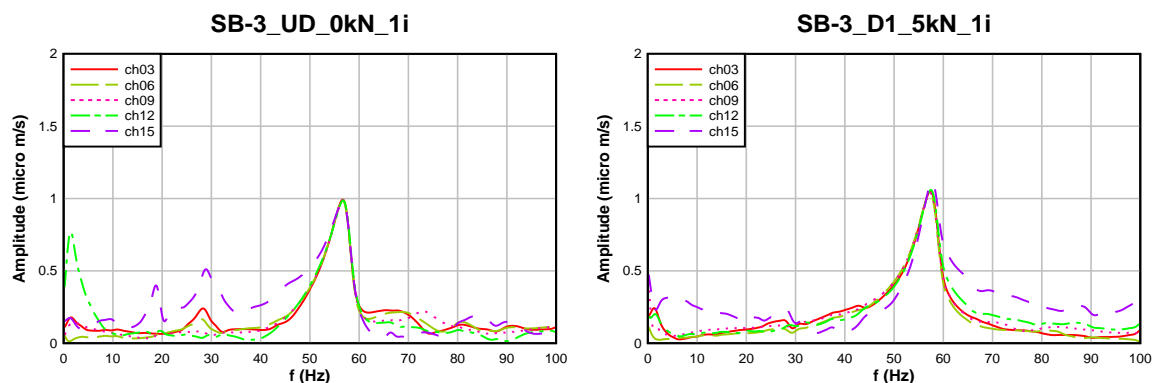
At damage level D1 (5kN) there was only one crack appeared below sensor-3 (ch09). In FFT plot we found no significant change in peaks from previous undamaged level.

At damage level D2 (10kN) multiple cracks appeared between the mid span of the beam. All of the cracks were between sensor-2, 3 &4 (ch06, 09, 12). In FFT plot all the channels showed a jump in a single point with a peak higher than the previous one.

At damage level D3 (15kN) only one new crack appeared below sensor-2 (ch06), all other cracks from previous damage level were propagated. In FFT plot there was no significant change in peak from previous damage level D2. Maximum damage occurred in this level as theoretical capacity of the beam was 209 N-m at single point loading and shear capacity of the beam was 15kN.

At damage level D4 (20kN) three new cracks appeared besides sensor-2 (ch06). In FFT plot we found that all the channels showed a single peak and peak was higher than the previous damage level D3.

At damage level D5 (Failure) no new cracks appeared only previous cracks were propagated. In FFT plot sensor-5(ch15) showed highest level of jump, followed by sensor-4 (ch12). All other channels showed same level of jump without any distinguished peak value. In this stage the beam was not taking any load which was clear from load-displacement curve in the Universal Testing machine (UTM) as displacement of the load cell was increasing without increasing load reading and thus indicated the failure stage of the beam. It is also clear from load-deflection curve of the beam that SB-3 was not taking any load after 24.2 kN.



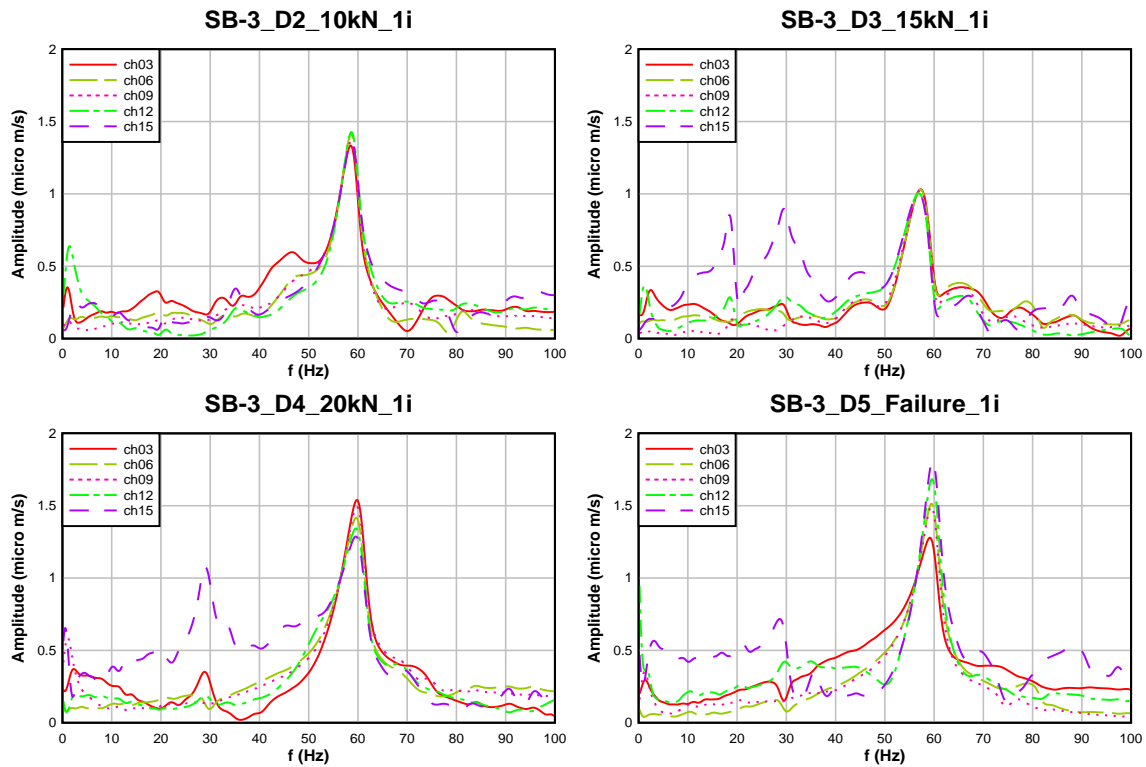
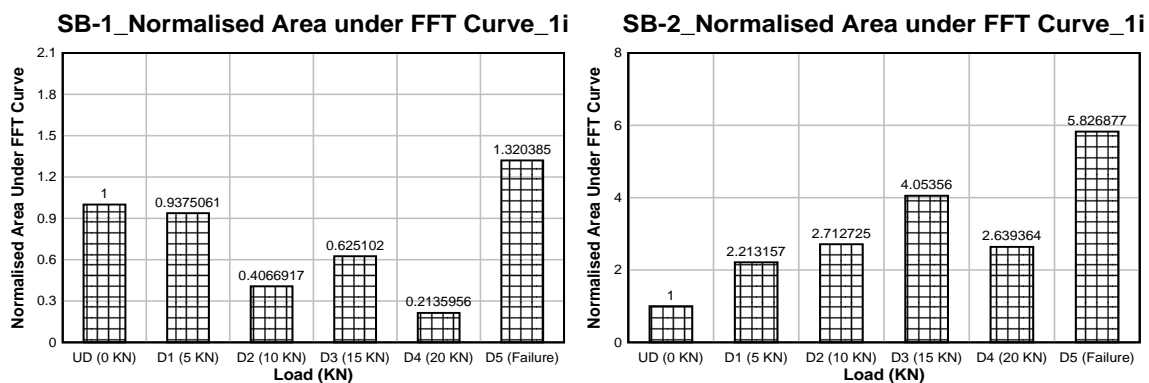


Figure 4.31: Normalized FFT Curve of Shear Control Beam-3 (SB-3) at One Impact Excitation

The following Fig. 4.32 shows the average area under the FFT curve normalized with respect to undamaged state UD (0kN) state. From the figure it is clear that there is a no definite pattern in increasing the area under FFT curve. It is clear from the figure that maximum area of FFT curve was achieved in damage level at failure D5 (Failure).



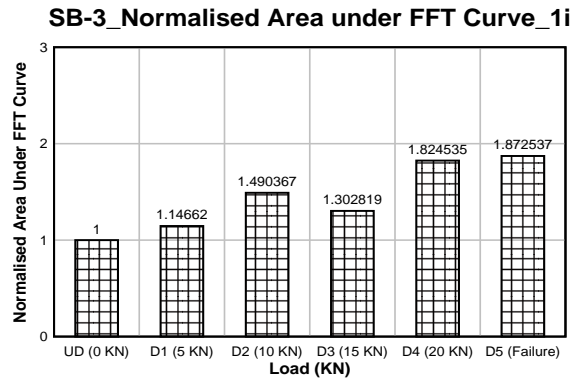


Figure 4.32: Area under the FFT Curve of Shear Control Beam at One Impact Excitation

4.8 Normalized FFT and Area under the Curve: Interval Impact Excitation

First time series data of undamaged beam as well as damaged beams were converted to frequency domain data and plotted against frequency. Only ch03, 06, 09, 12, 15 were used for analysis. As these channel data represents the vertical vibration. Then predominant frequency of each beam was determined. The damaged beam FFT plot was normalized with respect to predominant frequency of undamaged beam. The following Fig. 4.33 to 4.39 shows the normalized FFT plot of flexure and shear beam.

4.8.1 Flexure Control Beam

The following Fig. 4.33 shows the normalized FFT of flexure control beam-2 (FB-2) at Interval Impact Excitation at various damage levels. At UD (0kN) level there was no visible damage in the beam. The predominant frequency of undamaged beam was found to be 40.01 Hz. All the amplitude of damage level D1 to D5 was normalized with respect to this predominant frequency level.

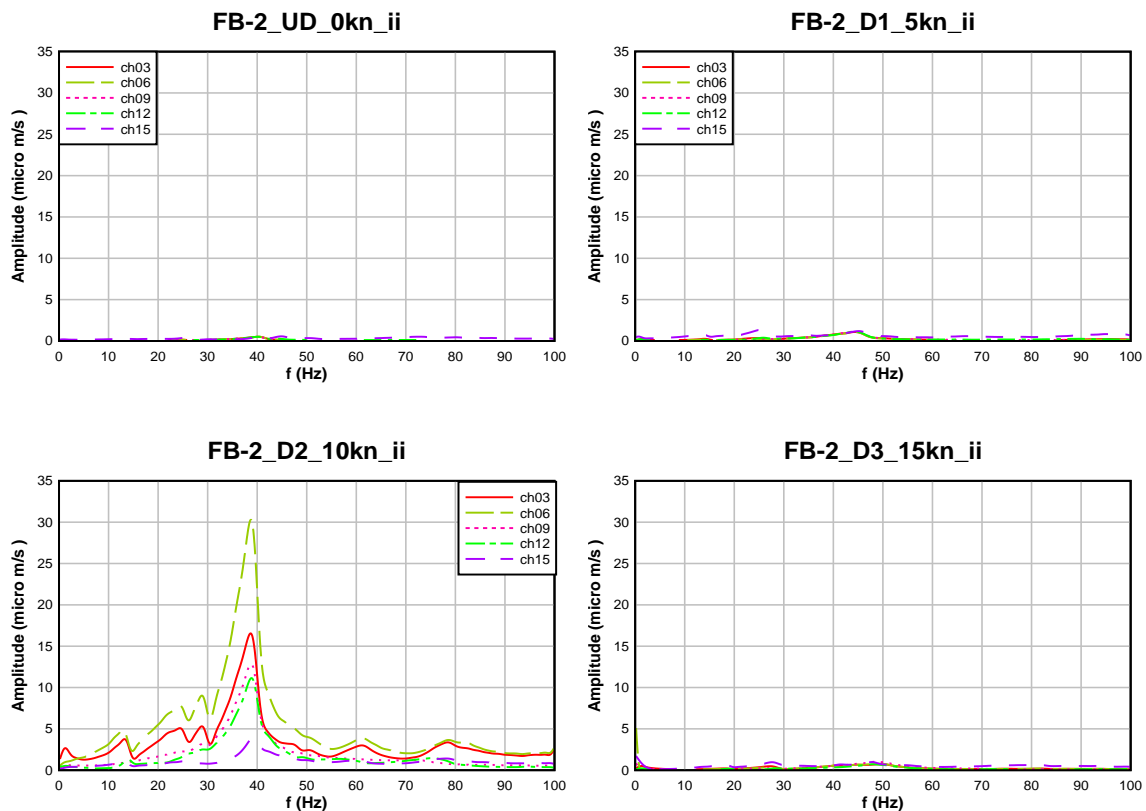
At damage level D1 there were two small cracks between sensor-2&3 (ch06 and ch09) another two were between sensor-3 & 4 (ch09 and ch12). From the normalized FFT plot it is clear that there were very little jump in all of the channels of FFT plot.

At damage level D2 (10kN) some new cracks appeared between sensor-2 and 3 (ch06 and ch09) and there were jump in FFT plot of all the channels than previous damage level. Ch06 had the highest level of jump followed by ch03 and ch09.

At damage level D3 (15kN) several cracks appeared between sensor- 2&3 (ch06 and ch09) there were no definite pattern in the normalized FFT plot. In FFT plot all the picks disappeared. Maximum damage occurred in this level as theoretical capacity of the beam was 140 N-m at single point loading of 13.24 kN.

At damage level D4 two new cracks appeared below sensor-3 (ch09) and from FFT plot it was clear that there were jump in sensor -2, 3 (ch06 & 09). No distinguished jump in channel plots rather all the channels showed a jump in a single point.

At damage level D5 (Failure) no new cracks appeared only previous cracks propagated in length and width. And FFT plot shows jump in all channels as cracks were increasing with applied load. The beam was not taking any load which was clear from load-displacement curve in the Universal Testing machine (UTM) as displacement of the load cell was increasing without increasing load reading and thus indicated the failure stage of the beam. It is also clear from load-deflection curve of the beam that FB-2 was not taking any load after 22.8 kN.



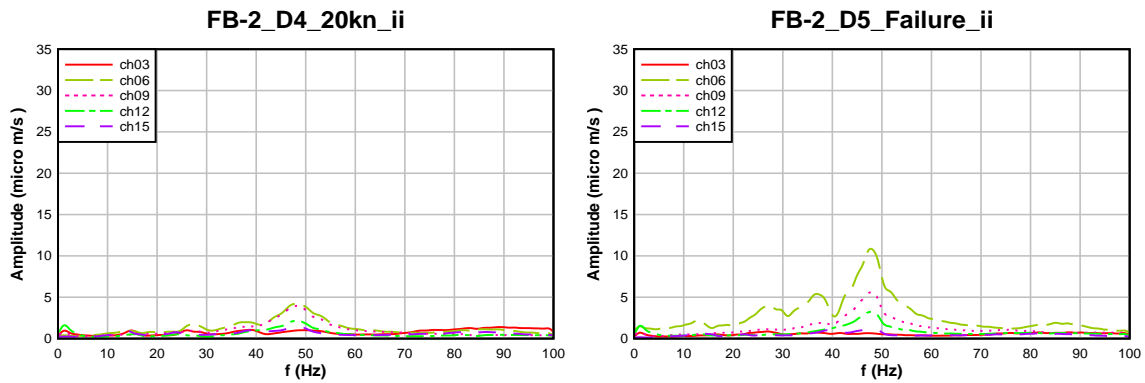


Figure 4.33: Normalized FFT Curve of Flexure Control Beam-2 (FB-2)

The following Fig. 4.34 shows the normalized FFT of Flexure Control Beam-3 (FB-3) at one impact excitation at various damage levels. At UD (0kN) level there was no visible damage in the beam. The predominant frequency of undamaged beam was found to be 38.47 Hz. All the amplitude of damage level D1 to D5 was normalized with respect to this predominant frequency level. At damage level D1 there were two small cracks between sensor-2&3 (ch06 and ch09) another two were between sensor-3 & 4 (ch09 and ch12). From the normalized FFT plot it is clear that there were jump in channels 6, 9, 12 of the FFT plot as well as channel 15.

At damage level D2 (10kN) some new cracks appeared between sensor-2 and 3 (ch06 and ch09) and there were jump in FFT plot of channels ch06 and ch09 but the peak was less than previous damage level D1.

At damage level D3 (15kN) several cracks appeared between sensor- 2&3 (ch06 and ch09). Highest jump was occurred in Sensor-2 (ch06) followed by sensor-3 (ch09). Other channels also showed some peaks. Maximum damage occurred in this level as theoretical capacity of the beam was 140 N-m at single point loading of 13.24 kN.

At damage level D4 two new cracks appeared below sensor-3 (ch09) and from FFT plot we found that sensor-2, 3 and 4 (ch06, 09 and 12) showed a clear pick.

At damage level D5 (Failure) no new cracks appeared only previous cracks propagated in length and width. And FFT plot showed jump in all channels as cracks were increasing with applied load. The beam was not taking any load which was clear from load-displacement curve in the Universal Testing machine (UTM) as displacement of the load cell was

increasing without increasing load reading and thus indicated the failure stage of the beam. It is also clear from load-deflection curve of the beam that FB-3 was not taking any load after 23.65 kN.

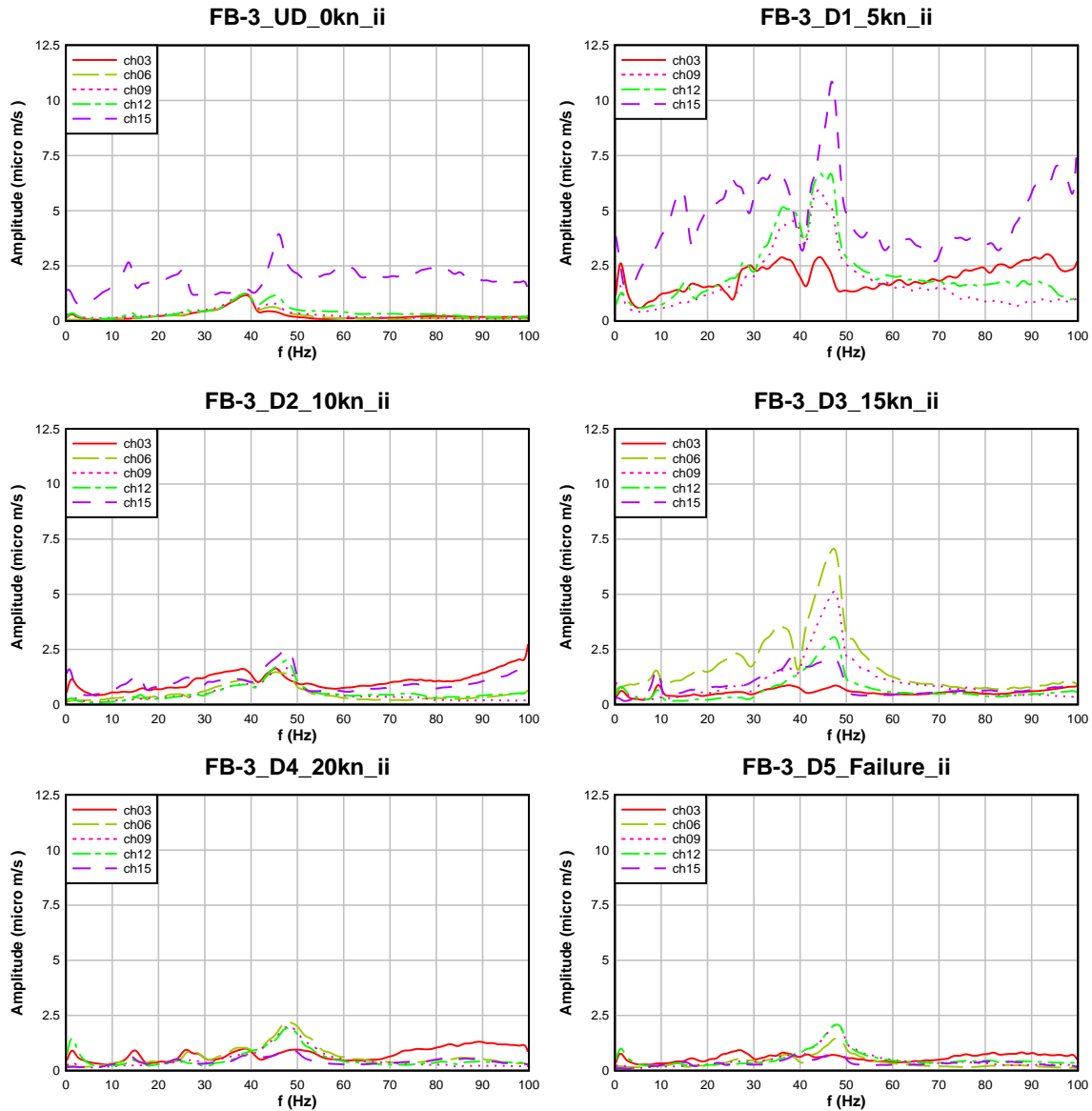


Figure 4.34: Normalized FFT Curve of Flexure Control beam-3 (FB-3)

The following Fig. 4.35 shows the average area under the FFT curve normalized with respect to undamaged state UD (0kN). For both of the beams it is clear that there is no definite pattern in changing of FFT area. For FB-2 we found that at maximum damage level (D3) the area was 2.18 times of the Undamaged (UD) stage and for FB-3 it was 1.59 times. It was also clear from the figure that FB-2 FFT plot had highest area for D2 (10kN) and FB-3 had

highest area in D1 (5kN). Moreover there was no definite pattern in increasing the FFT area of both the beams for Interval Impact Excitation.

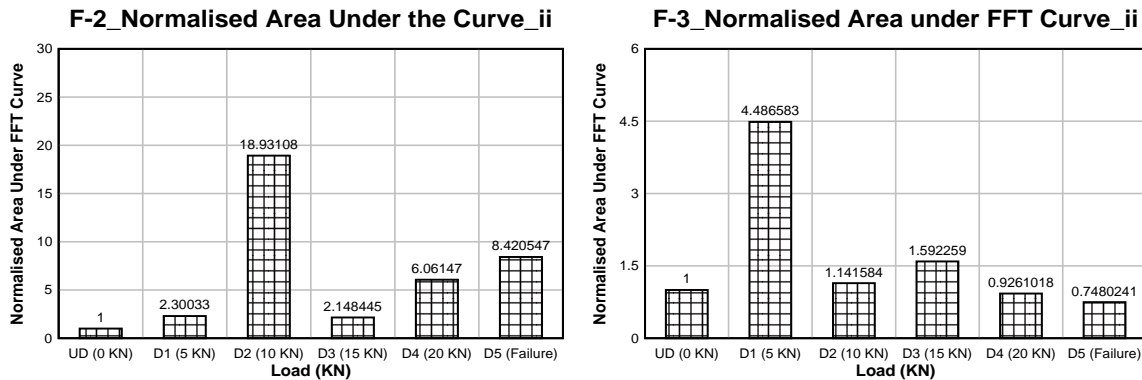


Figure 4.35: Area under the FFT Curve of Flexure Control Beam at One Impact Excitation

4.8.2 Shear Control beam

The following Fig. 4.36 shows the normalized FFT of Shear Control Beam-1 (SB-1) at Interval Impact Excitation at various damage levels. At UD (0kN) level there was no visible damage in the beam. The predominant frequency of undamaged beam was found to be 44.77 Hz. All the frequencies of damage level D1 to D5 were normalized with respect to this predominant frequency level.

At damage level D1 (5kN) there were no visible crack in the beam and there was a pick in FFT plot of all the channels in a single point and the peak was slightly higher than the previous UD level.

At damage level D2 (10kN) multiple small cracks appeared below Sensor-3 (ch09) at mid span of the beam. In FFT plot we observed that highest level of peak was shown by sensor-5 (ch15) followed by sensor-4 (ch12).

At damage level D3 (15kN) multiple cracks appeared at mid span of beam below sensor- 2, 3, 4 (ch06, 09, 12). From FFT plot it is clear that sensor-2, 3, 4 (ch06, 09, 12) showed highest level of jump at a single point followed by sensor-5, 1 (ch15, 03). Maximum damage occurred in this level as theoretical capacity of the beam was 209 N-m at single point loading and shear capacity of the beam was 15kN.

At damage level D4 (20kN) all cracks from previous damage level propagated in length and width and two new cracks appeared. One below sensor 1&2 (ch03 and ch06) and another one

below sensor 4&5 (ch12 and ch15). From FFT plot it is clear that all the channels showed some peak and highest peak was showed by sensor- 4 (ch12) followed by sensor-3 (ch09). At damage level D5 (Failure) two new cracks appeared below sensor-2 (ch06). In FFT plot we found that all the channels showed abrupt and scattered peaks without any pattern. Here all the channels showed a single point peak which was slightly higher than previous damage level D4. In this stage the beam was not taking any load which was clear from load-displacement curve in the Universal Testing machine (UTM) as displacement of the load cell was increasing without increasing load reading and thus indicated the failure stage of the beam. It is also clear from load-deflection curve of the beam that SB-1 was not taking any load after 22 kN.

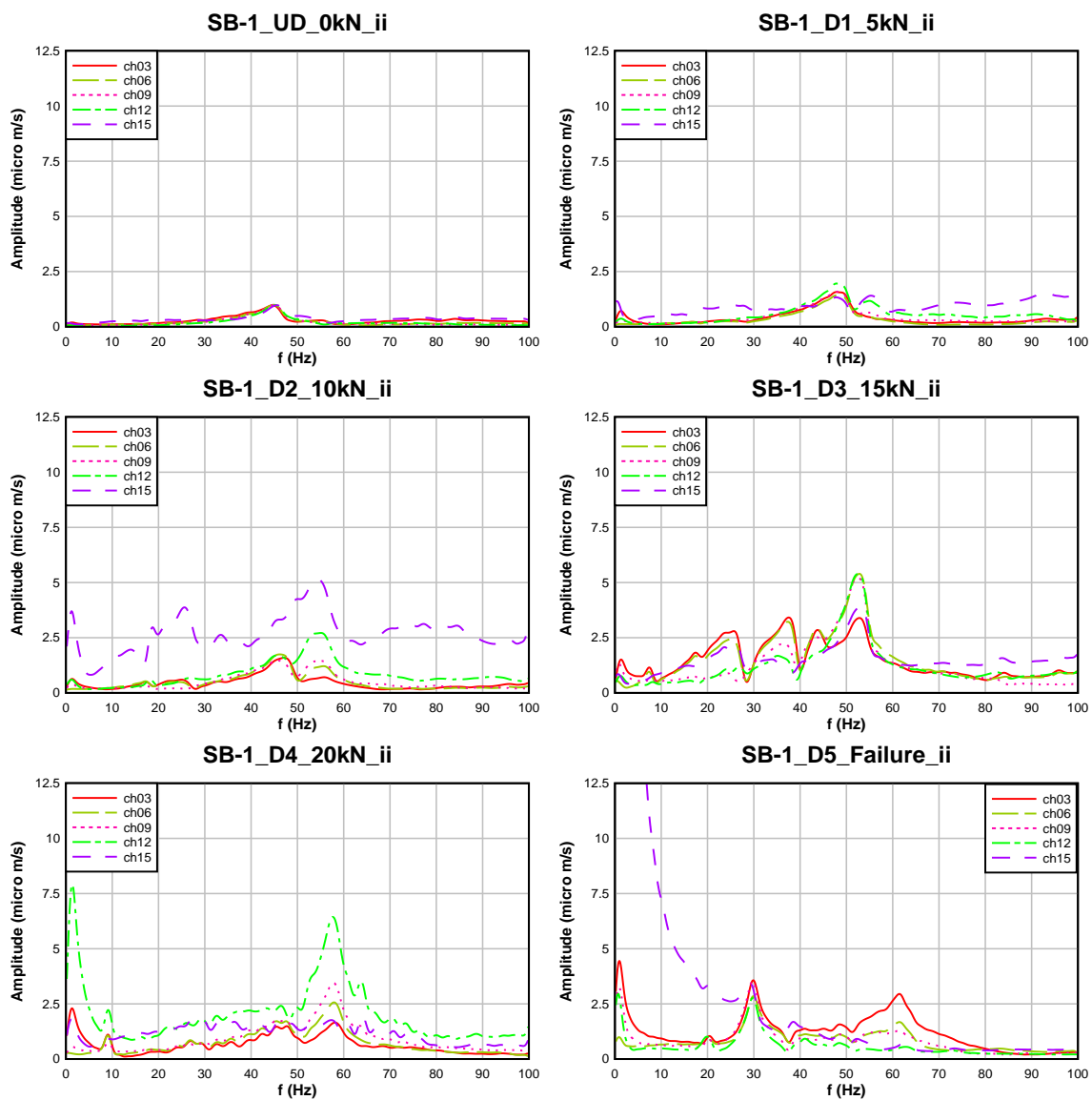


Figure 4.36: Normalized FFT Curve of Shear Control Beam-2 (SB-2)

The following Fig. 4.37 shows the normalized FFT of Shear Control Beam-2 (SB-2) at Interval Impact Excitation at various damage levels. At UD (0kN) level there was no visible damage in the beam. The predominant frequency of undamaged beam was found to be 53.17 Hz. All the frequencies of damage level D1 to D5 were normalized with respect to this predominant frequency level.

At damage level D1 (5kN) there were no visible crack in the beam and there were jump in all of the channels in FFT plot. Sensor-4 (ch12) showed the highest level of jump, followed by other channels.

At damage level D2 (10kN) multiple small cracks appeared below Sensor-2 & 3(ch06 & 09) at mid span of the beam. In FFT plot we found that there was highest level of jump in sensor-5 (ch15) followed by other channels. There was no visible difference in jump of all the channels in FFT plot except sensor-5 (ch15).

At damage level D3 (15kN) two new cracks appeared below sensor-3 (ch09) at mid span of the beam. All previous cracks were propagated in length and width. From FFT plot we found that sensor-5 (ch15) showed the highest level of jump. Other channels showed no distinguished difference in jump of FFT plot. Maximum damage occurred in this level as theoretical capacity of the beam was 209 N-m at single point loading and shear capacity of the beam was 15kN.

At damage level D4 (20kN) two new cracks were identified below sensor-2&4 (ch06 & ch12). There were more cracks between sensor-2, 3, and 4(ch06, 09, 12). From FFT plot we found that all the channels showed a single jump and no difference was observed.

At damage level D5 (Failure) no new cracks appeared only previous cracks were propagated. In FFT plot we found that sensor-5 (ch15) showed the highest level of jump, followed by sensor-3, 2 (ch09, 06). In this stage the beam was not taking any load which was clear from load-displacement curve in the Universal Testing machine (UTM) as displacement of the load cell was increasing without increasing load reading and thus indicated the failure stage of the beam. It is also clear from load-deflection curve of the beam that SB-2 was not taking any load after 21.5 kN.

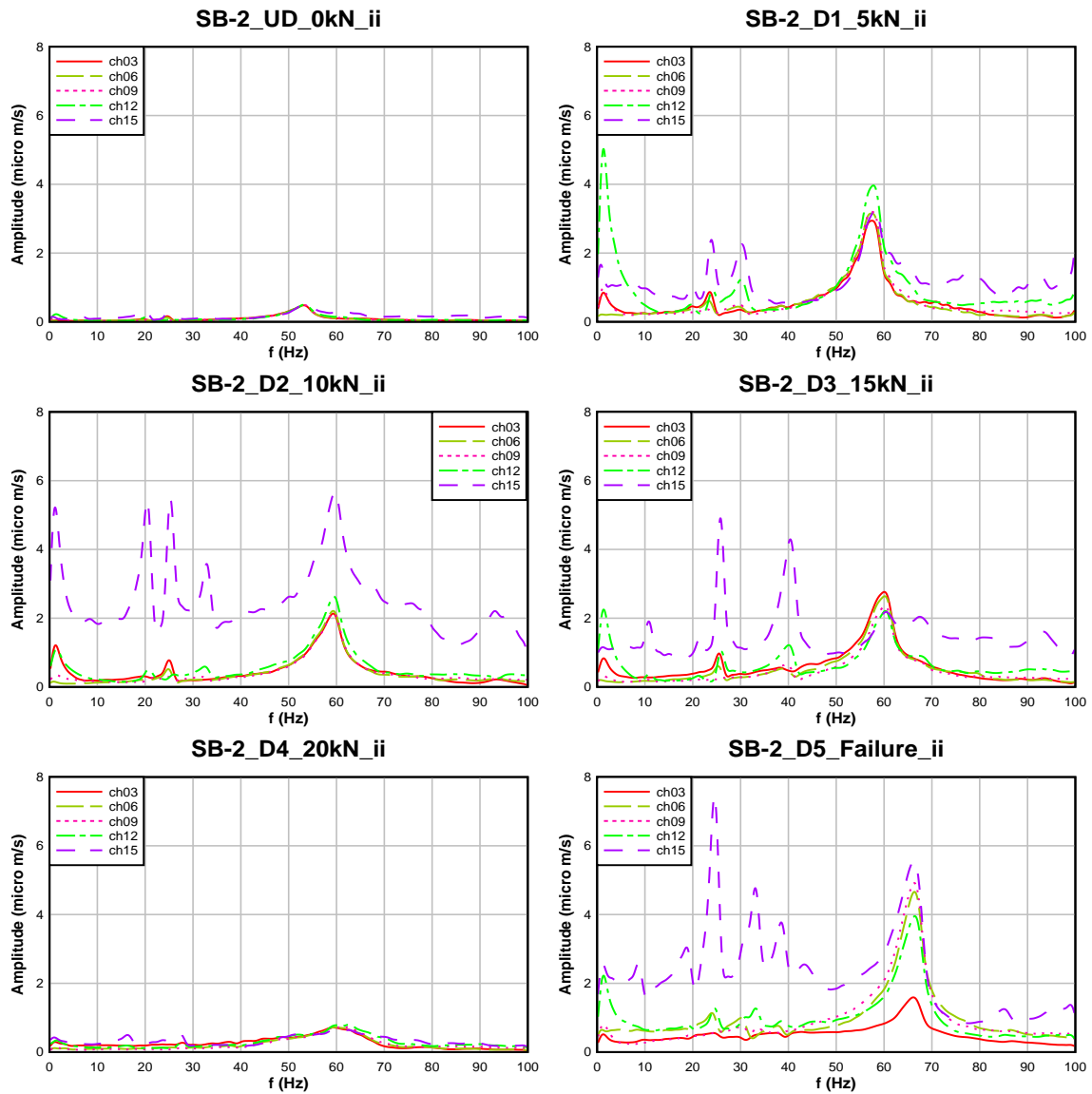


Figure 4.37: Normalized FFT Curve of Shear Control Beam-2 (SB-2) for Interval Impact Excitation

The following Fig. 4.38 shows the normalized FFT of Shear Control Beam-3 (SB-3) at ambient excitation at various damage levels. At UD (0kN) level there was no visible damage in the beam. The predominant frequency of undamaged beam was found to be 56.32 Hz. All the frequencies of damage level D1 to D5 were normalized with respect to this predominant frequency level.

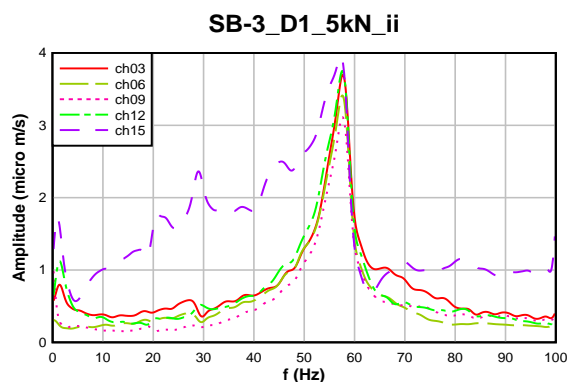
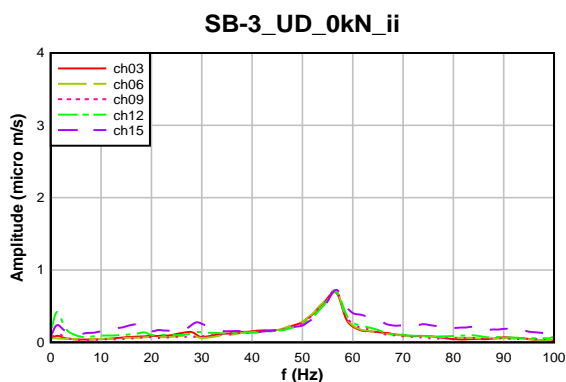
At damage level D1 (5kN) there was only one crack appeared below sensor-3 (ch09). In FFT plot we found that all the channels showed a single point jump and peak was higher than the previous undamaged state.

At damage level D2 (10kN) multiple cracks appeared between the mid span of the beam. All of the cracks were between sensor-2, 3 &4 (ch06, 09, 12). In FFT plot highest level of jump was shown by sensor-5(ch15) all other sensors showed same level of jump without any distinguished difference.

At damage level D3 (15kN) only one new crack appeared below sensor-2 (ch06), all other cracks from previous damage level were propagated. From FFT plot we found that sensor-4&5 (ch12&ch15) showed the highest level of jump followed by all other channels without any distinguished change in peak. Maximum damage occurred in this level as theoretical capacity of the beam was 209 N-m at single point loading and shear capacity of the beam was 15kN.

At damage level D4 (20kN) three new cracks appeared besides sensor-2 (ch06). In FFT plot we found that highest peak was achieved by sensor-5 (ch15) followed by all other channels.

At damage level D5 (Failure) no new cracks appeared only previous cracks were propagated. In FFT plot sensor-2(ch06) showed highest level of jump, but peak was lower than previous damage level. All other channels showed same level of jump without any distinguished peak value. In this stage the beam was not taking any load which was clear from load-displacement curve in the Universal Testing machine (UTM) as displacement of the load cell was increasing without increasing load reading and thus indicated the failure stage of the beam. It is also clear from load-deflection curve of the beam that SB-3 was not taking any load after 24.2 kN.



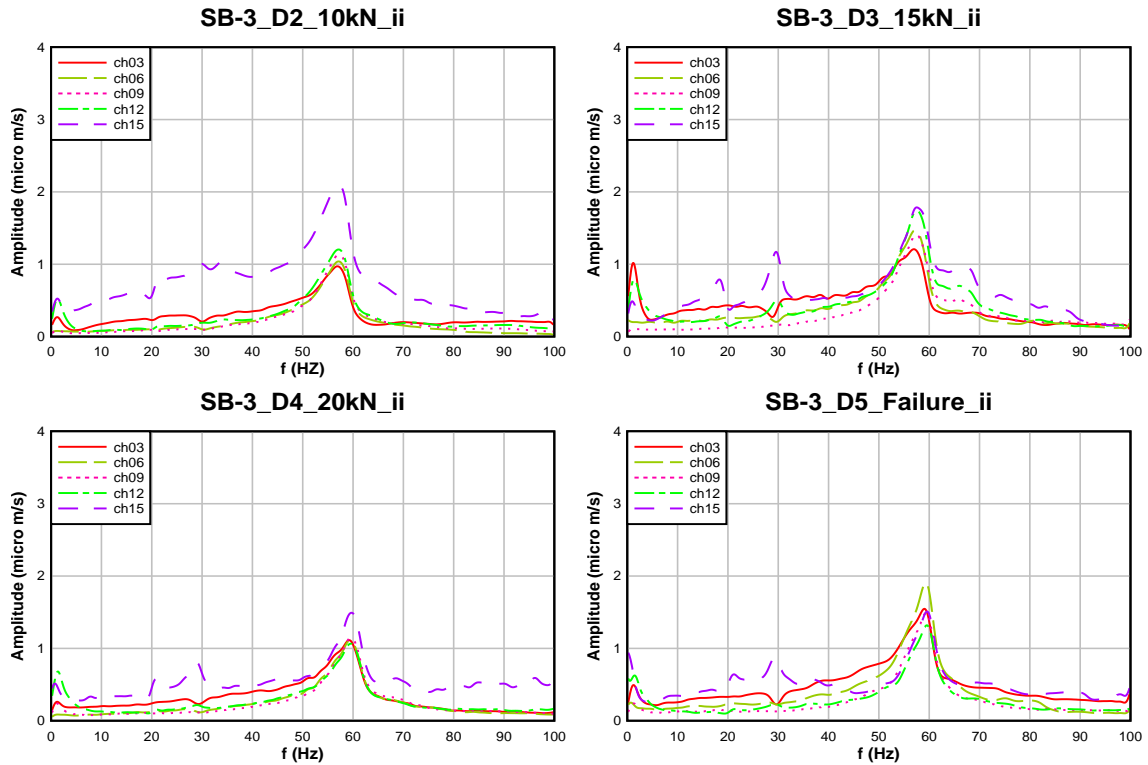
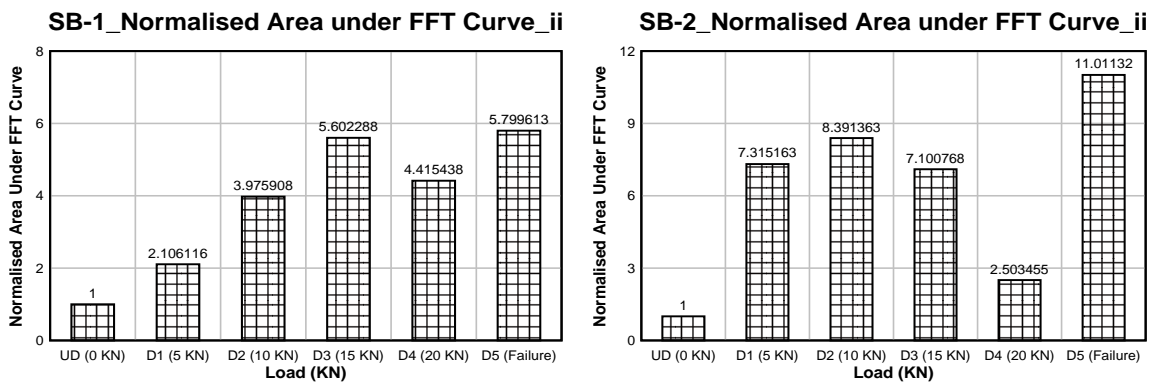


Figure 4.38: Normalized FFT Curve of Shear Control Beam-3 (SB-3) for Interval Impact Excitation

The following Fig. 4.39 shows the average area under the FFT curve normalized with respect to undamaged state UD (0kN) state. From the figure it is clear that there is a no definite pattern in increasing the area under FFT curve. For SB-1 highest area was achieved at damage level D3 (15kN) and damage level D5 (Failure) apart from these, SB-2 showed highest area for damage level D5 (Failure). On the other hand SB-3 showed highest area for damage level D1 (5kN), at the start of the loading.



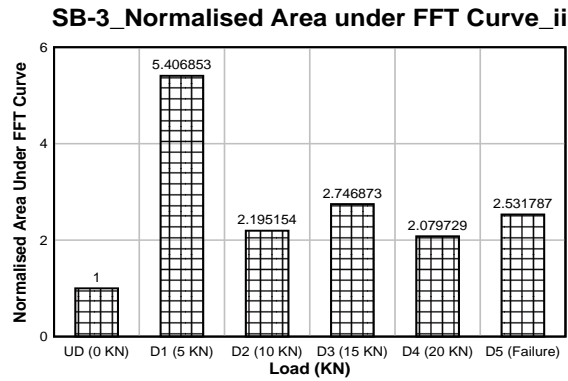


Figure 4.39: Area under the FFT Curve of Shear Control Beam at Interval Impact Excitation

4.9 Normalized FFT and Area under the Curve: Continuous Impact Excitation

First time series data of undamaged beam as well as damaged beams were converted to frequency domain data and plotted against frequency. Only ch03, 06, 09, 12, 15 were used for analysis. As these channel data represents the vertical vibration. Then predominant frequency of each beam was determined. The damaged beam FFT plot was normalized with respect to predominant frequency of undamaged beam. The following Fig. 4.40 to 4.46 shows the normalized FFT plot of flexure and shear beam.

4.9.1 Flexure Control Beam

The following Fig. 4.40 shows the normalized FFT of Flexure control beam-2 (FB-2) at Continuous impact excitation at various damage levels. At UD (0kN) level there was no visible damage in the beam. The predominant frequency of undamaged beam was found to be 40.55 Hz. All the amplitude of damage level D1 to D5 was normalized with respect to this predominant frequency level.

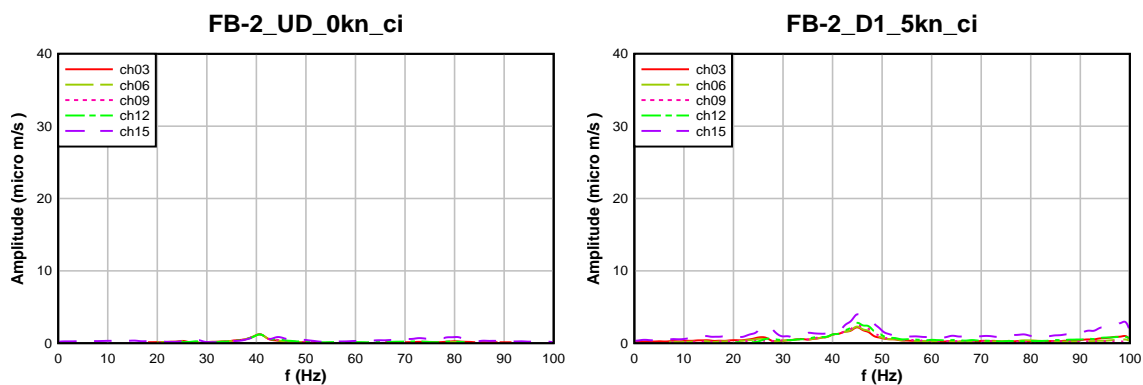
At damage level D1 (5kN) there were two small cracks between sensor-2&3 (ch06 and ch09) another two were between sensor-3 & 4 (ch09 and ch12). From the normalized FFT plot it is clear that there were very little jump in channel 6, 9, 12 of FFT plot. Apart from these channels there were also jump in channel 3.

At damage level D2 (10kN) some new cracks appeared between sensor-2 and 3 (ch06 and ch09) and there were equal jump in FFT plot of all the channels. All channels showed same peak.

At damage level D3 (15kN) several cracks appeared between sensor- 2&3 (ch06 and ch09). From FFT plot it is clear that channel 09 showed highest jump followed by channel 12 and 6. Channel 3 and 15 also showed picks higher than previous damage level. Maximum damage occurred in this level as theoretical capacity of the beam was 140 N-m at single point loading of 13.24 kN.

At damage level D4 (20kN) two new cracks appeared below sensor-3 (ch09) and from FFT plot it was clear that channel 9 and 6 showed same peak like the previous damage level D3. Only channel 3 showed higher pick than the previous damage level.

At damage level D5 (Failure) no new cracks appeared only previous cracks propagated in length and width. And FFT plot shows jump in all channels specially channel 9, as cracks were increasing with applied load. The beam was not taking any load which was clear from load-displacement curve in the Universal Testing machine (UTM) as displacement of the load cell was increasing without increasing load reading and thus indicated the failure stage of the beam. It is also clear from load-deflection curve of the beam that FB-2 was not taking any load after 22.8 kN.



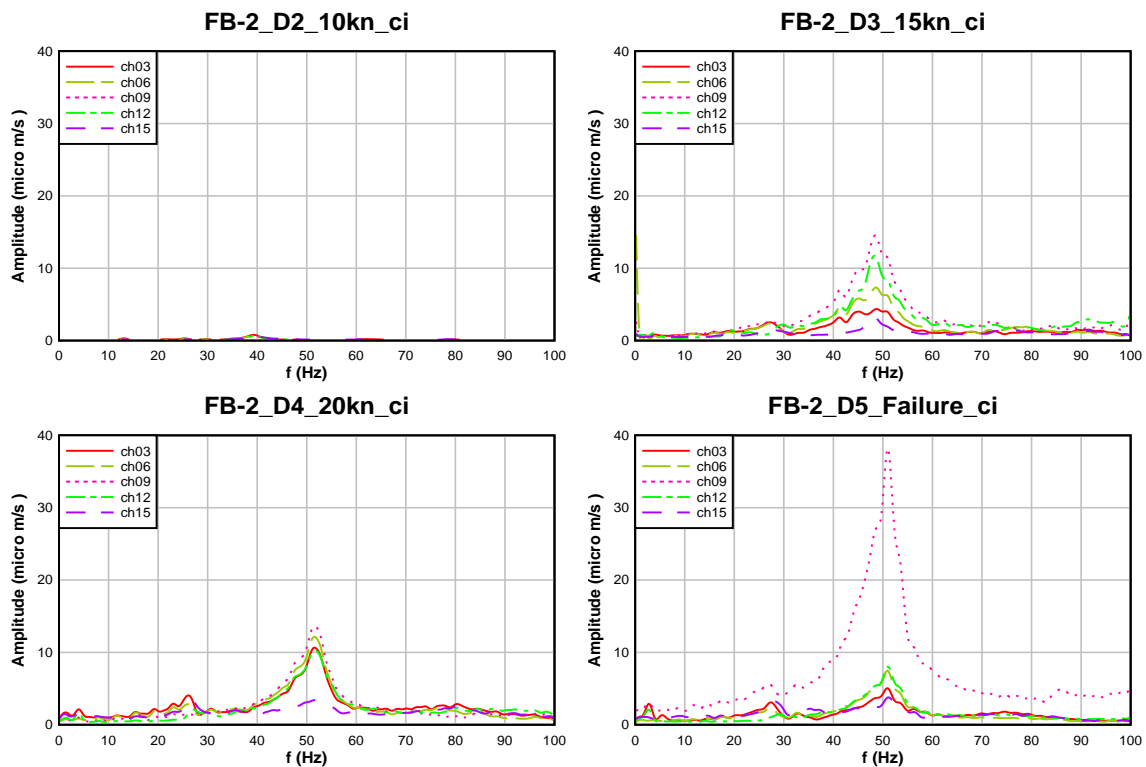


Figure 4.40: Normalized FFT curve of Flexure Control Beam-2 (FB-2) for Continuous Impact Excitation

The following Fig. 4.41 shows the normalized FFT of Flexure Control Beam-3 (FB-3) at one impact excitation at various damage levels. At UD (0kN) level there was no visible damage in the beam. The predominant frequency of undamaged beam was found to be 39.08 Hz. All the amplitude of damage level D1 to D5 was normalized with respect to this predominant frequency level.

At damage level D1 there were two small cracks between sensor-2&3 (ch06 and ch09) another two were between sensor-3 & 4 (ch09 and ch12). From the normalized FFT plot it is clear that there were jump in all the channels of the FFT plot.

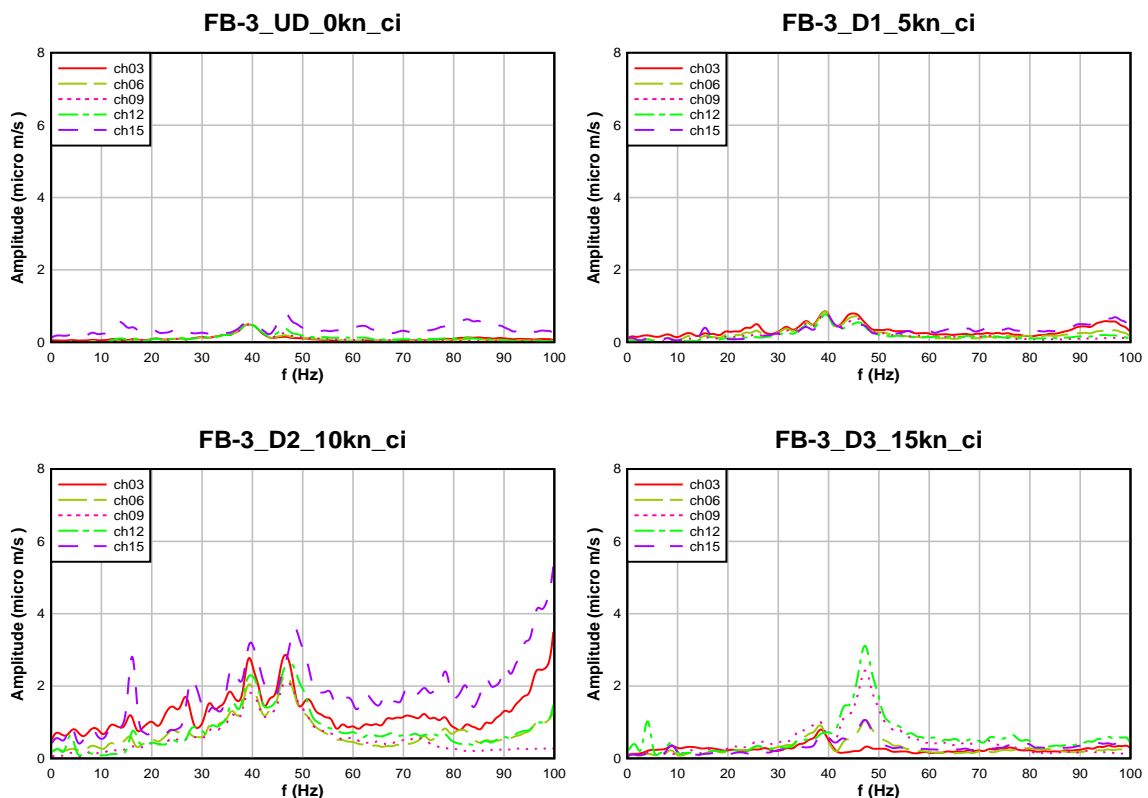
At damage level D2 (10kN) some new cracks appeared between sensor-2 and 3 (ch06 and ch09) and highest jump was occurred in Sensor-5 (ch15) followed by sensor-1 (ch03). Other channels also showed some peaks. All the peaks were higher than previous damage level D1.

At damage level D3 (15kN) several cracks appeared between sensor-2&3 (ch06 and ch09). Highest jump was occurred in Sensor-4 (ch12) followed by sensor-3 (ch09). Other channels

also showed some peaks. Maximum damage occurred in this level as theoretical capacity of the beam was 140 N-m at single point loading of 13.24 kN.

At damage level D4 (20kN) two new cracks appeared below sensor-3 (ch09) and from FFT plot we found that sensor- 5 (ch15) showed highest pick followed by sensor- 4 (ch12). All the channel peaks were higher than previous damage level.

At damage level D5 (Failure) no new cracks appeared only previous cracks propagated in length and width. And FFT plot showed jump in all channels as cracks were increasing with applied load. The beam was not taking any load which was clear from load-displacement curve in the Universal Testing machine (UTM) as displacement of the load cell was increasing without increasing load reading and thus indicated the failure stage of the beam. It is also clear from load-deflection curve of the beam that FB-3 was not taking any load after 23.65 kN.



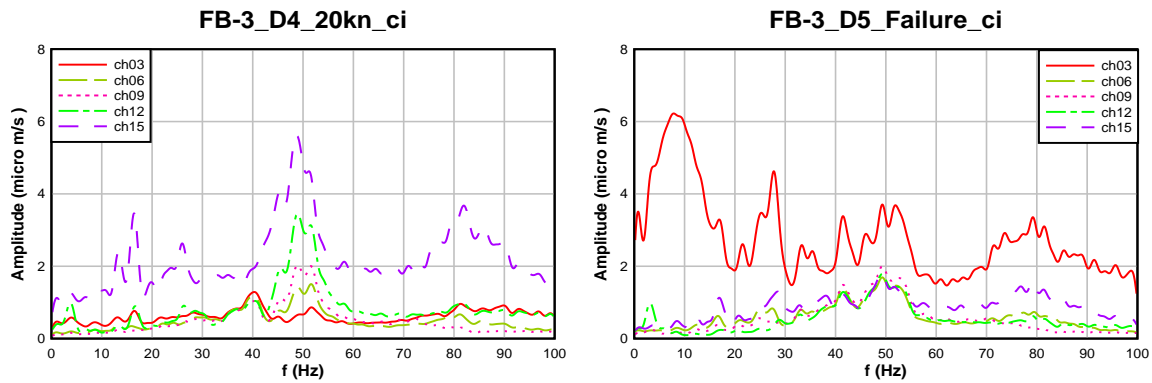


Figure 4.41: Normalized FFT Curve of Flexure Control Beam-3 (FB-3) for Continuous Impact Excitation

The following Fig. 4.42 shows the average area under the FFT curve normalized with respect to undamaged state UD (0kN). For both of the beams it is clear that there is no definite pattern in changing of FFT area. For FB-2 we found that at maximum damage level (D3) the area was 9.43times of the Undamaged (UD) stage and for FB-3 it was 2.5 times. It was also clear from the figure that FB-2 and FB-3 both had highest FFT area for D5 (Failure). Moreover there was no definite pattern in increasing the FFT area of both the beams for Continuous Impact excitation.

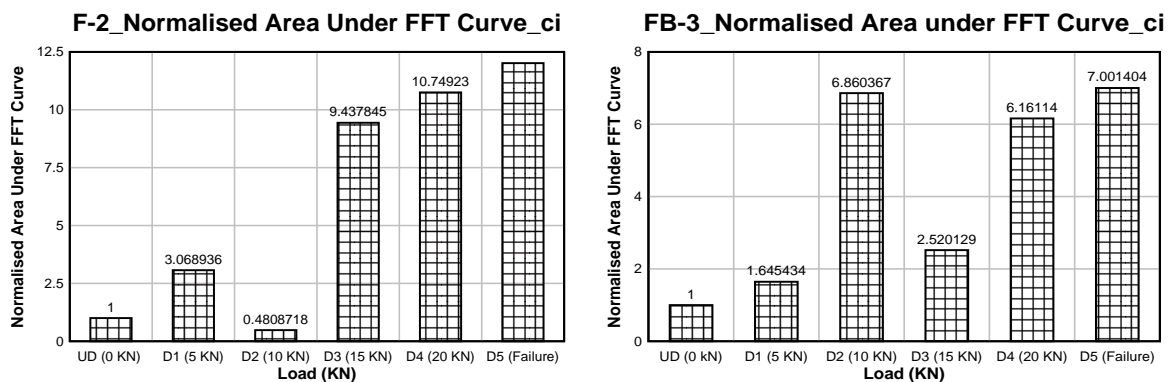


Figure 4.42: Area under the FFT Curve of Flexure Control Beam at Continuous Impact Excitation

4.9.2 Shear Control Beam

The following Fig. 4.43 shows the normalized FFT of Shear Control Beam-1 (SB-1) at Continuous Impact Excitation at various damage levels. At UD (0kN) level there was no visible damage in the beam. The predominant frequency of undamaged beam was found to be 45.70 Hz. All the frequencies of damage level D1 to D5 were normalized with respect to this predominant frequency level.

At damage level D1 (5kN) there were no visible crack in the beam and there was a pick in FFT plot of all the channels in a single point and the peak was slightly higher than the previous UD level.

At damage level D2 (10kN) multiple small cracks appeared below Sensor-3 (ch09) at mid span of the beam. In FFT plot we observed that highest level of peak was shown by sensor-5 (ch15) followed by sensor-4 and 3 (ch12, 09).

At damage level D3 (15kN) multiple cracks appeared at mid span of beam below sensor- 2, 3, 4 (ch06, 09, 12). From FFT plot it is clear that sensor-4 (ch12) showed highest level of peak followed by sensor-3 (ch09). Maximum damage occurred in this level as theoretical capacity of the beam was 209 N-m at single point loading and shear capacity of beam was 15kN.

At damage level D4 (20kN) all cracks from previous damage level propagated in length and width and two new cracks appeared. One below sensor 1&2 (ch03 and ch06) and another one below sensor 4&5 (ch12 and ch15). In FFT plot sensor-5 (ch15) showed the highest level of jump followed by sensor-4 (ch12). At damage level D5 (Failure) two new cracks appeared below sensor-2 (ch06). In FFT plot we found that sensor-5 (ch15) showed an abrupt peak followed by a small peak with all other channels. Here all the channels showed a single point peak which was lower than previous damage level D4. In this stage the beam was not taking any load which was clear from load-displacement curve in the Universal Testing machine (UTM) as displacement of the load cell was increasing without increasing load reading and thus indicated the failure stage of the beam. It is also clear from load-deflection curve of the beam that SB-1 was not taking any load after 22 kN.

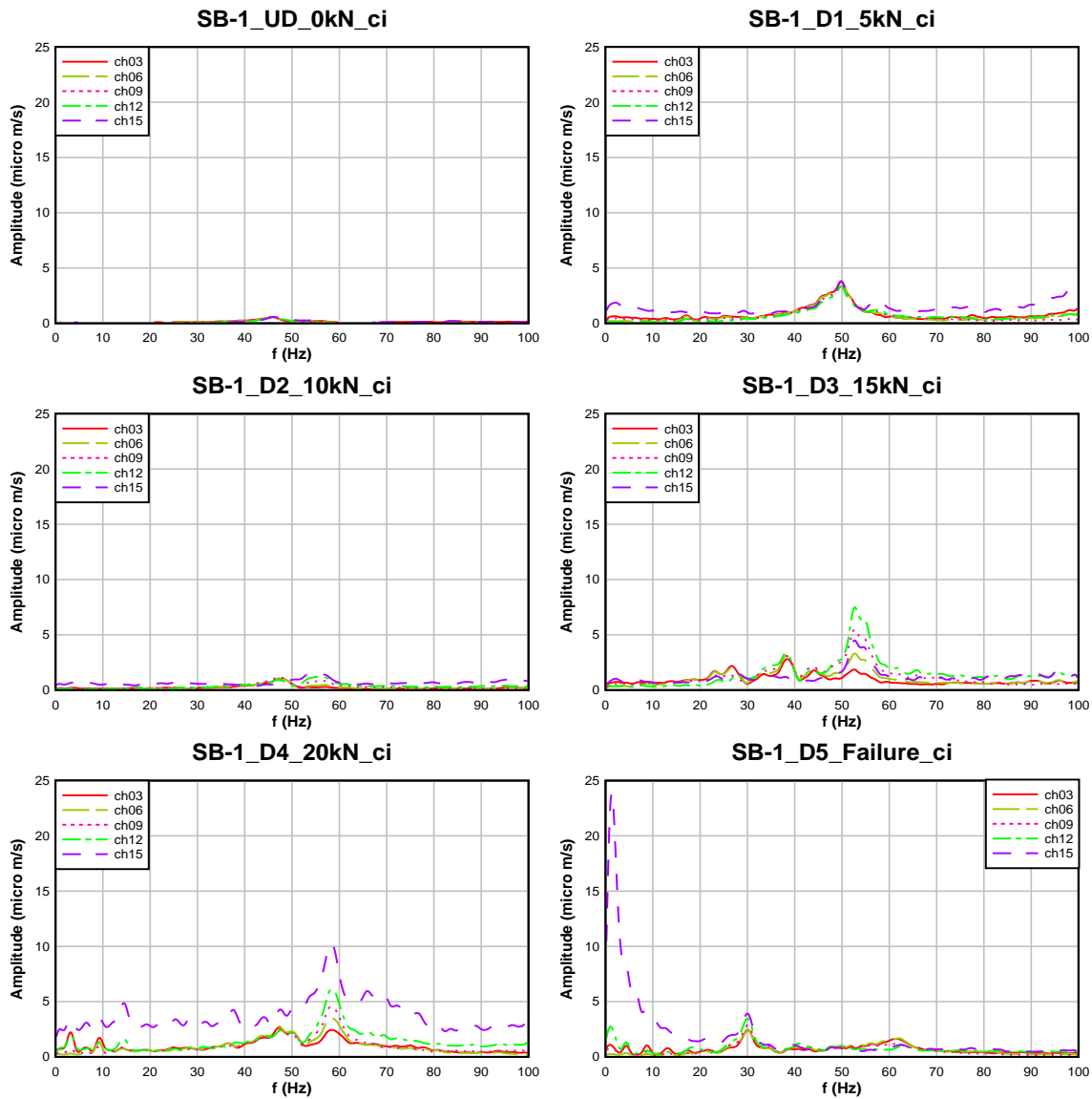


Figure 4.43: Normalized FFT Curve of Shear Control Beam-1 (SB-1) for Continuous Impact Excitation

The following Fig 4.44 shows the normalized FFT of Shear Control Beam-2 (SB-2) at ambient excitation at various damage levels. At UD (0kN) level there was no visible damage in the beam. The predominant frequency of undamaged beam was found to be 55.73 Hz. All the frequencies of damage level D1 to D5 were normalized with respect to this predominant frequency level.

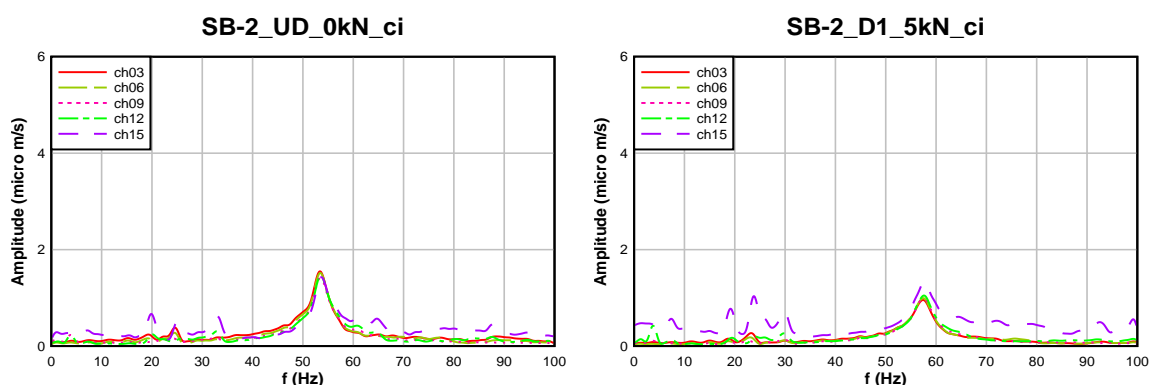
At damage level D1 (5kN) there were no visible crack in the beam and there were no significant change in peak of all the channels in FFT plot.

At damage level D2 (10kN) multiple small cracks appeared below Sensor-2 & 3(ch06 & 09) at mid span of the beam. In FFT plot we found no change in peak of the channels.

At damage level D3 (15kN) two new cracks appeared below sensor-3 (ch09) at mid span of the beam. All previous cracks were propagated in length and width. Highest jump was shown by sensor-3 (ch09). Followed by sensor-4 & 5 (ch12, 15). Maximum damage occurred in this level as theoretical capacity of the beam was 209 N-m at single point loading and shear capacity of beam was 15kN.

At damage level D4 (20kN) two new cracks were identified below sensor-2&4 (ch06 & ch12). There were more cracks between sensor-2, 3, and 4(ch06, 09, 12). From FFT plot we found that highest jump was given by sensor-4 (ch12) followed by sensor-5 (ch15), peaks were lower than the previous damage level.

At damage level D5 (Failure) no new cracks appeared only previous cracks were propagated. In FFT plot sensor-1 (ch03) showed highest level of jump. Followed by all other sensors with no significant difference in peak. In this stage the beam was not taking any load which was clear from load-displacement curve in the Universal Testing machine (UTM) as displacement of the load cell was increasing without increasing load reading and thus indicated the failure stage of the beam. It is also clear from load-deflection curve of the beam that SB-2 was not taking any load after 21.5 kN.



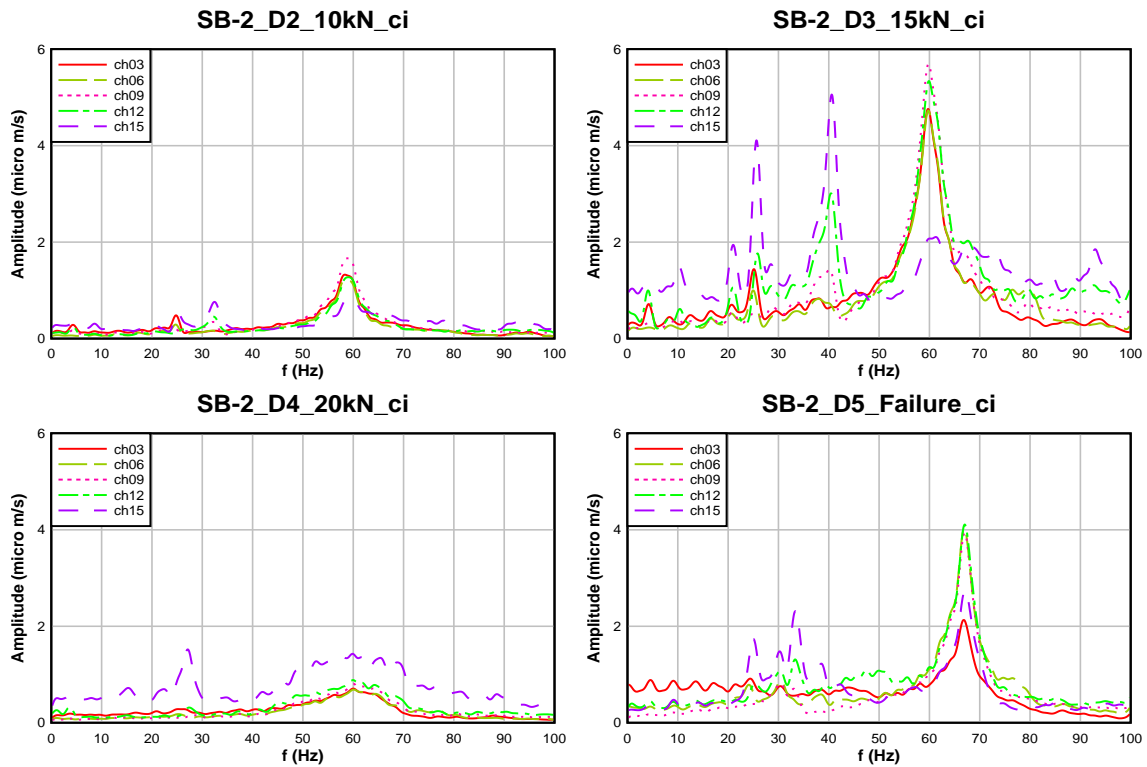


Figure 4.44: Normalized FFT Curve of Shear Control Beam-2 (SB-2) for Continuous Impact Excitation

The following Fig. 4.45 shows the normalized FFT of Shear Control Beam-3 (SB-3) at ambient excitation at various damage levels. At UD (0kN) level there was no visible damage in the beam. The predominant frequency of undamaged beam was found to be 56.78 Hz. All the frequencies of damage level D1 to D5 were normalized with respect to this predominant frequency level.

At damage level D1 (5kN) there was only one crack appeared below sensor-3 (ch09). In FFT plot we found that all the channels showed a single point jump and peak was slightly lower than the previous undamaged state.

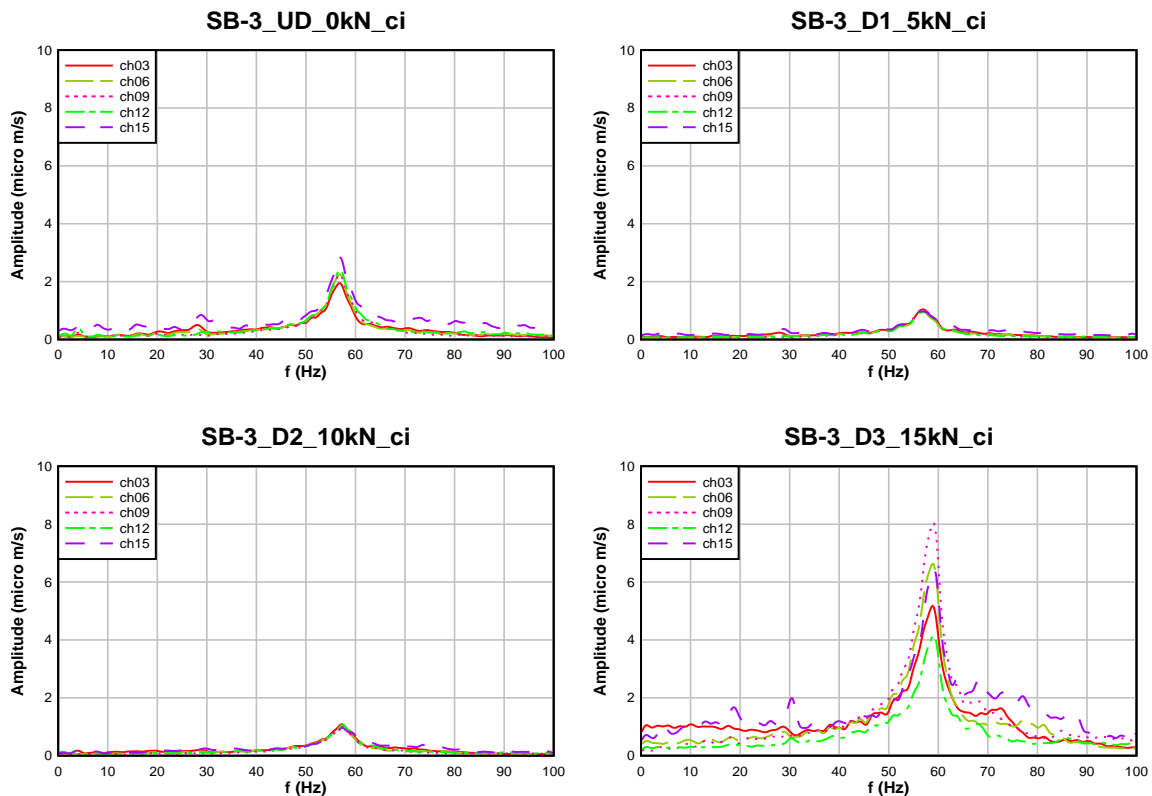
At damage level D2 (10kN) multiple cracks appeared between the mid span of the beam. All of the cracks were between sensor-2, 3 & 4 (ch06, 09, 12). In FFT plot we found that there was no significant change in FFT plot than the previous damage level.

At damage level D3 (15kN) only one new crack appeared below sensor-2 (ch06), all other cracks from previous damage level were propagated. From FFT plot we found that sensor-1 (ch03) showed the highest level of jump followed by sensor -2, 4 (ch06&ch12). All the peak

in this damage level were higher than the previous damage level D2. Maximum damage occurred in this level as theoretical capacity of the beam was 209 N-m at single point loading and shear capacity of the beam was 15kN.

At damage level D4 (20kN) three new cracks appeared besides sensor-2 (ch06). In FFT plot we found that highest peak was achieved by sensor-4 (ch12) followed by sensor-5 (ch15) and followed by all other channels.

At damage level D5 (Failure) no new cracks appeared only previous cracks were propagated. In FFT plot sensor-1(ch03) showed highest level of jump, but peak was lower than previous damage level. All other channels showed same level of jump without any distinguished peak value. In this stage the beam was not taking any load which was clear from load-displacement curve in the Universal Testing machine (UTM) as displacement of the load cell was increasing without increasing load reading and thus indicated the failure stage of the beam. It is also clear from load-deflection curve of the beam that SB-3 was not taking any load after 24.2 kN.



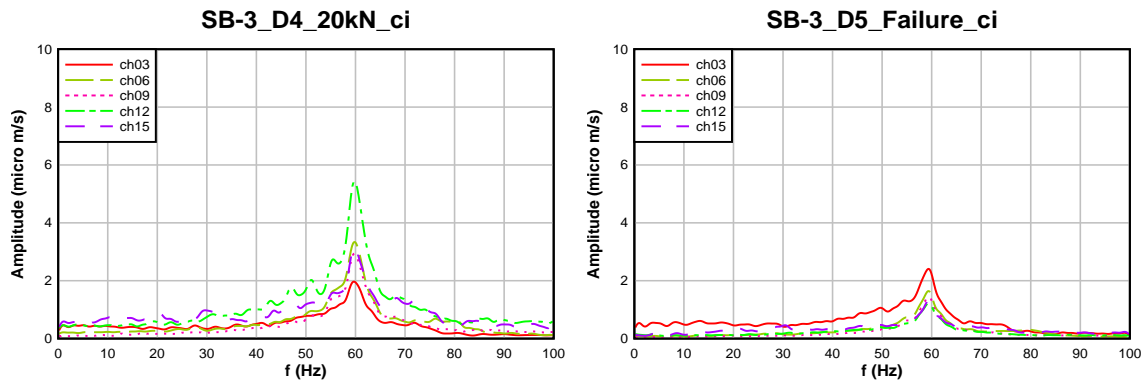
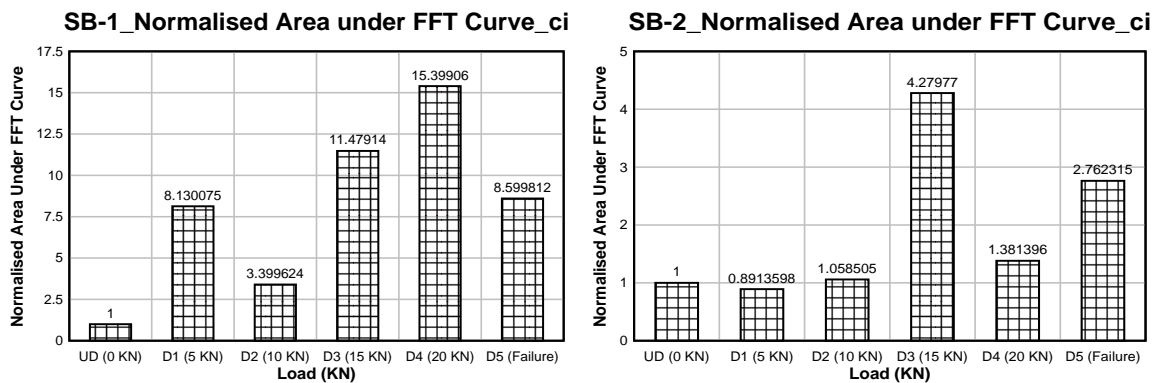


Figure 4.45: Normalized FFT Curve of Shear Control Beam-3 (SB-3) for Continuous Impact Excitation

The following Fig. 4.46 shows the average area under the FFT curve normalized with respect to undamaged state UD (0kN) state. From the figure it is clear that there is a no definite pattern in increasing the area under FFT curve. For SB-1 highest area was achieved at damage level D4 (20kN) but for SB-2 & 3 showed highest area for damage level D3 (15kN). For higher damage level SB-1&2 showed no definite pattern in increasing or decreasing FFT areas. Only SB-3 showed a definite pattern in decreasing areas. It is also clear that a for shear control beams failure occurred in a random way after achieving the maximum load.



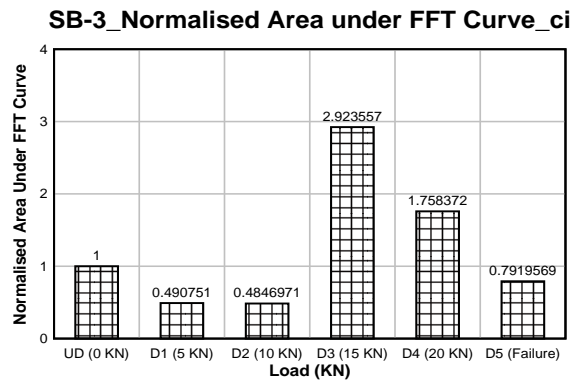


Figure 4.46: Area under the FFT Curve of Shear Control Beam at Continuous Impact Excitation

CHAPTER FIVE

CONCLUSIONS

5.1 General

The objectives of this study were to investigate the change of vibration time series properties of RC concrete beams with increasing nonlinearities, due to structural distress. A literature review has revealed that much work has been done in detecting damage in RC beams considering the vibration characteristics as linear. In contrast, very little work has been done on the nonlinear vibration properties of concrete beams. In addition to these, none of the discussed methods has quantified the extent of nonlinearity. Time series based measure of nonlinearity provided a good starting point in quantifying the nonlinearity.

The tested RC beams were so designed that two of them failed in flexure and three of them failed in shear. This was achieved by providing particular beam detailing. The flexure control beam had stirrup at minimum spacing to achieve flexural cracks and shear control beam had stirrup so designed to achieve shear cracks. Both types of beams had same concrete strength.

The test setup was challenging considering the space and management. The samples were transported with care so that no damage occurred in time of transportation. The Microtremor (MT) sensors were placed with great care to achieve the appropriate leveling before taking vibration data.

A dial gauge was placed at the middle of the beam to measure the deflection of the beam at loading. This data was used to plot load-deflection curve of the beams. Vibration data was recorded using MT at various excitations, Ambient, One Impact, Interval Impact and Continuous Impact Excitations. At time of providing impact manual hammer was used and highest effort was given to keep equal time interval for Interval Impact Excitation. These recorded time series data was used to determine NGI, NLI index followed by FFT plot to

observe the change in vibration time series properties with increasing nonlinearities induced in RC beams at various damage levels.

Load-Deflection curve of beams were plotted to observe the change of beam midspan deflection with increasing loads. Time series recorded at each damage level for four different vibrating conditions were tested to find the distribution of the signal followed by linearity test of the signal generating process. In addition to these FFT plot of the time series were observed and also area under the FFT curve were also used to correlate with the increasing nonlinearity of RC beams due to induced loads.

5.2 Conclusions

Following conclusion were drawn based on time series data analysis of the beam:

- A. Both NGI and NLI were good indicators in detecting nonlinearity in RC beams. For both Flexure and Shear control beams NLI correctly indicated the presence of nonlinearity in RC beams. But its change with increasing load had no definite pattern.
- B. Normalized FFT, with respect to undamaged beam showed good correlation with increasing damage for Ambient Excitation for both Flexure and shear Control beams.
- C. For both Flexure and Shear control beams, with propagation of crack below a certain sensor, showed a jump in normalized FFT plot of that sensor. In Flexure control beams area under the normalized FFT curve increased up to the theoretical capacity of the beam and decreased gradually to the state where it could not take any load.
- D. Ambient excitation time history data gave most reliable relation of FFT and Damage than other vibrating conditions such as: One Impact, Interval Impact and Continuous Impact excitation.

5.3 Recommendation for Future Studies

- A. The experimental results may be verified by FEM modeling.
- B. This experiment may be performed for steel beams and RC beam column joints.
- C. A uniform and controlled application of impact load may produce more reliable and certain results.

REFERENCES

- Alampalli, S., Fu, G., and Dillon, E. W. (1997). "Signal versus noise in damage detection by experimental modal analysis." *Journal of Structural Engineering*, 123(2), 237-245.
- Armon, D., Ben-Haim, Y., and Braun, S. (1994). "Crack detection in beams by rankordering of eigenfrequency shifts." *Mechanical Systems and Signal Processing*, 8(1), 81-91.
- C. Krüamer, C.A.M. De Smet, and G. De Roeck " bridge damage detection tests." *Proc., Proceedings of the International Modal Analysis Conference (IMAC)*, 1023—1029.
- Casas, J. R., and Aparicio, A. C. (1994). "Structural damage identification from dynamic-test data." *Journal of Structural Engineering*, 120(8), 2437-2450.
- Cawley, P., and Adams, R. (1979). "The location of defects in structures from measurements of natural frequencies." *The Journal of Strain Analysis for Engineering Design*, 14(2), 49-57.
- Choudhury, M. A. A. S., Shah, S. L., and Thornhill, N. F. (2004b). "Diagnosis of poor control-loop performance using higher-order statistics." *Automatica*, 40(10), 1719-1728.
- Choudhury, M. A. A. S., Shah, S. L., and Thornhill, N. F. (2006). "Linear or Nonlinear? A Bicoherence-Based Measure of Nonlinearity " *Diagnosis of Process Nonlinearities and Valve Stiction*, Springer-Verlag Berlin Heidelberg, 77-91.
- Choudhury, M. A. A. S., Shook, D. S., and Shah, S. L. "Linear or nonlinear? A bicoherence based metric of nonlinearity measure." *Proc., Fault Detection, Supervision and Safety of Technical Processes*, 617-622.
- Collis, W., White, P., and Hammond, J. (1998). "Higher-order spectra: the bispectrum and trispectrum." *Mechanical systems and signal processing*, 12(3), 375-394.
- Das, P., Owen, J., Eccles, B., Woodings, M., and Choo, B. (1997). "Role of Dynamic Testing in Assessment of Bridges." *Transportation Research Record: Journal of the Transportation Research Board*(1594), 115-124.
- Eccles, B., Owen, J., Woodings, M., and Choo, B. "A proposed new approach to full life quantitative bridge assessment." *Proc., Proceedings of the seventh international conference on structural faults and repair, held the assembly rooms, edinburgh, uk, 8 july 1997. Vol 1: extending the life of bridges*.
- Farrar, C., and James III, G. (1997). "System identification from ambient vibration measurements on a bridge." *Journal of Sound and Vibration*, 205(1), 1-18.

- Farrar, C. R., and Jauregui, D. A. (1998). "Comparative study of damage identification algorithms applied to a bridge: I. Experimental study." *Smart materials and structures*, 7(5), 704-719.
- Felber, A., and Ventura, C. "Frequency domain analysis of the ambient vibration data of the queensborough bridge main span." *Proc., Proceedings-spie the international society for optical engineering*, Spie international society for optical, 459-465.
- Goldsmith, A. (1999). "Damage detection in concrete beams using vibration measurements." *Fourth-Year Undergraduate Project Rep.*
- Humar, J., and Kashif, A. (1993). "Dynamic response of bridges under travelling loads." *Canadian Journal of Civil Engineering*, 20(2), 287-298.
- Kisa, M., and Brandon, J. (2000). "The effects of closure of cracks on the dynamics of a cracked cantilever beam." *Journal of Sound and Vibration*, 238(1), 1-18.
- Maeck, J., Wahab, M., and De Roeck, G. "Damage localization in reinforced concrete beams by dynamic stiffness determination." *Proc., Society for Experimental Mechanics, Inc, 17th International Modal Analysis Conference.*, 1289-1295.
- Maeck, J., Wahab, M. A., Peeters, B., De Roeck, G., De Visscher, J., De Wilde, W., Ndambi, J.-M., and Vantomme, J. (2000). "Damage identification in reinforced concrete structures by dynamic stiffness determination." *Engineering structures*, 22(10), 1339-1349.
- Maguire, J., and Severn, R. (1987). "Assessing the dynamic properties of prototype structures by hammer testing." *Proceedings of the Institution of Civil Engineers*, 83(4), 769-784.
- Mahmoud, M. A., Zaid, M. A., and Harashani, S. A. (1999). "Numerical frequency analysis of uniform beams with a transverse crack." *Communications in numerical methods in engineering*, 15(10), 709-715.
- Morassi, A. (2001). "Identification of a crack in a rod based on changes in a pair of natural frequencies." *Journal of Sound and Vibration*, 242(4), 577-596.
- Nandwana, B., and Maiti, S. (1997). "Detection of the location and size of a crack in stepped cantilever beams based on measurements of natural frequencies." *Journal of Sound and Vibration*, 203(3), 435-446.
- Narkis, Y. (1994). "Identification of crack location in vibrating simply supported beams." *Journal of sound and vibration*, 172(4), 549-558.
- Nikias, C. L., and Petropulu, A. P. (1993). "Higher-Order Spectra Analysis: A Nonlinear Signal Processing Framework. 1993." *PTR Prentice Hall, Englewood Cliffs, NJ.*

- Owen, J. S. (2001). "Structural health monitoring of bridges." *Civil Engineering Colloquium*, University of Oxford, University of Oxford.
- Owen, J. S., and Choo, B. S. (1998). "The use of dynamic testing methods for bridge assessment and monitoring (draft)." University of Nottingham Report No. SR98006.
- Pandey, A., and Biswas, M. (1994). "Damage detection in structures using changes in flexibility." *Journal of sound and vibration*, 169(1), 3-17.
- Pandey, A., Biswas, M., and Samman, M. (1991). "Damage detection from changes in curvature mode shapes." *Journal of sound and vibration*, 145(2), 321-332.
- Prakash Rao, D., Tamhankar, M., and Sharma, S. (1983). "Literature survey on in situ testing of concrete bridges." *Materials and Structures*, 16(6), 457-466.
- Raghavendrachar, M., and Aktan, A. E. (1992). "Flexibility by multireference impact testing for bridge diagnostics." *Journal of Structural Engineering*, 118(8), 2186-2203.
- Rao, T. S., and Gabr, M. (1980). "A test for linearity of stationary time series." *Journal of time series analysis*, 1(2), 145-158.
- Ratcliffe, C. P. (1997). "Damage detection using a modified Laplacian operator on mode shape data." *Journal of Sound and Vibration*, 204(3), 505-517.
- Rivola, A., and White, P. (1998). "Bispectral analysis of the bilinear oscillator with application to the detection of fatigue cracks." *Journal of Sound and Vibration*, 216(5), 889-910.
- Rizos, P., Aspragathos, N., and Dimarogonas, A. (1990). "Identification of crack location and magnitude in a cantilever beam from the vibration modes." *Journal of sound and vibration*, 138(3), 381-388.
- Roberts, G. P. "Recent experience in dynamic monitoring of a multi-span bridge." *Proc., Analysis and Testing of Bridges Seminar*, The Institution of Structural Engineers,.
- Salane, H., and Baldwin Jr, J. (1990). "Identification of modal properties of bridges." *Journal of Structural Engineering*, 116(7), 2008-2021.
- Salawu, O. S. (1997). "Assessment of bridges: use of dynamic testing." *Canadian Journal of Civil Engineering*, 24(2), 218-228.
- Salawu, O. S., and Williams, C. (1995). "Bridge assessment using forced-vibration testing." *Journal of structural engineering*, 121(2), 161-173.
- Shifrin, E., and Ruotolo, R. (1999). "Natural frequencies of a beam with an arbitrary number of cracks." *Journal of Sound and Vibration*, 222(3), 409-423.

- Sundermeyer, J. N., and Weaver, R. (1995). "On crack identification and characterization in a beam by non-linear vibration analysis." *Journal of Sound and Vibration*, 183(5), 857-871.
- Thyagarajan, S., Schulz, M., Pai, P., and Chung, J. (1998). "Detecting structural damage using frequency response functions." *Journal of Sound and Vibration*, 210(1), 162-170.
- Tsyfansky, S., and Beresnevich, V. (2000). "Non-linear vibration method for detection of fatigue cracks in aircraft wings." *Journal of sound and vibration*, 236(1), 49-60.
- Van Den Abeele, K., and De Visscher, J. (2000). "Damage assessment in reinforced concrete using spectral and temporal nonlinear vibration techniques." *Cement and Concrete Research*, 30(9), 1453-1464.
- Wahab, M. A., and De Roeck, G. (1997). "Effect of temperature on dynamic system parameters of a highway bridge." *Structural Engineering International*, 7(4), 266-270.
- Worden, K., and Tomlinson, G. (2001). "Nonlinearity in experimental modal analysis." *Philosophical Transactions of the Royal Society of London A: Mathematical, Physical and Engineering Sciences*, 359(1778), 113-130.

APPENDIX-A

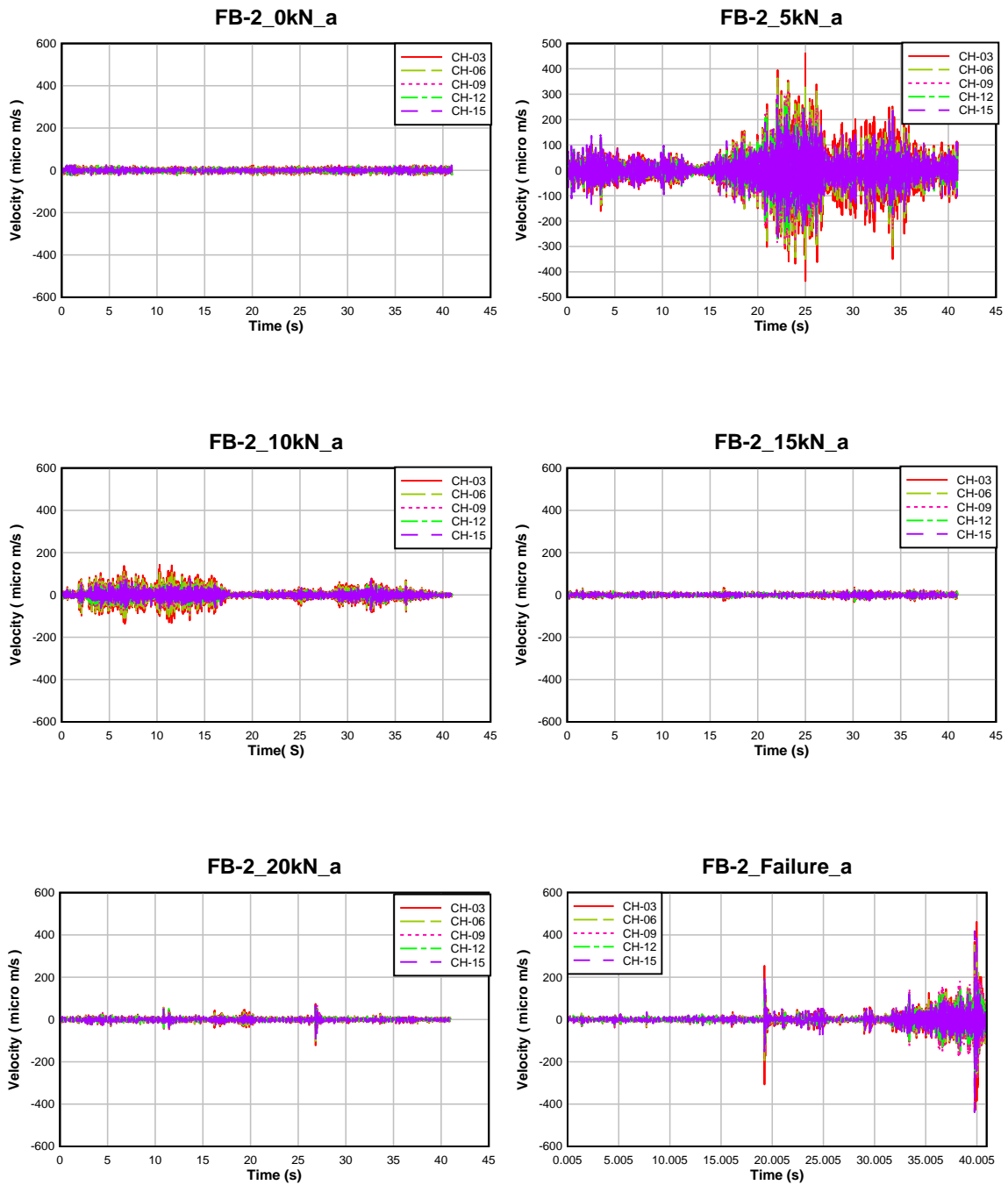


Figure A47: Ambient Time History Recording for Flexure Control Beam-2

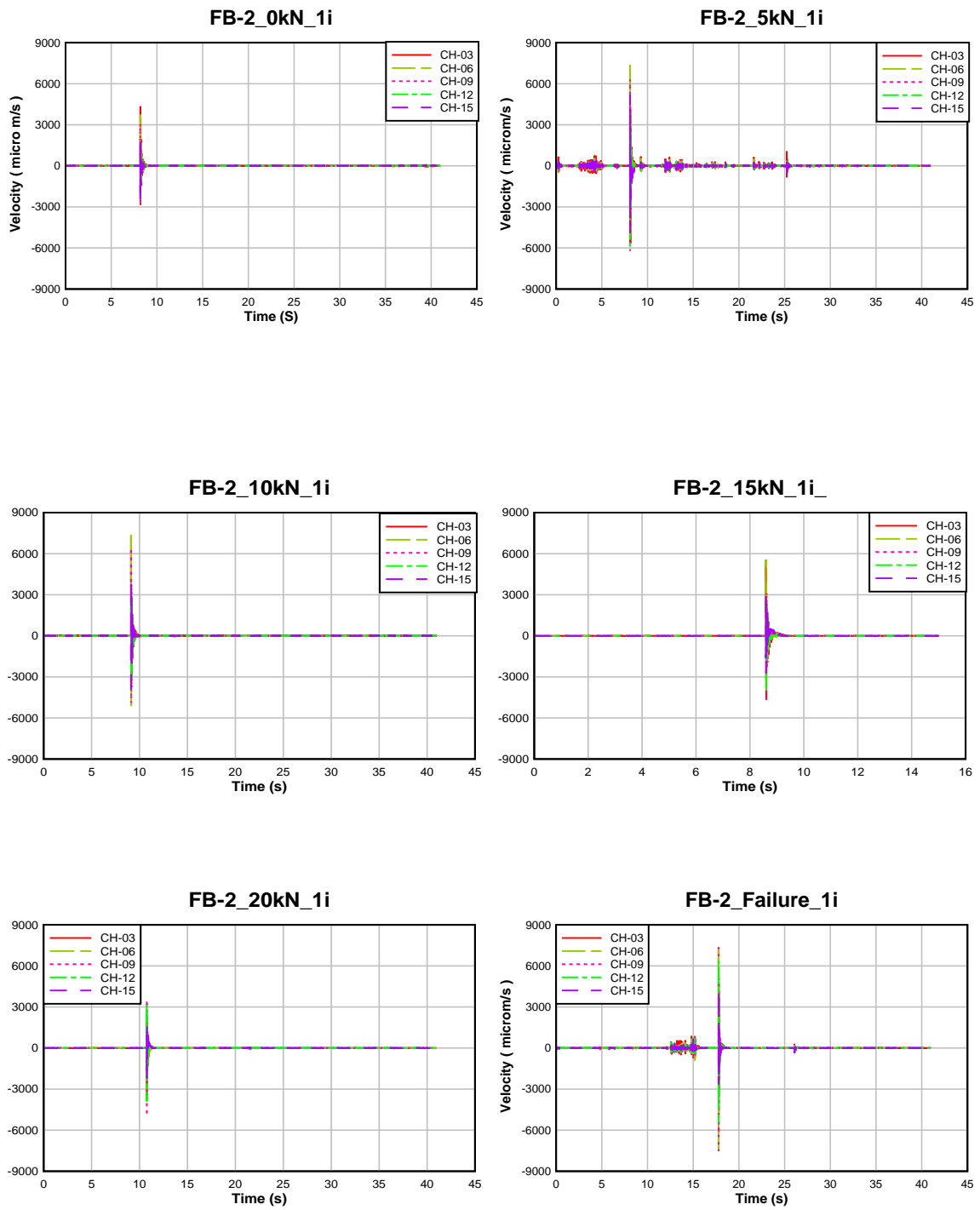


Figure A48: One Impact Time History Recording for Flexure Control Beam-2

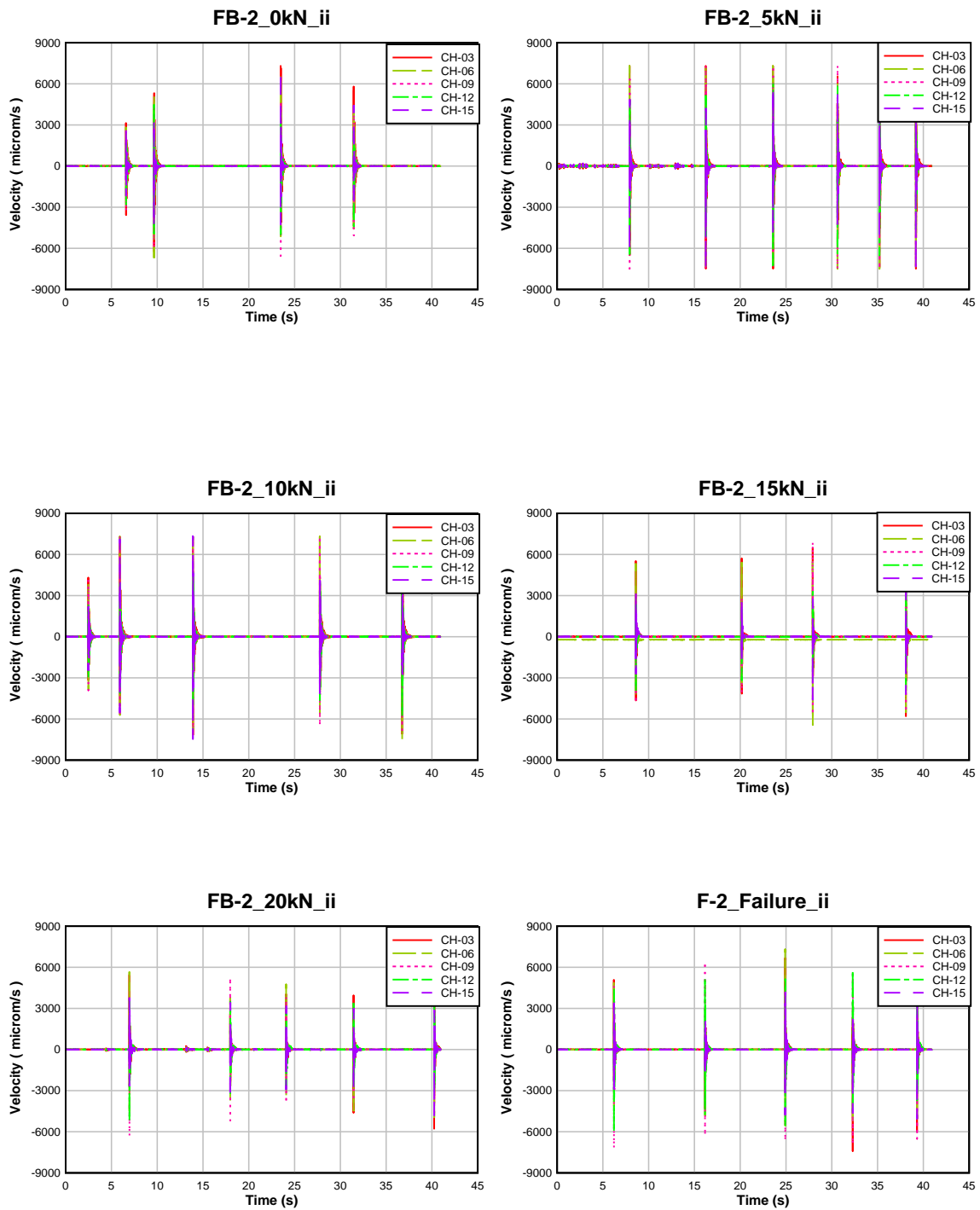


Figure A49: Interval Impact Time History Recording for Flexure Control Beam-2

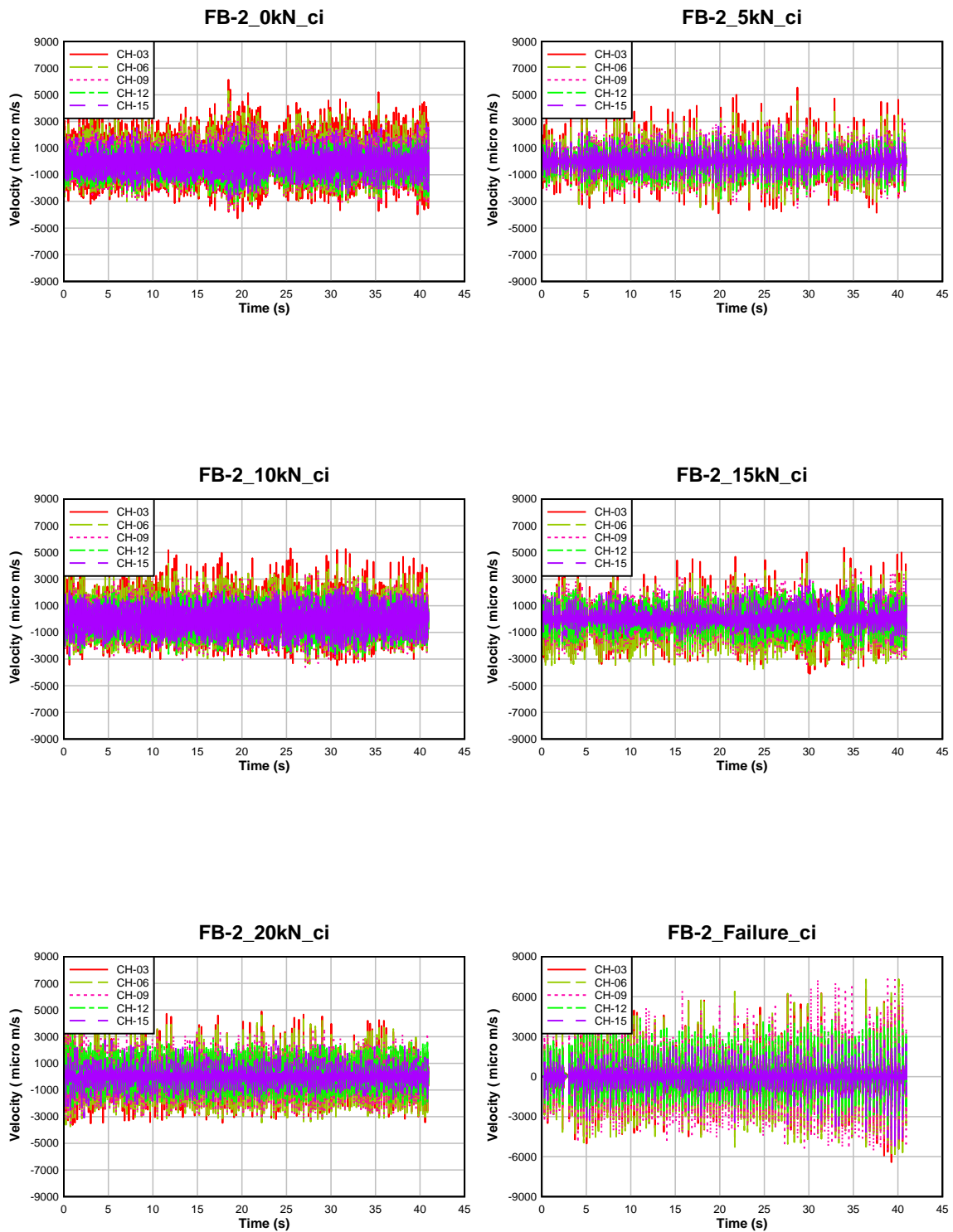


Figure A50: Continuous Impact Time History Recording for Flexure Control Beam-2

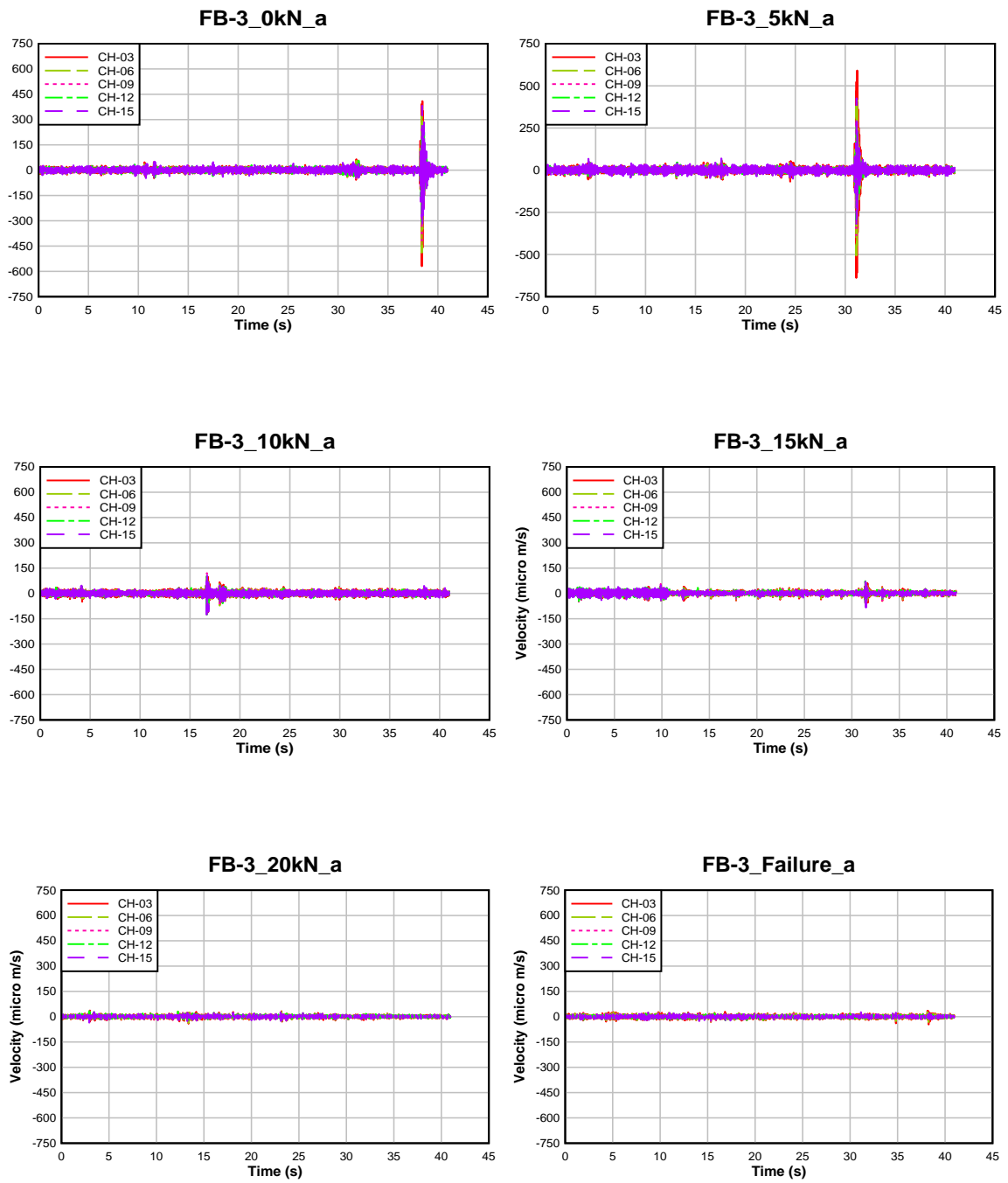


Figure A51: Ambient Time History Recording for Flexure Control Beam-3

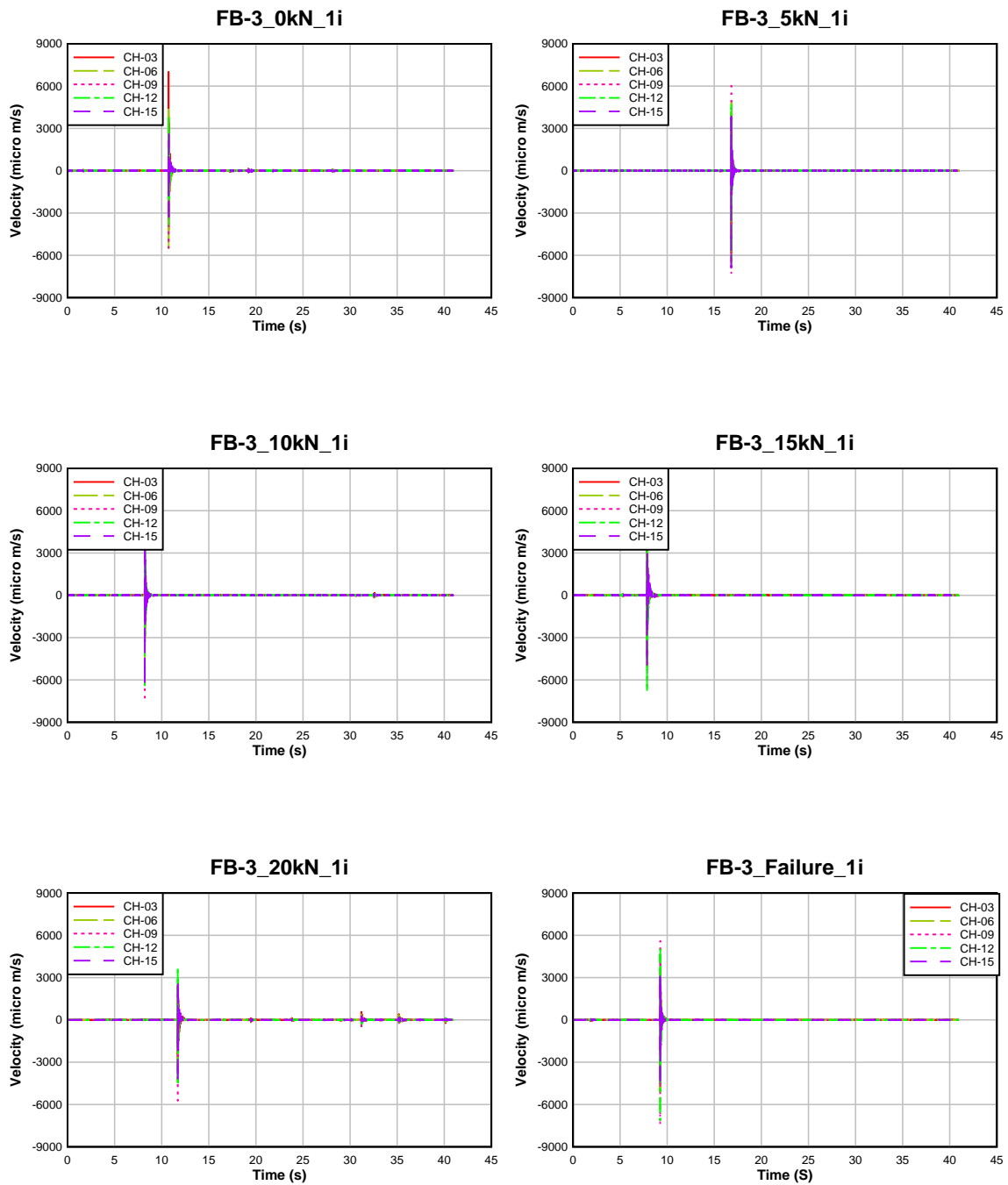


Figure A52: One Impact Time History Recording for Flexure Control Beam-3

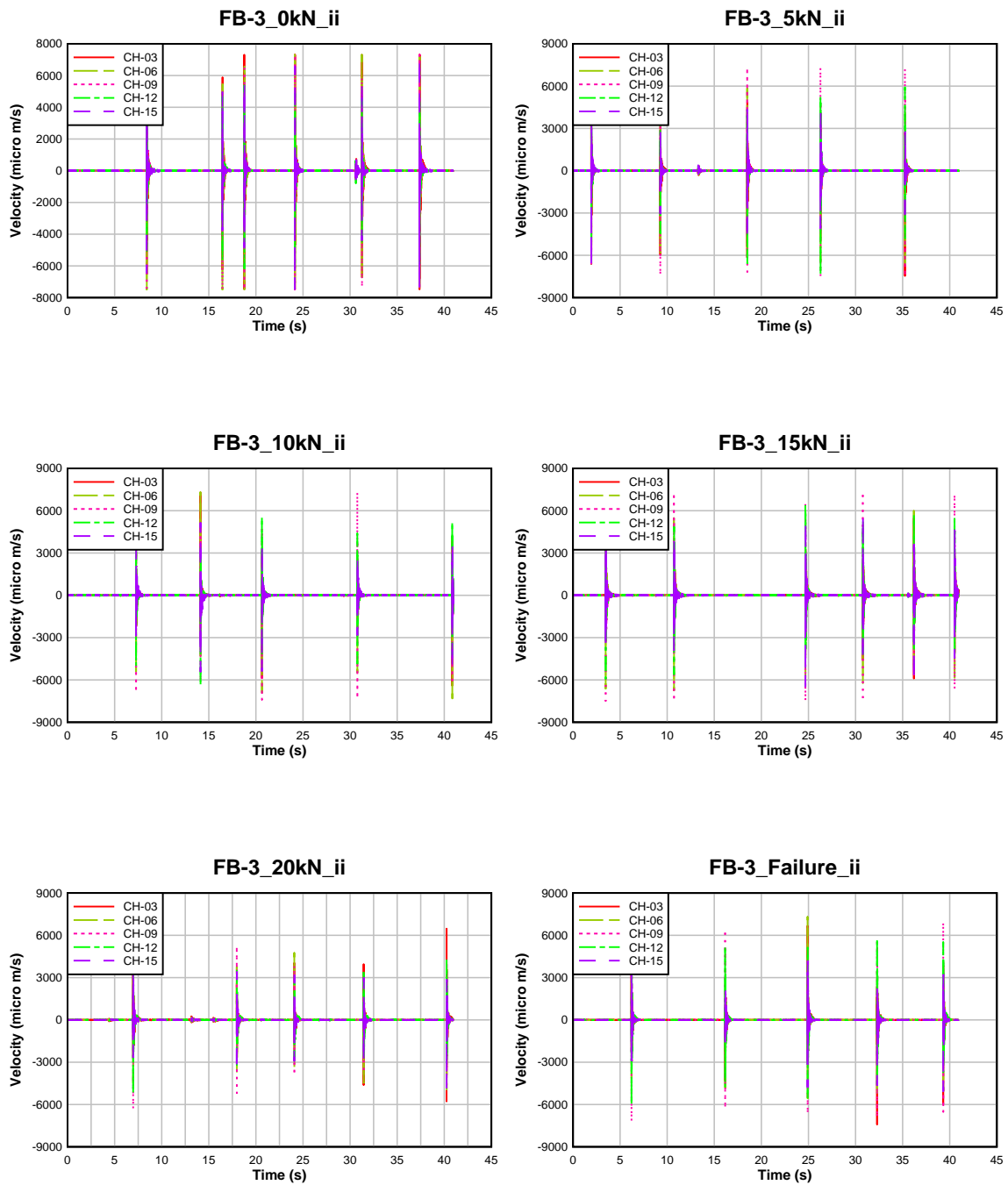


Figure A53: Interval Impact Time History Recording for Flexure Control Beam-3

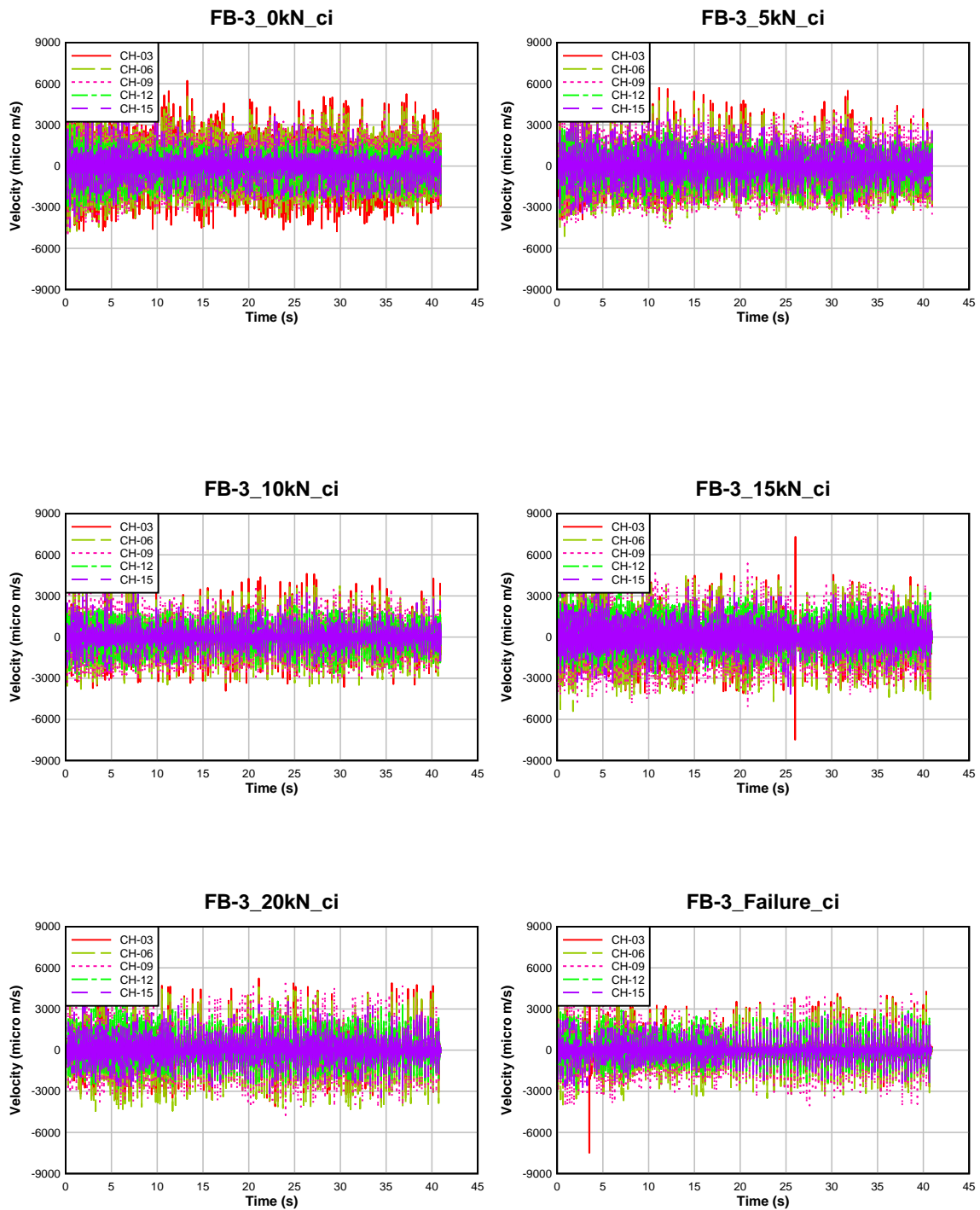


Figure A54: Continuous Impact Time History Recording for Flexure Control Beam-3

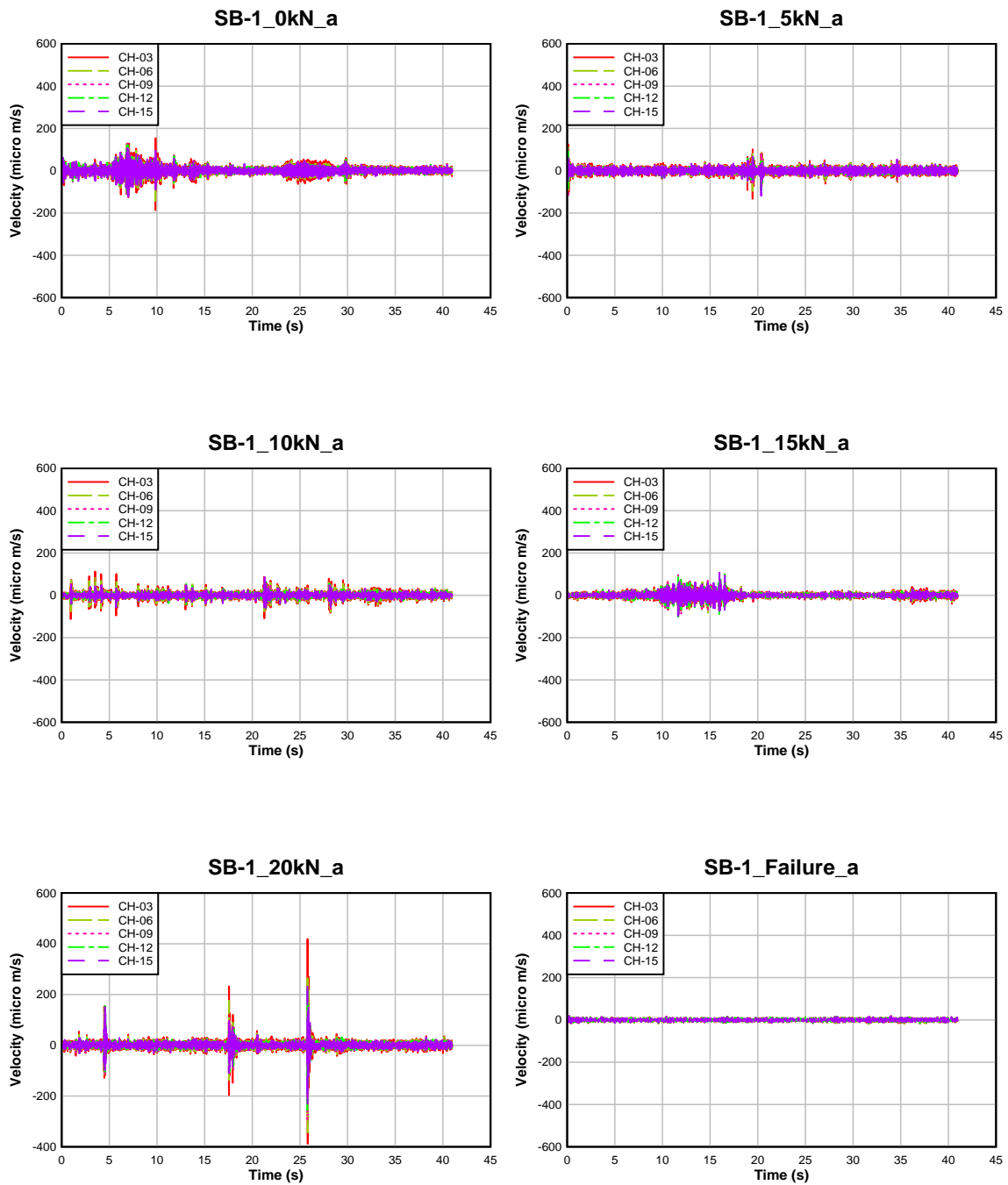


Figure A55: Ambient Time History Recording for Shear Control Beam-1

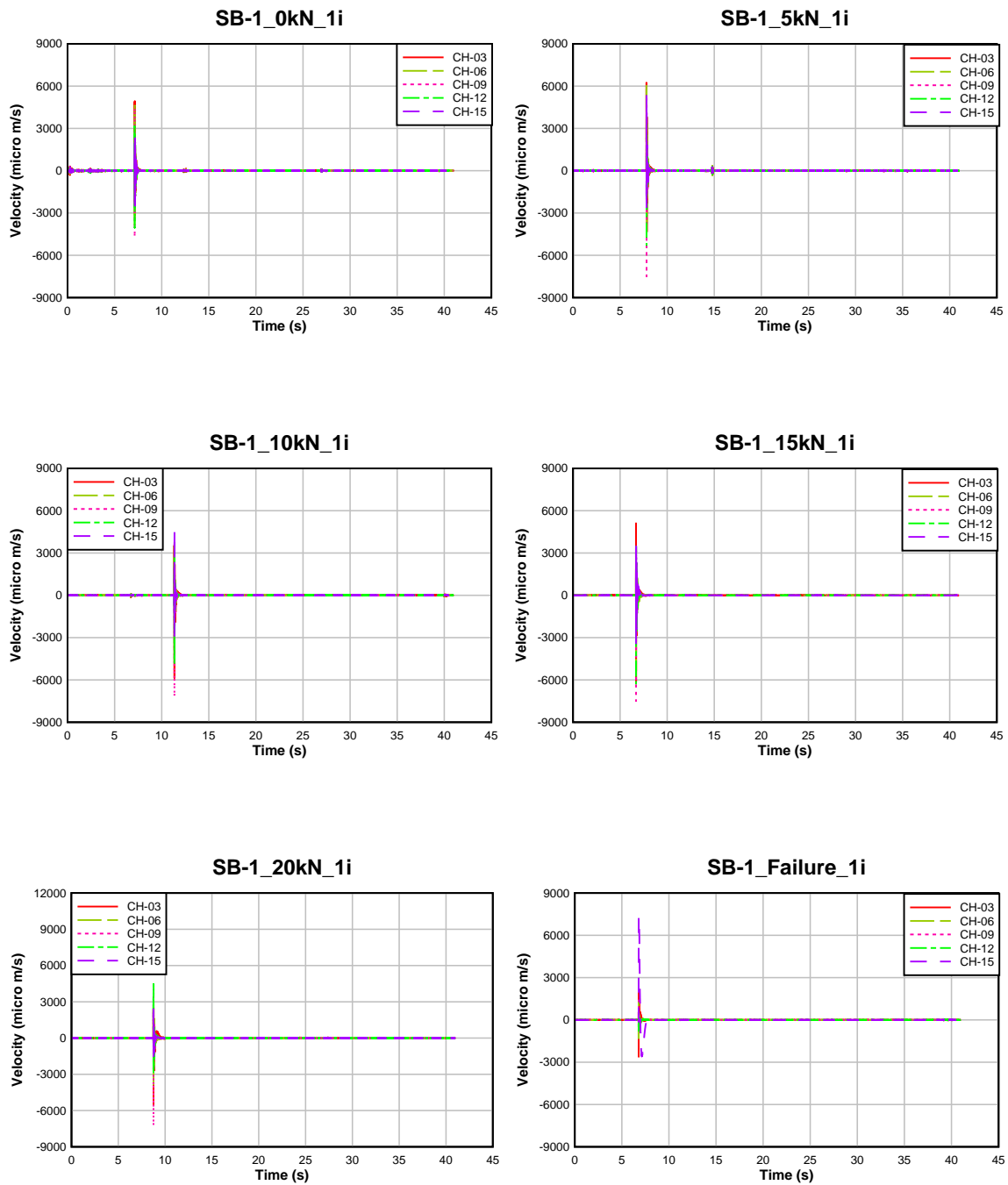


Figure A56: One Impact Time History Recording for Shear Control Beam-1

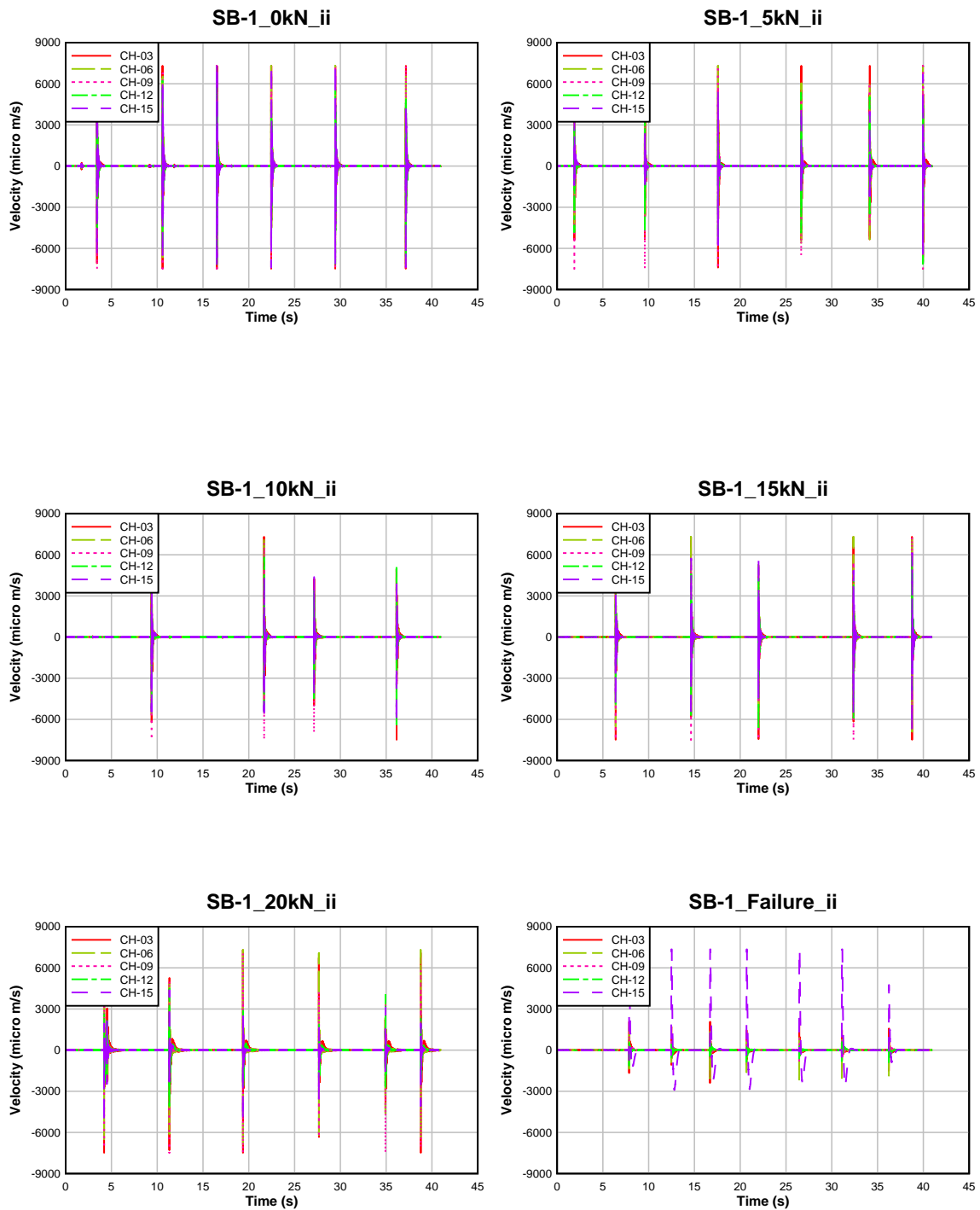


Figure A57: Interval Impact Time History Recording for Shear Control Beam-1

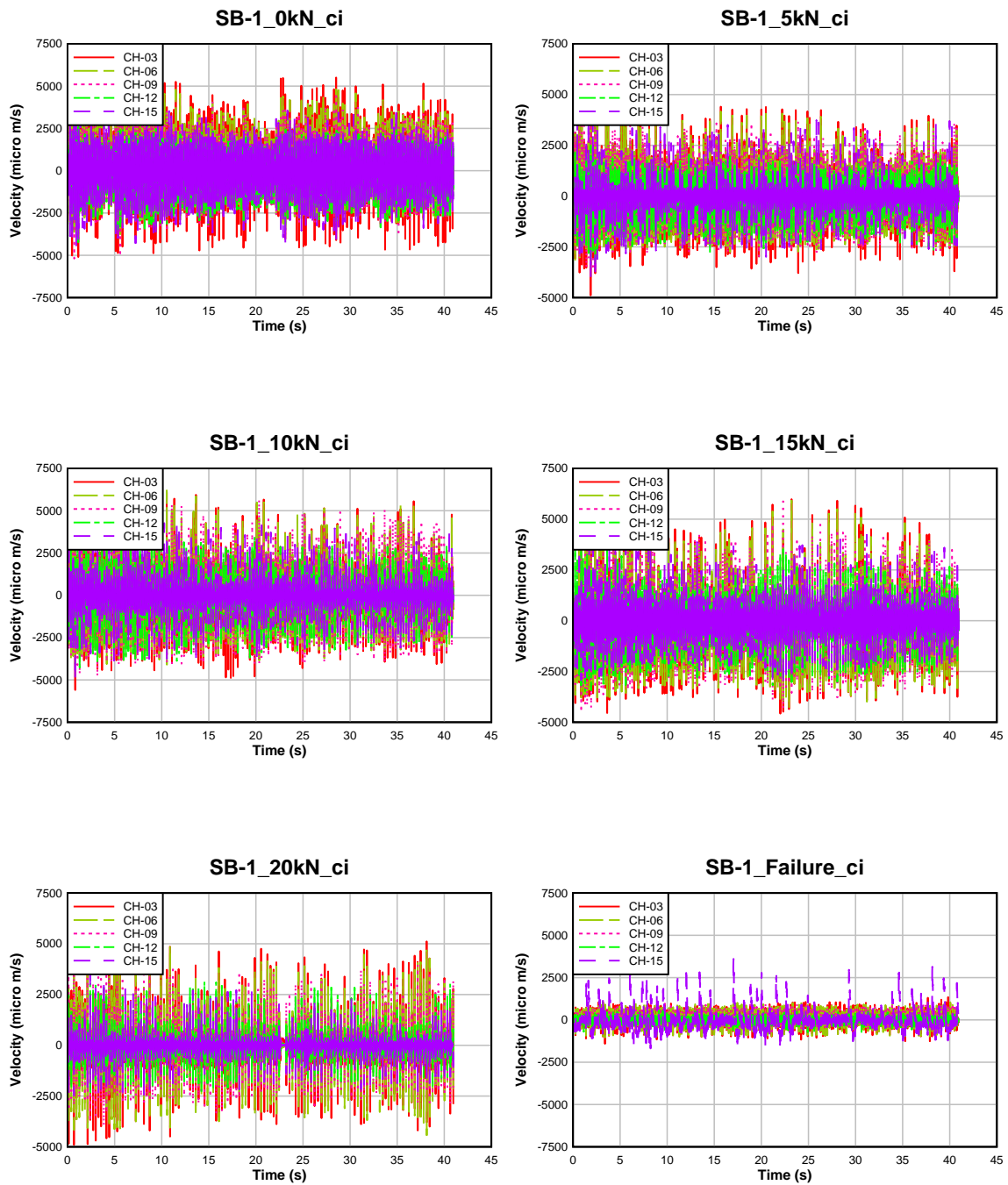


Figure A58: Continuous Impact Time History Recording for Shear Control Beam-1

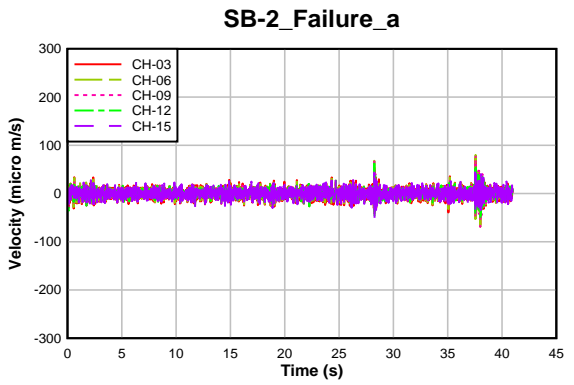
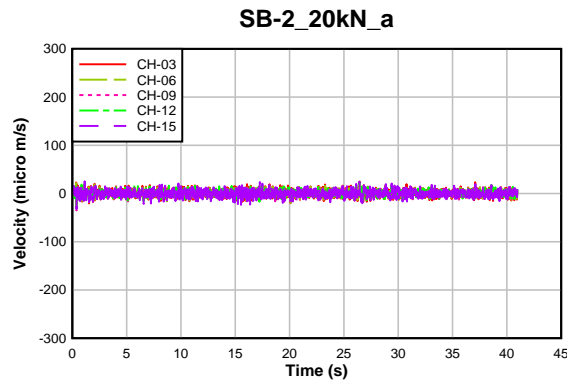
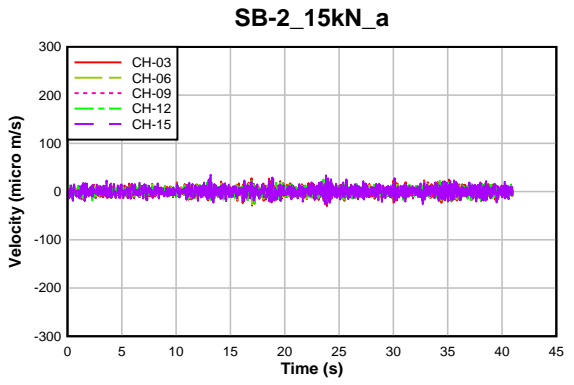
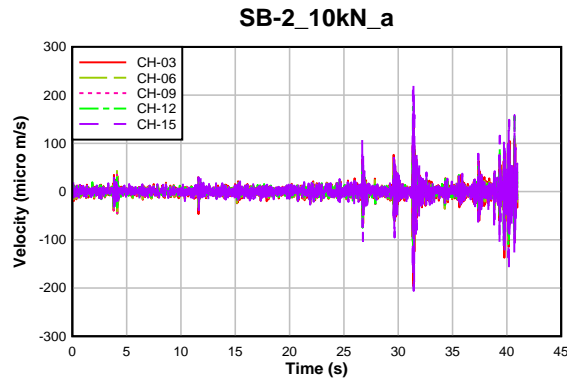
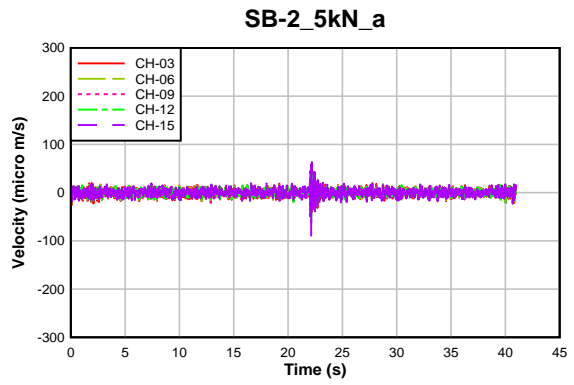
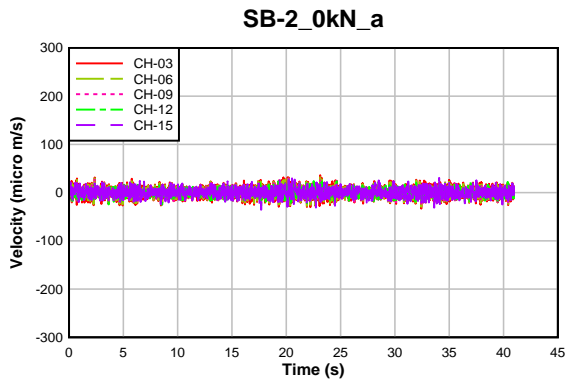


Figure A59: Ambient Time History Recording for Shear Control Beam-2

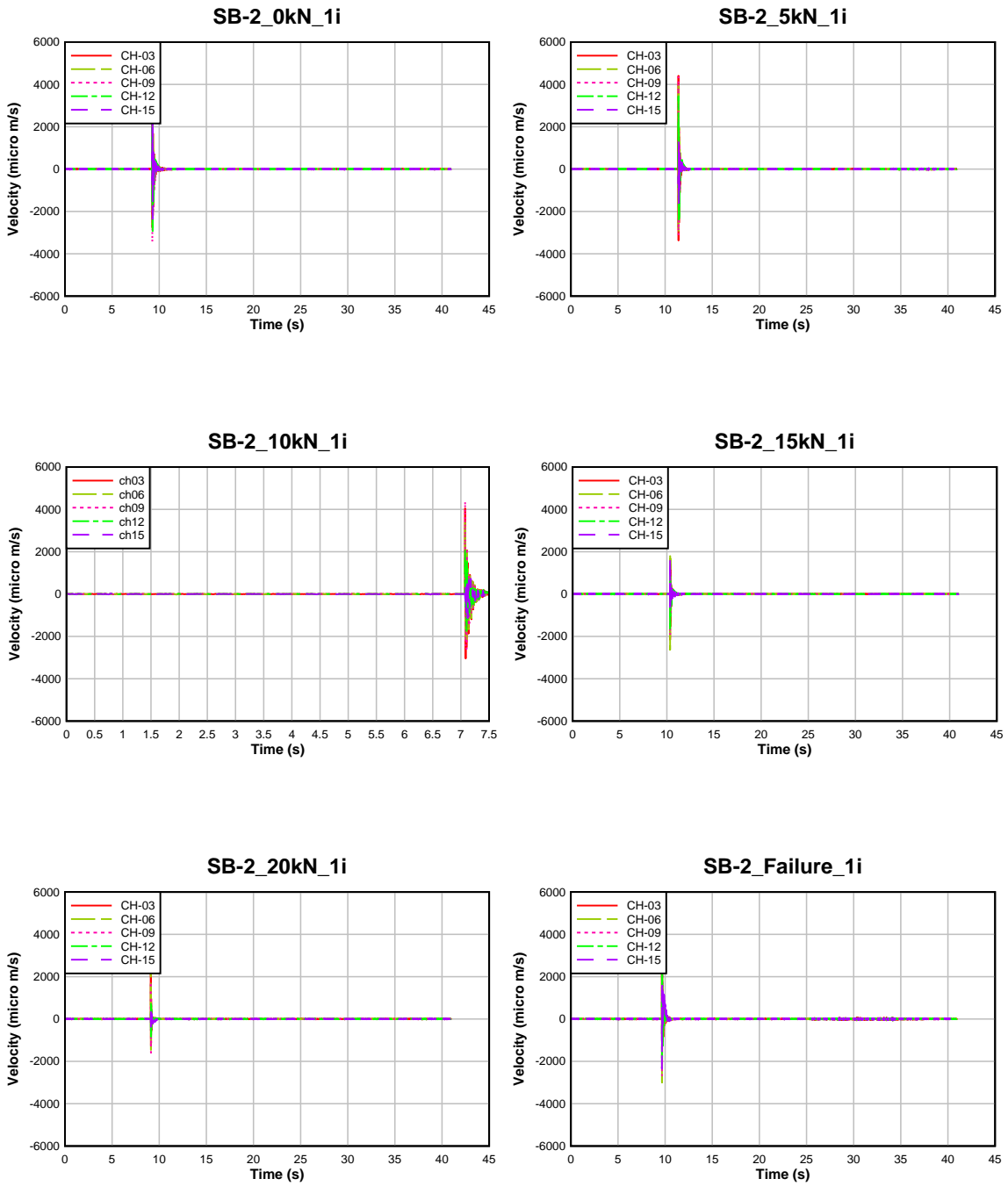


Figure A60: One Impact Time History Recording for Shear Control Beam-2

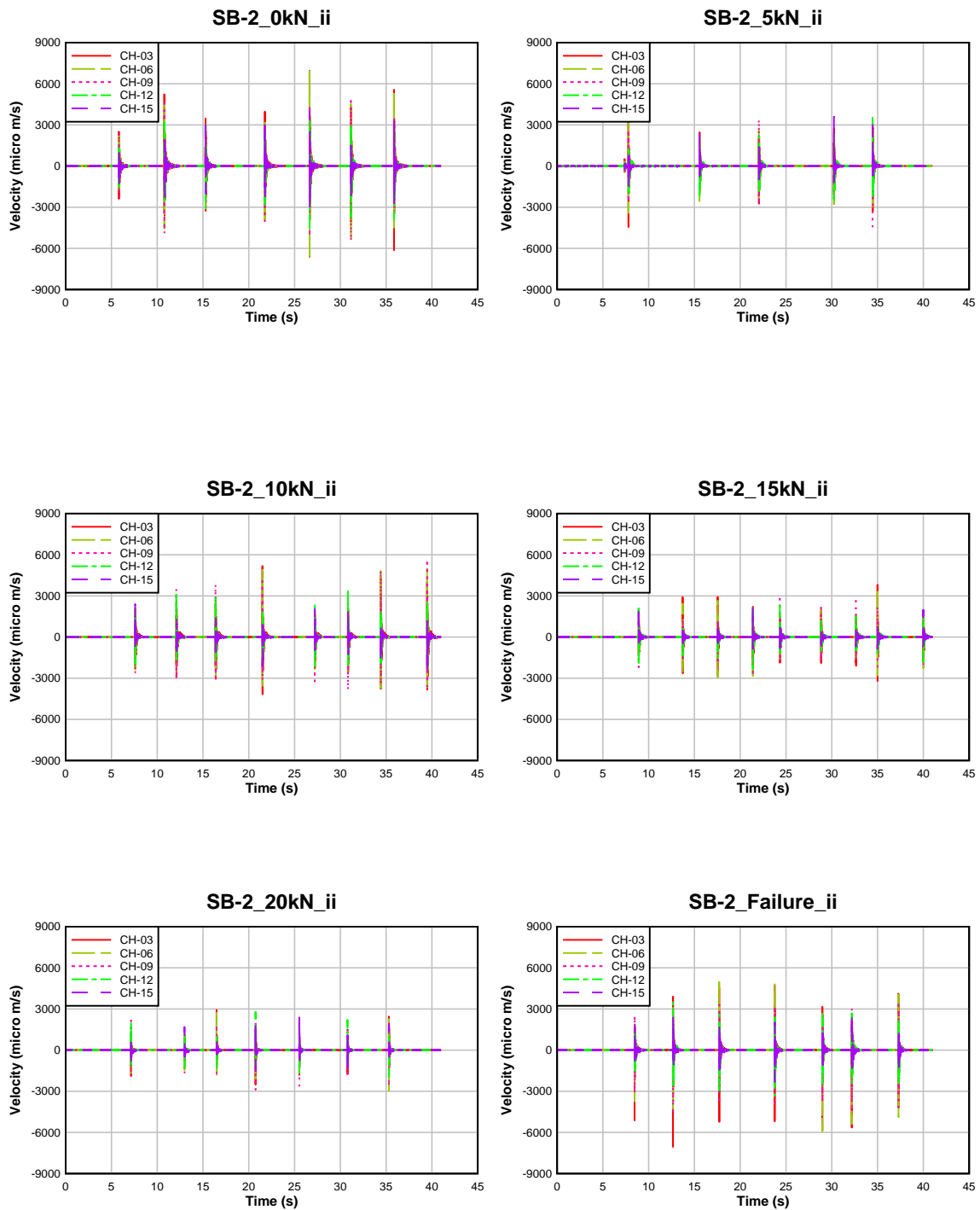


Figure A61: Interval Impact Time History Recording for Shear Control Beam-2

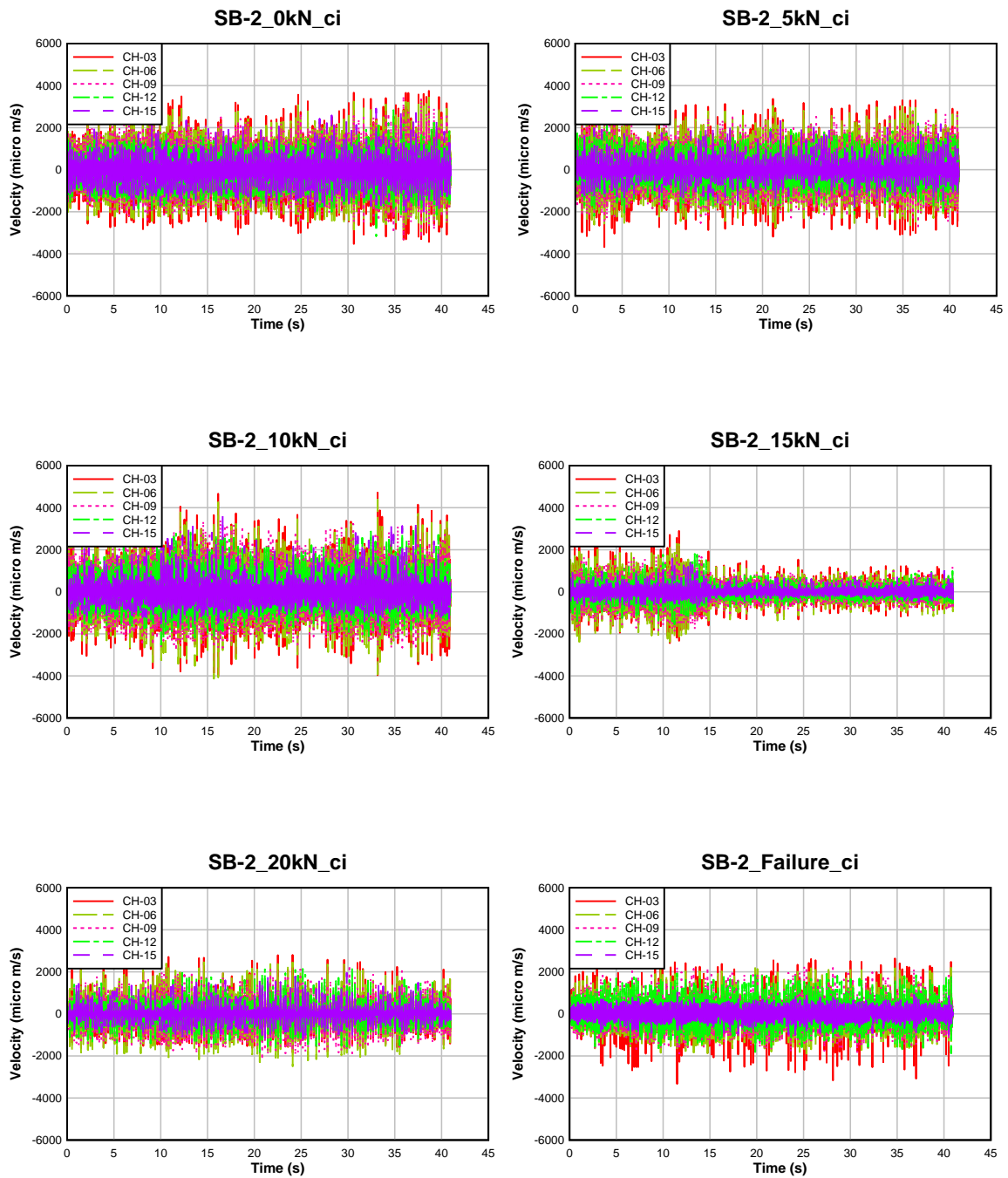


Figure A62: Continuous Impact Time History Recording for Shear Control Beam-2

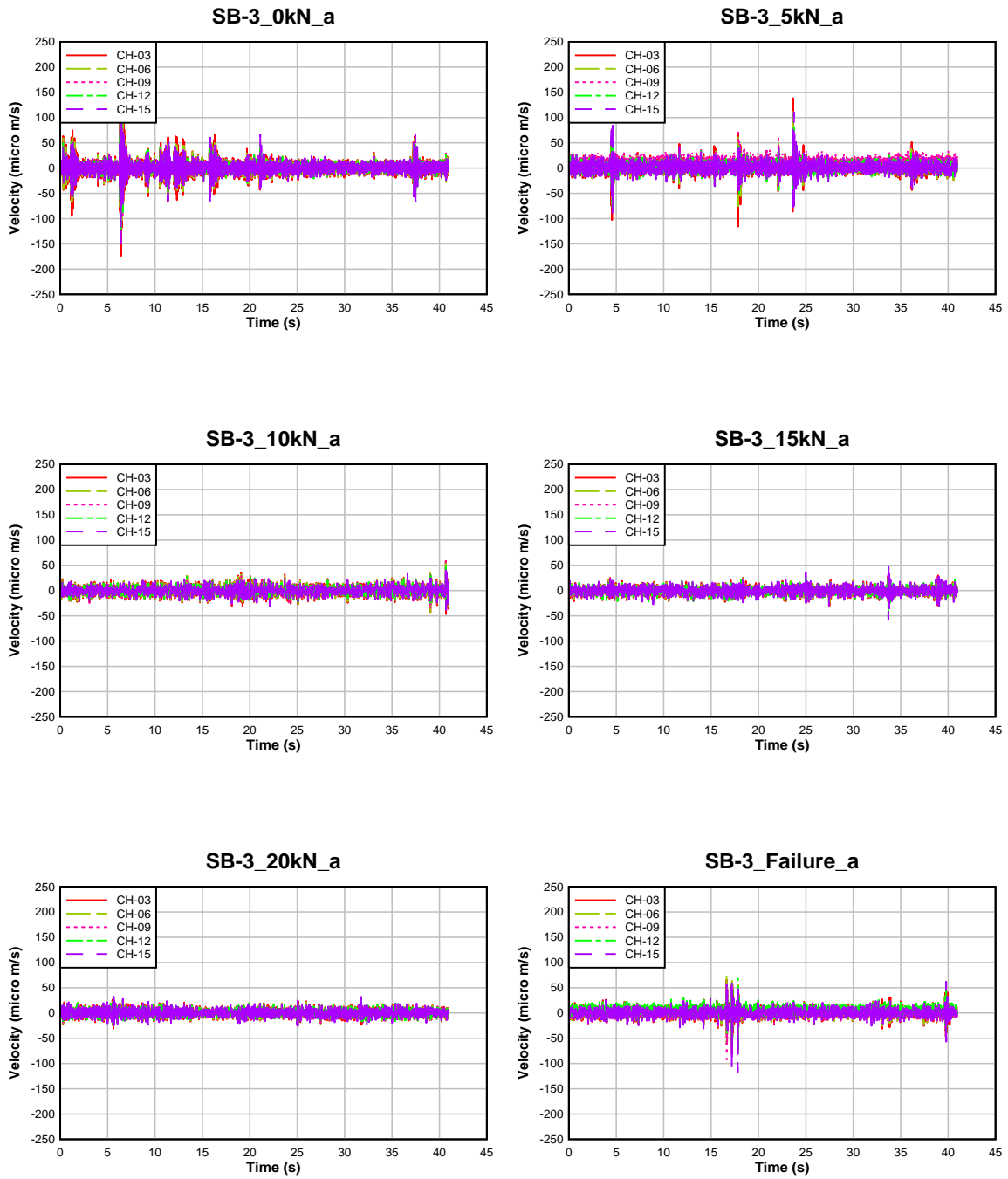


Figure A63: Ambient Time History Recording for Shear Control Beam-3

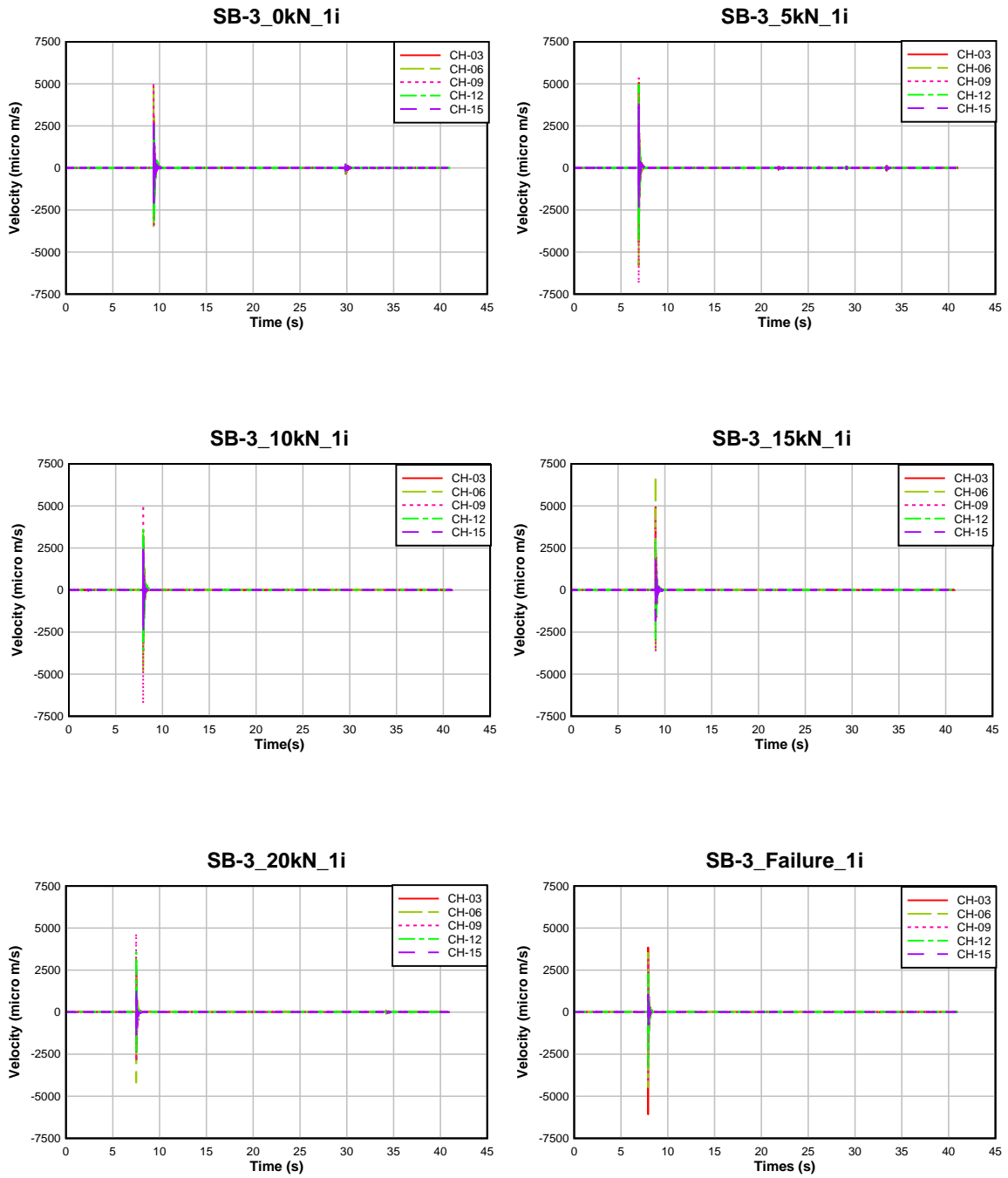


Figure A64: One Impact Time History Recording for Shear Control Beam-3

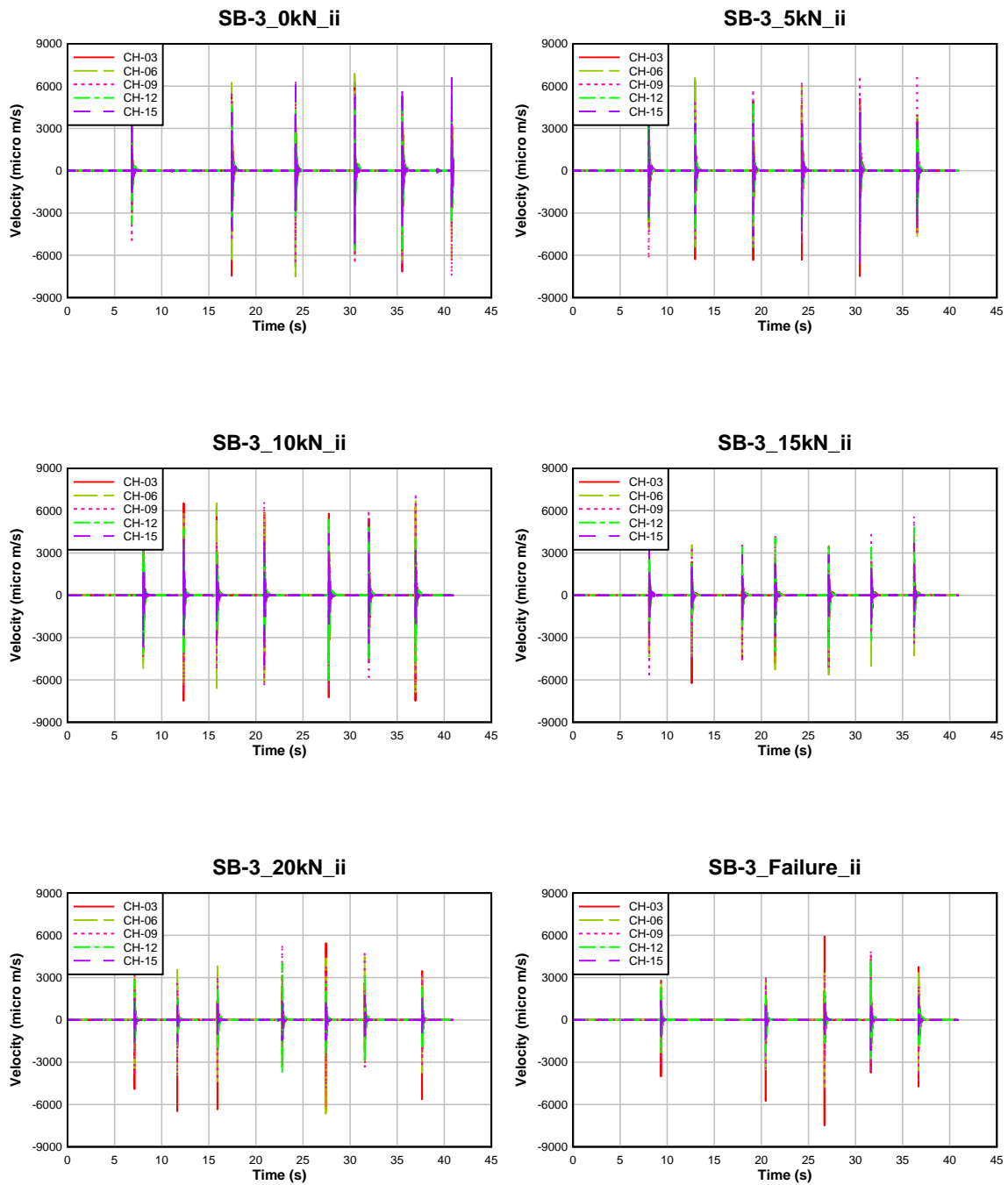


Figure A65: Interval Impact Time History Recording for Shear Control Beam-3

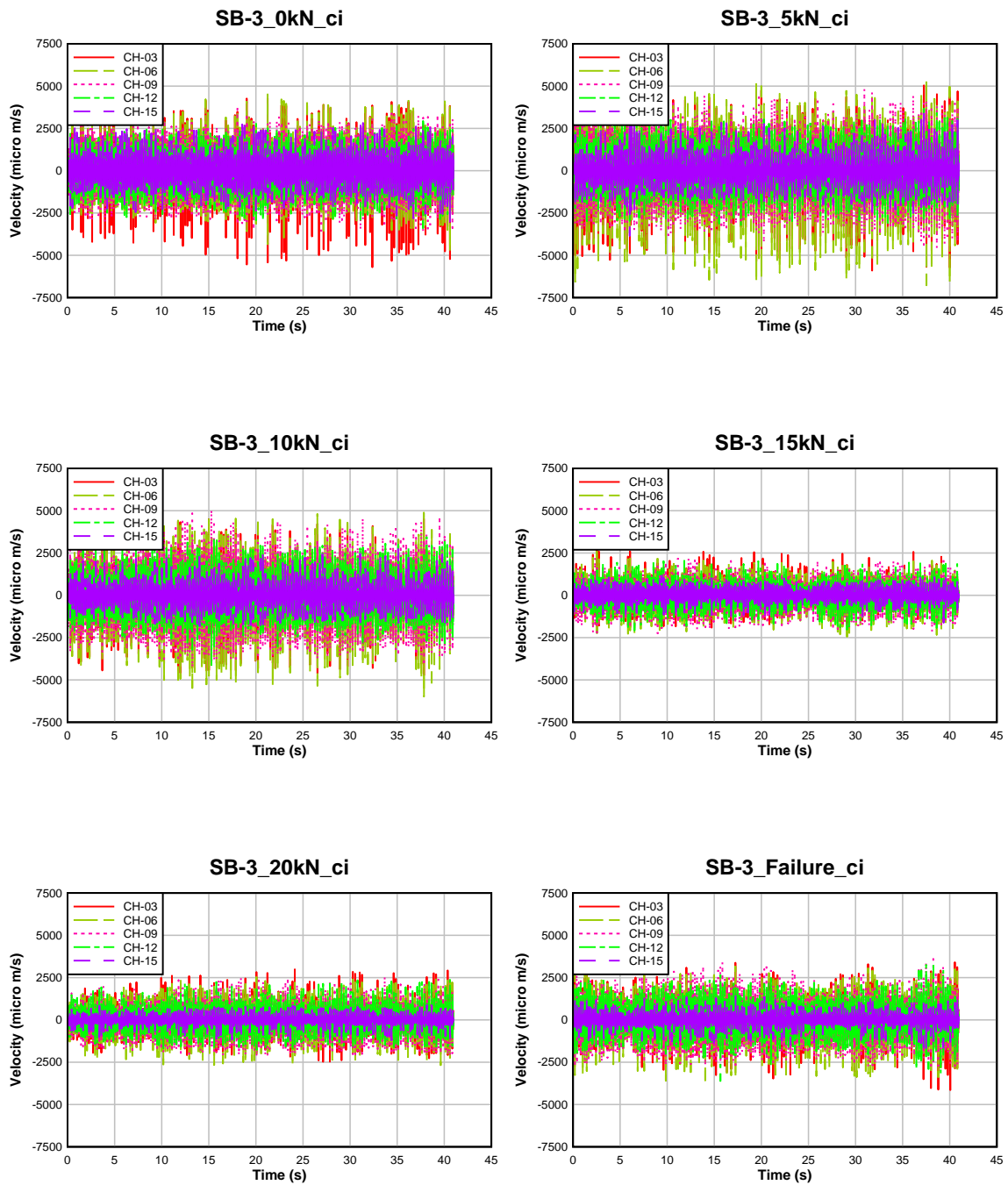


Figure A66: Continuous Impact Time History Recording for Shear Control Beam-3

APPENDIX-B

Material Properties of Fine Aggregate

Table B6: Sieve Analysis of Fine Aggregate

SIEVE SIZE	MASS RETAIN (gm)	INDIVIDUAL % RETAIN	CUMULATIVE % RETAIN	% PASSING
4.75 mm (No. 4)	0	0	0	100
2.36 mm (No. 8)	11	2	2	98
1.18 mm (No. 16)	45	9	11	89
600 μm (No. 30)	112	22	34	66
300 μm (No. 50)	190	38	72	28
150 μm (No. 100)	109	22	94	6
75 μm (No. 200)	22	4	98	2
pan	11	2	96	4
TOTAL	500		2.13	

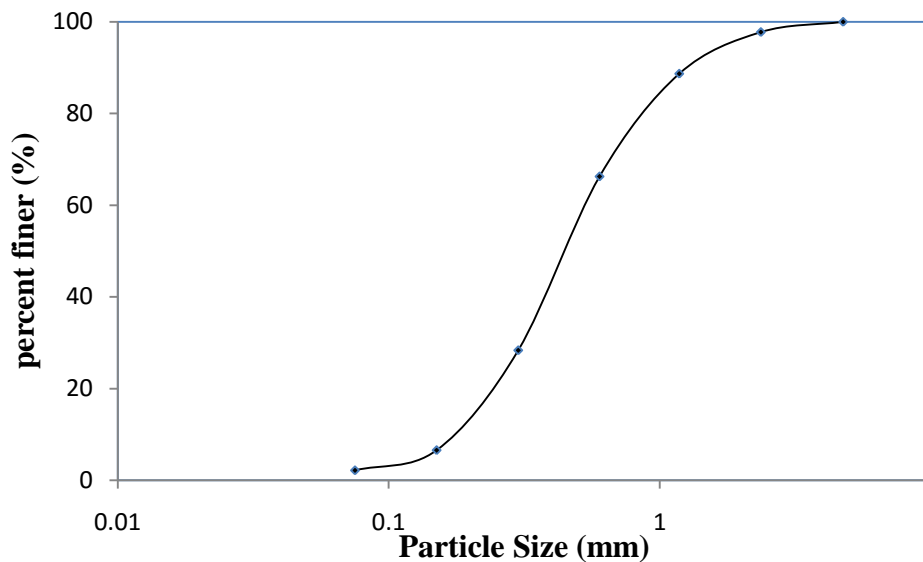


Figure B67: Grain Size Distribution of Fine Aggregate

Table B7: Specific Gravity and Absorption Capacity of Sand

Test for Specific Gravity and Absorption Capacity of Sand							
Test Method ASTM C128-88							
Oven Dry Sample (gm)	Pyc+Water (gm)	pyc+Water +Sample (gm)	SSD wt of Sample(gm)	Absorption Capacity (nearest 0.1%)	Specific Gravity (nearest 0.01)		
					Bulk	SSD	Aparent
492.6	1321.4	1629.7	500	1.5	2.57	2.61	2.67

Table B8: Unit Wt of Fine Aggregate

UNIT Wt OF FINE AGGREGATE		
Weight of Mold (T)	2625	gm
Weight of Sand + Mold (G)	7102	gm
Volume of Mold (V)	2832	cm3
Unit Wt	1.581	gm/cm3
	1581	kg/m3

Material Properties of Coarse Aggregate

Table B9: Grain Size Analysis of Coarse Aggregate

SIEVE SIZE	SIZE	MASS RETAIN (gm)	INDIVIDUAL % RETAIN	CUMULATIVE % RETAIN	% PASSING
25 mm (1in)	25	0	0	0	100
19 mm (3/4 in)	19	0	0	0	100
12.5 mm (1/2 in)	12.5	33	2	2	98
9.5 mm (3/8 in)	9.5	303	15	17	83
4.755 mm (No. 4)	4.75	1477.3	74	91	9
2.36 mm (No. 8)	2.36	181.3	9	100	0
Pan	-	5.4			0
TOTAL		2000			

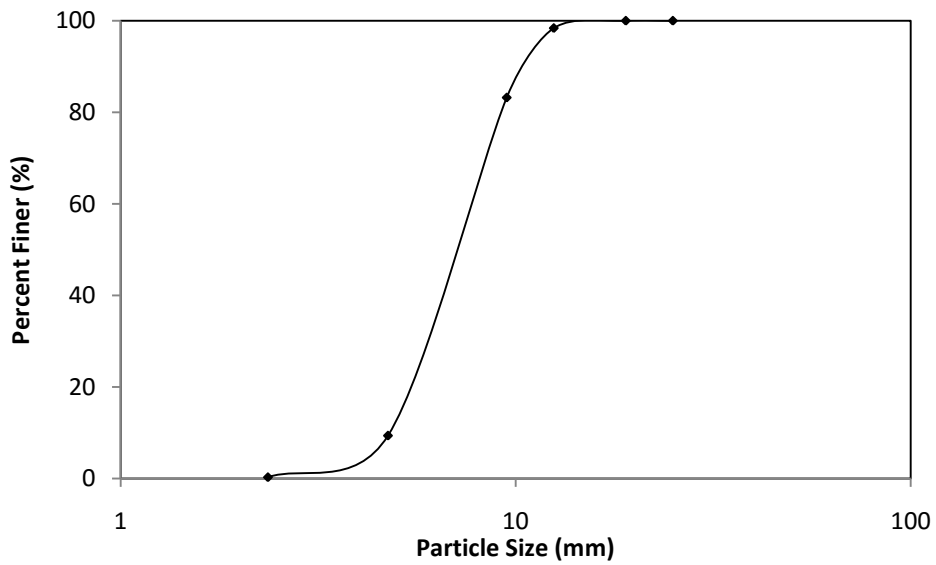


Figure B68: Grain Size Distribution of Fine Aggregate

Table B10: Specific Gravity and Absorption Capacity of Coarse Aggregate

Test for Specific Gravity and Absorption Capacity of Coarse Aggregate						
Test Method ASTM C128-88						
Oven Dry Sample (gm)	SSD wt in air (gm)	SSD wt in water (gm)	Absorption Capacity (nearest 0.1%)	Specific Gravity (nearest 0.01)		
				Bulk	SSD	Apparent
1942.6	1982	1796.6	2.03	10.48	10.69	13.31

Table B11: Unit Wt of Coarse Aggregate

UNIT Wt OF COARSE AGGREGATE			
Weight of Mold (T)	2625	gm	
Weight of Stone + Mold (G)	6686	gm	
Volume of Mold (V)	2832	cm ³	
Unit Wt	1.434	gm/cm ³	
	1434	kg/m ³	

Table B12: Mix Design for Beam Casting

MATERIAL	For 1m ³ of Concrete (SSD Basis)	Adjusted Mass (Kg)	For Beam And Cylinder (Kg)
Water	216	203	41.3
Cement	415	415	84.3
F.A	789	682	138.6
C.A	855	817	166

APPENDIX- C

		NGI	NLI			NGI	NLI
f-2_0kn_a	CH03	0.28	0.54	f-2_0kn_li	CH03	0.44	0.74
	CH06	0.28	0.52		CH06	0.44	0.77
	CH09 (mid)	0.26	0.54		CH09 (mid)	0.39	0.65
	CH12	0.26	0.48		CH12	0.42	0.73
	CH15	0.27	0.51		CH15	0.35	0.45
	Avg	0.27	0.518		Avg	0.408	0.668
f-2_5kn_a	CH03	0.3	0.63	f-2_5kn_li	CH03	0.38	0.68
	CH06	0.3	0.62		CH06	0.36	0.64
	CH09 (mid)	0.29	0.59		CH09 (mid)	0.42	0.56
	CH12	0.29	0.57		CH12	0.37	0.58
	CH15	0.29	0.66		CH15	0.35	0.8
	Avg	0.294	0.614		Avg	0.376	0.652
f-2_10kn_a	CH03	0.27	0.45	f-2_10kn_li	CH03	0.4	0.7
	CH06	0.26	0.47		CH06	0.38	0.69
	CH09 (mid)	0.28	0.6		CH09 (mid)	0.4	0.65
	CH12	0.26	0.47		CH12	0.48	0.73
	CH15	0.28	0.52		CH15	0.41	0.68
	Avg	0.27	0.502		Avg	0.414	0.69
f-2_15kn_a	CH03	0.26	0.44	f-2_15kn_li	CH03	0.82	0.63
	CH06	0.26	0.45		CH06	0.79	0.51
	CH09 (mid)	0.27	0.43		CH09 (mid)	0.88	0.65
	CH12	0.27	0.47		CH12	0.86	0.68
	CH15	0.27	0.46		CH15	0.82	0.85
	Avg	0.266	0.45		Avg	0.834	0.664
f-2_20kn_a	CH03	0.26	0.47	f-2_20kn_li	CH03	0.39	0.64
	CH06	0.27	0.49		CH06	0.38	0.68
	CH09 (mid)	0.27	0.55		CH09 (mid)	0.45	0.63
	CH12	0.28	0.59		CH12	0.46	0.69
	CH15	0.26	0.57		CH15	0.4	0.81
	Avg	0.268	0.534		Avg	0.416	0.69
f-2_failure_a	CH03	0.37	0.84	f-2_failure_li	CH03	0.4	0.65
	CH06	0.34	0.85		CH06	0.38	0.56
	CH09 (mid)	0.4	0.9		CH09 (mid)	0.43	0.64
	CH12	0.39	0.91		CH12	0.4	0.69
	CH15	0.34	0.74		CH15	0.32	0.51
	Avg	0.368	0.848		Avg	0.386	0.61

		NGI	NLI				NGI	NLI
f-2_0kn_ii	CH03	0.37	0.55	f-2_0kn_ci	CH03	0.26	0.47	
	CH06	0.39	0.61		CH06	0.25	0.54	
	CH09 (mid)	0.36	0.71		CH09 (mid)	0.24	0.34	
	CH12	0.36	0.57		CH12	0.27	0.45	
	CH15	0.29	0.37		CH15	0.25	0.41	
	Avg	0.354	0.562		Avg	0.254	0.442	
f-2_5kn_ii	CH03	0.36	0.64	f-2_5kn_ci	CH03	0.25	0.33	
	CH06	0.31	0.4		CH06	0.25	0.35	
	CH09 (mid)	0.38	0.5		CH09 (mid)	0.26	0.4	
	CH12	0.42	0.59		CH12	0.26	0.44	
	CH15	0.29	0.39		CH15	0.25	0.41	
	Avg	0.352	0.504		Avg	0.254	0.386	
f-2_10kn_ii	CH03	0.37	0.66	f-2_10kn_ci	CH03	0.27	0.53	
	CH06	0.35	0.63		CH06	0.28	0.68	
	CH09 (mid)	0.39	0.6		CH09 (mid)	0.29	0.7	
	CH12	0.46	0.64		CH12	0.26	0.48	
	CH15	0.35	0.52		CH15	0.27	0.59	
	Avg	0.384	0.61		Avg	0.274	0.596	
f-2_15kn_ii	CH03	0.37	0.58	f-2_15kn_ci	CH03	0.24	0.31	
	CH06	0.38	0.42		CH06	0.24	0.31	
	CH09 (mid)	0.39	0.55		CH09 (mid)	0.25	0.42	
	CH12	0.39	0.62		CH12	0.26	0.41	
	CH15	0.27	0.36		CH15	0.25	0.37	
	Avg	0.36	0.506		Avg	0.248	0.364	
f-2_20kn_ii	CH03			f-2_20kn_ci	CH03	0.34	0.7	
	CH06				CH06	0.28	0.71	
	CH09 (mid)				CH09 (mid)	0.26	0.49	
	CH12				CH12	0.35	0.76	
	CH15				CH15	0.25	0.49	
	Avg				Avg	0.296	0.63	
f-2_failure_ii	CH03			f-2_failure_ci	CH03	0.32	0.66	
	CH06				CH06	0.25	0.37	
	CH09 (mid)				CH09 (mid)	0.26	0.55	
	CH12				CH12	0.35	0.71	
	CH15				CH15	0.24	0.38	
	Avg				Avg	0.284	0.534	

		NGI	NLI				NGI	NLI
f-3_0kn_a	CH03	0.42	0.76	f-3_0kn_li	CH03	0.4	0.66	
	CH06	0.48	0.77		CH06	0.39	0.62	
	CH09 (mid)	0.52	0.79		CH09 (mid)	0.37	0.63	
	CH12	0.47	0.83		CH12	0.39	0.6	
	CH15	0.46	0.84		CH15	0.34	0.67	
	Avg	0.47	0.798		Avg	0.378	0.636	
f-3_5kn_a	CH03	0.44	0.82	f-3_5kn_li	CH03	0.41	0.49	
	CH06	0.46	0.82		CH06	0.41	0.53	
	CH09 (mid)	0.45	0.8		CH09 (mid)	0.42	0.48	
	CH12	0.43	0.79		CH12	0.35	0.57	
	CH15	0.4	0.77		CH15	0.36	0.6	
	Avg	0.436	0.8		Avg	0.39	0.534	
f-3_10kn_a	CH03	0.31	0.72	f-3_10kn_li	CH03	0.35	0.54	
	CH06	0.31	0.68		CH06	0.43	0.51	
	CH09 (mid)	0.3	0.71		CH09 (mid)	0.35	0.52	
	CH12	0.3	0.7		CH12	0.37	0.59	
	CH15	0.29	0.6		CH15	0.41	0.49	
	Avg	0.302	0.682		Avg	0.382	0.53	
f-3_15kn_a	CH03	0.25	0.34	f-3_15kn_li	CH03	0.34	0.59	
	CH06	0.24	0.35		CH06	0.44	0.68	
	CH09 (mid)	0.24	0.38		CH09 (mid)	0.42	0.66	
	CH12	0.28	0.48		CH12	0.47	0.69	
	CH15	0.3	0.61		CH15	0.5	0.74	
	Avg	0.262	0.432		Avg	0.434	0.672	
f-3_20kn_a	CH03	0.29	0.62	f-3_20kn_li	CH03	0.34	0.71	
	CH06	0.3	0.65		CH06	0.38	0.51	
	CH09 (mid)	0.28	0.64		CH09 (mid)	0.36	0.49	
	CH12	0.27	0.45		CH12	0.46	0.59	
	CH15	0.26	0.44		CH15	0.46	0.59	
	Avg	0.28	0.56		Avg	0.4	0.578	
f-3_failure_a	CH03	0.25	0.37	f-3_failure_li	CH03	0.32	0.64	
	CH06	0.25	0.37		CH06	0.4	0.61	
	CH09 (mid)	0.25	0.53		CH09 (mid)	0.41	0.61	
	CH12	0.25	0.59		CH12	0.44	0.63	
	CH15	0.24	0.4		CH15	0.42	0.55	
	Avg	0.248	0.452		Avg	0.398	0.608	

		NGI	NLI				NGI	NLI
f-3_0kn_ii	CH03	0.39	0.69		f-3_0kn_ci	CH03	0.25	0.47
	CH06	0.33	0.67			CH06	0.26	0.47
	CH09 (mid)	0.3	0.55			CH09 (mid)	0.26	0.46
	CH12	0.33	0.57			CH12	0.26	0.41
	CH15	0.26	0.43			CH15	0.25	0.48
	Avg	0.322	0.582			Avg	0.256	0.458
f-3_5kn_ii	CH03	0.31	0.38		f-3_5kn_ci	CH03	0.25	0.41
	CH06	0.32	0.37			CH06	0.25	0.48
	CH09 (mid)	0.32	0.34			CH09 (mid)	0.24	0.54
	CH12	0.35	0.33			CH12	0.27	0.58
	CH15	0.32	0.53			CH15	0.25	0.38
	Avg	0.324	0.39			Avg	0.252	0.478
f-3_10kn_ii	CH03	0.28	0.34		f-3_10kn_ci	CH03	0.25	0.37
	CH06	0.32	0.36			CH06	0.25	0.37
	CH09 (mid)	0.33	0.42			CH09 (mid)	0.25	0.39
	CH12	0.34	0.52			CH12	0.27	0.46
	CH15	0.33	0.52			CH15	0.26	0.41
	Avg	0.32	0.432			Avg	0.256	0.4
f-3_15kn_ii	CH03	0.33	0.59		f-3_15kn_ci	CH03	0.29	0.43
	CH06	0.29	0.45			CH06	0.27	0.43
	CH09 (mid)	0.32	0.5			CH09 (mid)	0.26	0.43
	CH12	0.35	0.59			CH12	0.32	0.68
	CH15	0.35	0.65			CH15	0.25	0.43
	Avg	0.328	0.556			Avg	0.278	0.48
f-3_20kn_ii	CH03	0.34	0.58		f-3_20kn_ci	CH03	0.23	0.35
	CH06	0.27	0.37			CH06	0.25	0.36
	CH09 (mid)	0.32	0.56			CH09 (mid)	0.26	0.38
	CH12	0.52	0.72			CH12	0.28	0.59
	CH15	0.25	0.28			CH15	0.24	0.41
	Avg	0.34	0.502			Avg	0.252	0.418
f-3_failure_ii	CH03	0.3	0.46		f-3_failure_ci	CH03	0.51	0.79
	CH06	0.24	0.27			CH06	0.25	0.38
	CH09 (mid)	0.31	0.51			CH09 (mid)	0.26	0.47
	CH12	0.36	0.67			CH12	0.29	0.68
	CH15	0.27	0.35			CH15	0.26	0.39
	Avg	0.296	0.452			Avg	0.314	0.542

		NGI	NLI				NGI	NLI
S-1_0kn_a	CH03	0.32	0.79		S-1_0kn_li	CH03	0.43	0.7
	CH06	0.32	0.73			CH06	0.43	0.7
	CH09 (mid)	0.35	0.8			CH09 (mid)	0.42	0.74
	CH12	0.32	0.67			CH12	0.43	0.72
	CH15	0.31	0.66			CH15	0.41	0.7
	Avg	0.324	0.73			Avg	0.424	0.712
S-1_5kn_a	CH03	0.27	0.45		S-1_5kn_li	CH03	0.47	0.64
	CH06	0.27	0.46			CH06	0.4	0.65
	CH09 (mid)	0.26	0.41			CH09 (mid)	0.41	0.65
	CH12	0.27	0.44			CH12	0.39	0.58
	CH15	0.25	0.38			CH15	0.36	0.5
	Avg	0.264	0.428			Avg	0.406	0.604
S-1_10kn_a	CH03	0.22	0.26		S-1_10kn_li	CH03	0.39	0.6
	CH06	0.23	0.27			CH06	0.4	0.43
	CH09 (mid)	0.24	0.32			CH09 (mid)	0.4	0.49
	CH12	0.25	0.41			CH12	0.41	0.57
	CH15	0.24	0.31			CH15	0.35	0.51
	Avg	0.236	0.314			Avg	0.39	0.52
S-1_15kn_a	CH03	0.29	0.6		S-1_15kn_li	CH03	0.38	0.52
	CH06	0.28	0.64			CH06	0.39	0.6
	CH09 (mid)	0.3	0.65			CH09 (mid)	0.4	0.68
	CH12	0.29	0.61			CH12	0.4	0.62
	CH15	0.3	0.74			CH15	0.44	0.68
	Avg	0.292	0.648			Avg	0.402	0.62
S-1_20kn_a	CH03	0.37	0.71		S-1_20kn_li	CH03	0.48	0.82
	CH06	0.35	0.67			CH06	0.38	0.73
	CH09 (mid)	0.31	0.65			CH09 (mid)	0.41	0.68
	CH12	0.32	0.66			CH12	0.41	0.7
	CH15	0.32	0.71			CH15	0.37	0.58
	Avg	0.334	0.68			Avg	0.41	0.702
S-1_failure_a	CH03	0.23	0.27		S-1_failure_li	CH03	0.42	0.83
	CH06	0.24	0.28			CH06	0.44	0.8
	CH09 (mid)	0.23	0.29			CH09 (mid)	0.42	0.77
	CH12	0.23	0.26			CH12	0.47	0.81
	CH15	0.23	0.28			CH15	0.58	0.78
	Avg	0.232	0.276			Avg	0.466	0.798

		NGI	NLI			NGI	NLI
S-2_0kn_a	CH03	0.24	0.44	S-2_0kn_li	CH03	0.46	0.71
	CH06	0.25	0.45		CH06	0.39	0.73
	CH09 (mid)	0.26	0.47		CH09 (mid)	0.5	0.73
	CH12	0.26	0.44		CH12	0.51	0.7
	CH15	0.25	0.45		CH15	0.39	0.69
	Avg	0.252	0.45		Avg	0.45	0.712
S-2_5kn_a	CH03	0.29	0.55	S-2_5kn_li	CH03	0.47	0.74
	CH06	0.26	0.51		CH06	0.44	0.73
	CH09 (mid)	0.26	0.54		CH09 (mid)	0.45	0.71
	CH12	0.3	0.72		CH12	0.55	0.7
	CH15	0.32	0.74		CH15	0.38	0.72
	Avg	0.286	0.612		Avg	0.458	0.72
S-2_10kn_a	CH03	0.3	0.63	S-2_10kn_li	CH03	0.43	0.81
	CH06	0.29	0.61		CH06	0.43	0.8
	CH09 (mid)	0.29	0.59		CH09 (mid)	0.45	0.81
	CH12	0.3	0.65		CH12	0.45	0.83
	CH15	0.31	0.71		CH15	0.38	0.74
	Avg	0.298	0.638		Avg	0.428	0.798
S-2_15kn_a	CH03	0.24	0.41	S-2_15kn_li	CH03	0.45	0.76
	CH06	0.24	0.35		CH06	0.48	0.68
	CH09 (mid)	0.24	0.46		CH09 (mid)	0.44	0.75
	CH12	0.24	0.46		CH12	0.43	0.78
	CH15	0.25	0.41		CH15	0.34	0.68
	Avg	0.242	0.418		Avg	0.428	0.73
S-2_20kn_a	CH03	0.25	0.39	S-2_20kn_li	CH03	0.38	0.5
	CH06	0.25	0.4		CH06	0.39	0.52
	CH09 (mid)	0.25	0.42		CH09 (mid)	0.39	0.56
	CH12	0.25	0.4		CH12	0.43	0.69
	CH15	0.25	0.41		CH15	0.47	0.9
	Avg	0.25	0.404		Avg	0.412	0.634
S-2_failure_a	CH03	0.27	0.42	S-2_failure_li	CH03	0.47	0.73
	CH06	0.35	0.85		CH06	0.45	0.69
	CH09 (mid)	0.39	0.88		CH09 (mid)	0.49	0.73
	CH12	0.36	0.8		CH12	0.5	0.71
	CH15	0.29	0.74		CH15	0.44	0.91
	Avg	0.332	0.738		Avg	0.47	0.754

		NGI	NLI				NGI	NLI
S-2_0kn_ii	CH03	0.32	0.56		S-2_0kn_ci	CH03	0.26	0.38
	CH06	0.33	0.56			CH06	0.27	0.48
	CH09 (mid)	0.36	0.55			CH09 (mid)	0.35	0.67
	CH12	0.47	0.72			CH12	0.35	0.71
	CH15	0.3	0.49			CH15	0.25	0.44
	Avg	0.356	0.576			Avg	0.296	0.536
S-2_5kn_ii	CH03	0.42	0.8		S-2_5kn_ci	CH03	0.31	0.64
	CH06	0.27	0.35			CH06	0.25	0.32
	CH09 (mid)	0.5	0.82			CH09 (mid)	0.38	0.72
	CH12	0.57	0.74			CH12	0.4	0.85
	CH15	0.3	0.43			CH15	0.25	0.4
	Avg	0.412	0.628			Avg	0.318	0.586
S-2_10kn_ii	CH03	0.45	0.75		S-2_10kn_ci	CH03	0.33	0.59
	CH06	0.31	0.45			CH06	0.23	0.31
	CH09 (mid)	0.32	0.6			CH09 (mid)	0.28	0.47
	CH12	0.43	0.74			CH12	0.33	0.6
	CH15	0.28	0.44			CH15	0.24	0.33
	Avg	0.358	0.596			Avg	0.282	0.46
S-2_15kn_ii	CH03	0.36	0.77		S-2_15kn_ci	CH03	0.32	0.73
	CH06	0.25	0.43			CH06	0.26	0.44
	CH09 (mid)	0.39	0.71			CH09 (mid)	0.26	0.47
	CH12	0.45	0.77			CH12	0.31	0.68
	CH15	0.25	0.35			CH15	0.27	0.58
	Avg	0.34	0.606			Avg	0.284	0.58
S-2_20kn_ii	CH03	0.33	0.54		S-2_20kn_ci	CH03	0.25	0.41
	CH06	0.29	0.51			CH06	0.23	0.29
	CH09 (mid)	0.3	0.5			CH09 (mid)	0.24	0.36
	CH12	0.33	0.49			CH12	0.27	0.56
	CH15	0.3	0.39			CH15	0.24	0.36
	Avg	0.31	0.486			Avg	0.246	0.396
S-2_failure_ii	CH03	0.33	0.57		S-2_failure_ci	CH03	0.24	0.44
	CH06	0	0.13			CH06	0.25	0.49
	CH09 (mid)	0.48	0.78			CH09 (mid)	0.25	0.41
	CH12	0.38	0.68			CH12	0.25	0.37
	CH15	0.32	0.58			CH15	0.25	0.46
	Avg	0.302	0.548			Avg	0.248	0.434

		NGI	NLI				NGI	NLI
S-3_0kn_a	CH03	0.33	0.72		S-3_0kn_li	CH03	0.43	0.68
	CH06	0.33	0.72			CH06	0.42	0.64
	CH09 (mid)	0.29	0.57			CH09 (mid)	0.45	0.7
	CH12	0.29	0.6			CH12	0.56	0.63
	CH15	0.29	0.69			CH15	0.4	0.65
	Avg	0.306	0.66			Avg	0.452	0.66
S-3_5kn_a	CH03	0.25	0.39		S-3_5kn_li	CH03	0.41	0.68
	CH06	0.26	0.47			CH06	0.4	0.71
	CH09 (mid)	0.27	0.46			CH09 (mid)	0.41	0.67
	CH12	0.27	0.44			CH12	0.45	0.68
	CH15	0.28	0.51			CH15	0.4	0.7
	Avg	0.266	0.454			Avg	0.414	0.688
S-3_10kn_a	CH03	0.24	0.42		S-3_10kn_li	CH03	0.38	0.69
	CH06	0.24	0.43			CH06	0.44	0.73
	CH09 (mid)	0.25	0.46			CH09 (mid)	0.41	0.69
	CH12	0.25	0.49			CH12	0.49	0.71
	CH15	0.25	0.44			CH15	0.4	0.63
	Avg	0.246	0.448			Avg	0.424	0.69
S-3_15kn_a	CH03	0.25	0.45		S-3_15kn_li	CH03	0.41	0.72
	CH06	0.25	0.41			CH06	0.4	0.62
	CH09 (mid)	0.25	0.38			CH09 (mid)	0.42	0.66
	CH12	0.25	0.36			CH12	0.39	0.68
	CH15	0.25	0.37			CH15	0.4	0.66
	Avg	0.25	0.394			Avg	0.404	0.668
S-3_20kn_a	CH03	0.24	0.33		S-3_20kn_li	CH03	0.44	0.71
	CH06	0.24	0.31			CH06	0.41	0.65
	CH09 (mid)	0.24	0.38			CH09 (mid)	0.46	0.74
	CH12	0.24	0.33			CH12	0.42	0.61
	CH15	0.24	0.32			CH15	0.37	0.69
	Avg	0.24	0.334			Avg	0.42	0.68
S-3_failure_a	CH03	0.32	0.71		S-3_failure_li	CH03	0.36	0.58
	CH06	0.28	0.62			CH06	0.5	0.67
	CH09 (mid)	0.29	0.58			CH09 (mid)	0.43	0.72
	CH12	0.32	0.74			CH12	0.39	0.71
	CH15	0.29	0.63			CH15	0.42	0.65
	Avg	0.3	0.656			Avg	0.42	0.666

		NGI	NLI				NGI	NLI
S-3_0kn_ii	CH03	0.37	0.64		S-3_0kn_ci	CH03	0.28	0.61
	CH06	0.3	0.43			CH06	0.24	0.38
	CH09 (mid)	0.4	0.76			CH09 (mid)	0.36	0.77
	CH12	0.37	0.71			CH12	0.37	0.77
	CH15	0.29	0.43			CH15	0.26	0.42
	Avg	0.346	0.594			Avg	0.302	0.59
S-3_5kn_ii	CH03	0.34	0.56		S-3_5kn_ci	CH03	0.31	0.54
	CH06	0.33	0.52			CH06	0.24	0.31
	CH09 (mid)	0.31	0.47			CH09 (mid)	0.31	0.61
	CH12	0.4	0.61			CH12	0.25	0.5
	CH15	0.32	0.42			CH15	0.28	0.48
	Avg	0.34	0.516			Avg	0.278	0.488
S-3_10kn_ii	CH03	0.28	0.47		S-3_10kn_ci	CH03	0.32	0.6
	CH06	0.27	0.33			CH06	0.24	0.34
	CH09 (mid)	0.36	0.54			CH09 (mid)	0.33	0.67
	CH12	0.41	0.57			CH12	0.32	0.7
	CH15	0.26	0.28			CH15	0.29	0.54
	Avg	0.316	0.438			Avg	0.3	0.57
S-3_15kn_ii	CH03	0.34	0.74		S-3_15kn_ci	CH03	0.25	0.42
	CH06	0.29	0.43			CH06	0.23	0.33
	CH09 (mid)	0.3	0.35			CH09 (mid)	0.27	0.41
	CH12	0.36	0.61			CH12	0.24	0.31
	CH15	0.25	0.24			CH15	0.28	0.45
	Avg	0.308	0.474			Avg	0.254	0.384
S-3_20kn_ii	CH03	0.28	0.39		S-3_20kn_ci	CH03	0.23	0.27
	CH06	0.23	0.26			CH06	0.25	0.42
	CH09 (mid)	0.39	0.66			CH09 (mid)	0.24	0.35
	CH12	0.42	0.65			CH12	0.27	0.41
	CH15	0.28	0.48			CH15	0.24	0.31
	Avg	0.32	0.488			Avg	0.246	0.352
S-3_failure_ii	CH03	0.32	0.55		S-3_failure_ci	CH03	0.24	0.34
	CH06	0.25	0.31			CH06	0.24	0.35
	CH09 (mid)	0.33	0.67			CH09 (mid)	0.26	0.38
	CH12	0.36	0.66			CH12	0.25	0.37
	CH15	0.27	0.47			CH15	0.25	0.34
	Avg	0.306	0.532			Avg	0.248	0.356

